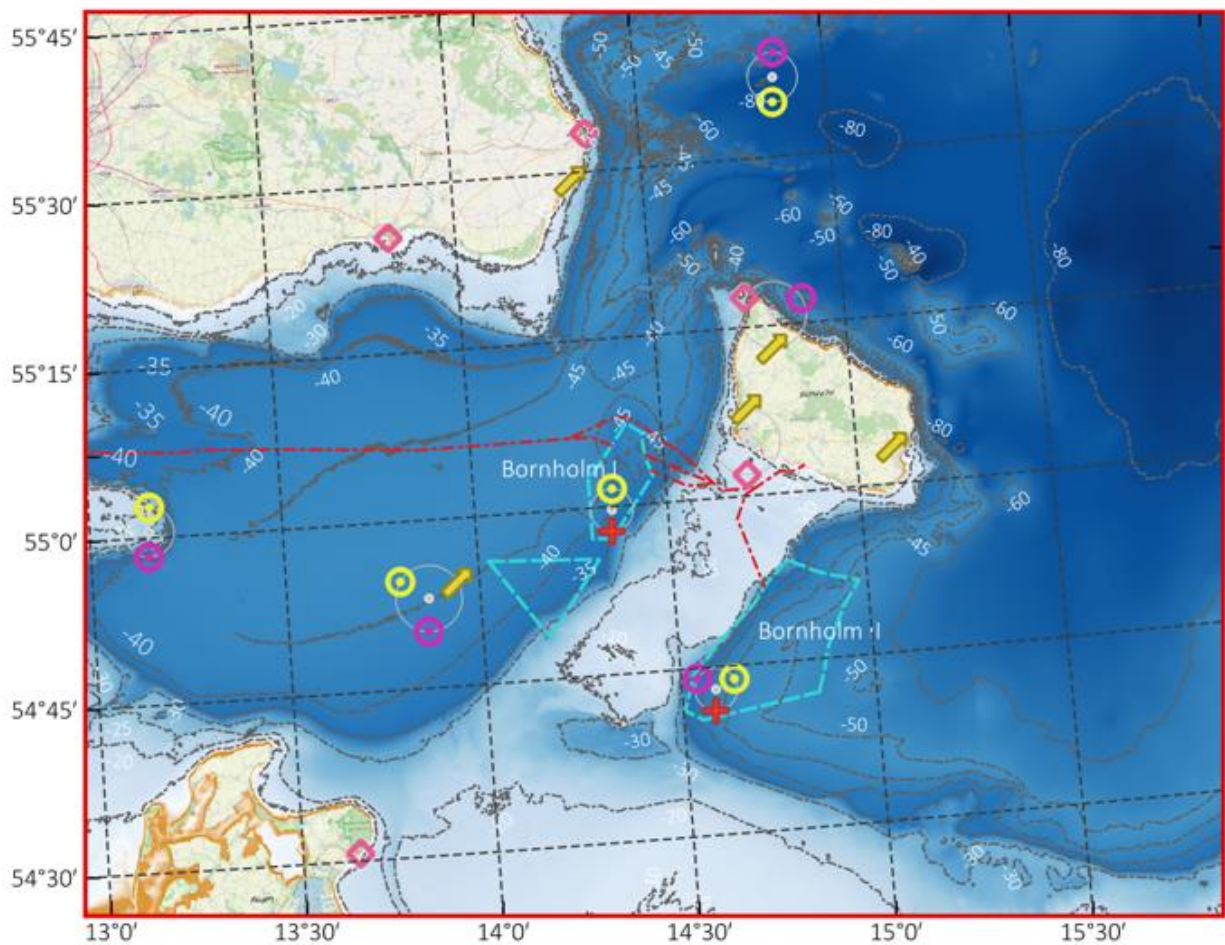


Ice Assessment, Energy Island Baltic Sea Bornholm I and II OWF

Site Ice Conditions Assessment



Change list

Ver:	Date:	Description of the change	Reviewed	Approved by
01	10/11 2023	First version	LARJ, SABA, AUOL	HLG
02	03/01 2024	General update	LARJ, SABA, AUOL	HLG
03	16/02 2024	General update	LARJ, AUOL	HLG

Project Name: Ice Assessment Energy Island Baltic Sea
Bornholm I and II OWF
Project Number: 41007612
Document number: 41007612-001
Client: Energinet
Ver: 03
Date: 16/02/2024
Author: Lars Bülow Jørgensen, Sabine Bäckström-
Andreasen, August Olrik
Controlled by Helge Gravesen
Approved by Lars Bülow Jørgensen
Document Reference: p:\tm\41007612_ice_assessment_bornholm_e
nergiz\000\04_output\report\ice assessment
bornholm energiz ver 03.docx

Table of contents

Change list.....	2
1 Introduction.....	12
1.1 Codes, standards and references	12
2 Input data.....	13
2.1 Ice observation reports.....	13
2.2 Model data.....	13
2.2.1 ERA5 model data	13
2.2.2 NORA3 model data	14
2.2.3 Data availability	14
2.3 Measured data.....	15
2.3.1 FINO2 platform.....	15
2.3.2 Arkona Becken platform and buoy	15
2.3.3 Arkona Lighthouse	16
2.3.4 LOT3 and LOT4 air temperature data.....	17
2.3.5 Air temperature calibration	18
2.3.6 Wind data	19
2.3.7 Current speed data.....	21
3 Project site.....	23
4 Sea ice observations	25
4.1 General ice observations.....	25
4.2 Local ice observations.....	35
4.3 Observed types of ice.....	40
4.4 Climate change effects	41
4.4.1 Gulf Stream weakening.....	43
5 Frost index and ice occurrence	44
5.1 Frost index.....	44
5.2 Ice thickness (50-year return period).....	46
5.3 Ice occurrence distribution	48
5.4 Ice floe size.....	50
5.5 Free ice floe speed.....	50
6 Climate properties	59
6.1 Air properties	59
6.2 Water levels and tidal range.....	59
6.2.1 Sea level rise due to climate changes.....	60
6.3 Temperature	60
6.4 Salinity	61
6.5 Seawater and ice density	61
7 Ice properties.....	62
7.1 Ice brine volume	62
7.2 Porosity.....	62
7.3 Poisson ratio.....	62
7.4 Young's modulus	62
7.5 Ice friction coefficient.....	63
8 Ice strength.....	64
8.1 Bending strength	64
8.2 Tensile strength	66

8.3	Ice strength coefficient	66
9	Ice loads	70
9.1	Horizontal ice loads	70
9.2	Vertical ice loads	71
9.3	Local ice pressures.....	71
9.4	Dynamic ice loads	72
10	Ice ridges	80
10.1	Ice ridge generation pressure.....	81
10.2	Design loads for ice ridge	82
11	Icing (marine and atmospheric).....	86
12	Design load cases	88
13	References	90
13.1	Project specific documents.....	90
13.2	Normative and general references	90
	Annex A Recorded ice data, Area 16	92
	Annex B Ice ridge case study	94
B.1	Ice ridge generation in a wind farm.	94
B.2	Ice blocking effect for Bornholm I and II OWF	94
B.3	Foundations with cones.....	94
B.4	Monopiles and jackets without cones.....	95
B.5	Summation of ice ridge blocking effects.....	95
	Annex C Discussion of dynamic ice loading scenarios	97

Sweco Danmark
Ørestads Boulevard 41

DK 2300 København S, Denmark
Telephone +45 72 20 72 07
Fax +45 72 42 89 00
www.sweco.dk

Sweco Danmark A/S
Reg. No.: 48233511
Reg. Office: Ørestad

Member of the Sweco Group

Lars Bülow Jørgensen
Wind Energy Expert
Coastal Engineering
Telephone direct +45 43 48 64 14
Mobile +45 27 23 64 14
larsbulow.jorgensen@sweco.dk

Summary

Below in Table 1-1 is a list of the key sea ice design parameters for the Energy Island Baltic Sea's two Offshore Windfarm Farm (OWF) area's Bornholm I (BH I) and Bornholm II (BH II) located in the Baltic Sea in the Danish waters 15 km southwest of the island Bornholm with the reference coordinate:

- Bornholm I Latitude / Longitude (degrees) 54.995°N, 14.356°E
- Bornholm II Latitude / Longitude (degrees) 54.717°N, 14.588°E

The key sea ice design parameters in relation to the reference coordinate for Bornholm I and II OWF respectively are considered to be valid for the entire of the two sites.

References to the report sections are given in the last column of Table 1-1. Background documentations are listed in the reference list in Section 13.

Table 1-1 Overall ice design parameters for the Bornholm OWF.

Parameter	Probability	Values BH I	Values BH II	Unit	Internal ref.
Frost index 1/5 years	1/5y	51	56	[deg days]	5.1
Frost index 1/50 years	1/50y	224	223	[deg days]	5.1
Frost index 1/100 years	1/100y	276	273	[deg days]	5.1
Ice thickness 1/1 year	1/1y	0	0	[m]	5.2
Ice thickness 1/5 years	1/5y	0	0.01	[m]	5.2
Ice thickness 1/50 years	1/50y	0.30	0.29	[m]	5.2
Ice thickness 1/100 years	1/100y	0.34	0.34	[m]	5.2
Ice floe speed	1hr/1y	0.94	0.88	[m/s]	5.5
Average high tide (winter months)		0.10	0.09	[mMSL]	6.2
Average low tide (winter months)		-0.11	-0.11	[mMSL]	6.2
High water level (winter months)	1hr/1y	1.07	1.07	[mMSL]	6.2
Low water level (winter months)	1hr/1y	-1.02	-1.02	[mMSL]	6.2
Ice floe size	-	2	2	[km]	5.4
Ice strength coefficient, C_R ice floe (*)	1/1y	0.85	0.85	[MPa]	8.3
Ice strength coefficient, C_R ice floe (*)	1/50y	1.31	1.31	[MPa]	8.3
Ice strength coefficient, C_R ice floe (*)	1/100y	1.40	1.40	[MPa]	8.3
Ice strength coefficient, C_R ice ridge (*)(**)	1/1y	0.85	0.85	[MPa]	8.3
Ice bending strength 1/50 years	1/50y	0.36	0.35	[MPa]	8.1
Ice bending strength 1/100 years	1/100y	0.42	0.41	[MPa]	8.1
Ice ridge consolidated layer	1/50y	0.48	0.48	[m]	10.2
Ice ridge keel depth	1/50y	8.45	8.45	[m]	10.2
Ice ridge consolidated layer	1/100y	0.54	0.54	[m]	10.2

Ice ridge keel depth	1/100y	8.45	8.45	[m]	10.2
Marine icing		0-100	0-100	[mm]	11
Atmospheric icing		30	30	[mm]	11

(*) The ice strength coefficient shall be adjusted for velocity and compliance effects ref. Section 8.3 and Section 9.4.

(**) The ice strength coefficient is to be used in static calculation for ice ridge design following section A.8.2.4.5.1 of ISO 19906 [103]. Dynamic effects can be omitted due to the damping effect of the loose ice blocks in the ice ridge keel.

The 1/50y or 1/100y ice thickness event shall be combined with the 1/1y ice strength coefficient, a relevant ice floe speed (Section 5.5) and water level (Section 6.2). As the water level has little correlation to the extreme ice floe impact it would be natural to combine the extreme ice to a 1hr/1y water level event. Furthermore, it is reasonable to assume that the 1/50y or 1/100y ice thickness does not coincide with 1hr/50y or 1hr/100y ice floe speed, but rather the 1hr/1y ice floe speed.

The area around Bornholm I and II OWF has experienced ice ridges during the past 40 years according to the ice observation records, therefore it is found relevant to design for ice ridges. Further it is likely that the wind turbine foundations or nearby wind turbine foundation will generate ice ridges as described in Section 10.

Horizontal load due to temperature fluctuation in a fast ice cover (thermal ice pressure) is not expected as an overall load for the Bornholm I and II OWF foundations due to the location in the open waters and assumed distance between foundations (>1km). Further the ice cover estimate predicts less than 80% ice cover. Thermal loads shall be considered for structures adjacent to the main structure and for jackup structures.

Horizontal load from a fast ice cover subject to water level fluctuations and arch effect is not expected for the Bornholm I and II OWF foundations due to the location in the open waters (coast distance >10km) on water depth of more than 15m. Further the ice cover estimate predicts less than 80% ice cover.

Horizontal load from moving ice shall be evaluated based on the assessment of ice thickness, frequency, movement, and ice strength for Bornholm I and II OWF as described in the report. The ice movement is described for free moving ice. When the ice floes interact with the foundation structures the movement (speed) will be affected (reduced) and this effect shall be incorporated when assessing the resulting ice movement and resulting ice strength ref. [123].

Pressure from hummocked ice and ice ridges due to both subduction and ridging processes is covered by the assessment of the magnitude of ice ridges and ice strength.

Vertical force from fast ice covers subject to water level fluctuations is covered by the assessment of water level fluctuations and ice strength.

Nomenclature

Abbreviations

BHS	Bundesamt für Seeschifffahrt und Hydrographie
CFSR	Climate Forecast System Reanalysis
DLC	Design load case
ECMWF	European Centre for Medium-Range Weather Forecasts
ERA5	European Environment Agency fifth generation
EWM	Extreme wind speed model
F	Fatigue
GMSL	Global mean sea level
IPCC	Intergovernmental Panel on Climate Change
N	Normal
NCEP	The National Centers for Environmental Prediction
NSIDC	National Snow and Ice Data Center
NTM	Normal turbulence model
NWLR	Normal water level range
OWF	Offshore wind farm
PSMSL	Permanent Service for mean sea level
RCP	Representative Concentration Pathways
SMHI	Sveriges meteorologiska och hydrologiska institut
SOK	The Danish national defence marine department
U	Ultimate strength
WTG	Wind turbine generator

Symbols

A	Contact surface
A_{local}	Local area
a	Slope of frost index distribution
b	Offset of frost index distribution

b_k	Width of the base of the keel
C_R	Ice strength coefficient
c	Apparent keel cohesion, Section 10.2 or chord length, Section 11
D	Width of the ice feature
E_f	Effective elastic modulus
e	Keel porosity
F_G	Global horizontal crushing ice load
F_c	Action component due to the consolidated part of the ridge
F_k	Keel action component
f	Frequency
f_{AR}	Empirical term in relation to determine p_G
g	Gravitational acceleration
H, F	Ice action
H_0	Peak value of ice action
H_k	Keel depth
H_{max}, F_{max}	Maximum value of ice action
H_{min}	Minimum value of ice action
H_s	Sail height
h, t, t_{open}	Ice thickness, ice thickness in open waters or time in Section 9.4
h_c	Consolidated layer thickness
h_k	Vertical distance between the base of the consolidated layer and the base of the keel
h_p	Parent ice floe thickness
h_s	Sail height
K, K_{max}	Frost index summarized in a winter period
k	Stiffness of the structure at the waterline
n, m	Empirical exponents to take account of the size effect in relation to determine p_G
p_D	Ridge-building action per unit width

p_G	External global ice pressure
p_{local}	Characteristic local ice pressure for use in design in design against moving ice
R	Coefficient in relation to determine p_D , Section 10.1 or rotor radius, Section 11
S	Security surcharge
S_B	Bulk salinity after completed ice growth
T	Period of ice action
T_R	Return period
U	Impact velocity
U_c	Current speed
$U_{w,10m}$	Wind speed 10 m above water
U_{wind}	Wind speed
u	Structure displacement
u_w	Waterline displacement
V_{hub}	Mean wind speed at hub height
V_b	Vertical load limited by the bending strength if the ice is broken in a ring around the support structure
V_{ice}	Free ice floe speed
V_t	Vertical load limited by shear strength at adhesion to the support structure
v_0	Reference volume
v_b	Ice brine volume
w	Width of the structure
γ_S	Compliance parameter
γ_e	Effective buoyancy
ΔH	Difference between maximum and minimum values of ice action
Δz	Water level difference
ε	Strain rate, depending on the rate of interaction (ice drift velocity)
θ	Coefficient in relation to determine ξ_n
θ_f	Freezing temperature of water

θ_k	Keel angle from horizontal
μ_E	Mass distribution on the leading edge of the rotor blade at half the rotor radius
μ_d	Dynamic friction coefficient
μ_{d0}	Constant depending on the structure surface
μ_ϕ	Passive pressure coefficient
ξ_n	Damping of the n'th eigenmode as a fraction of critical damping
ρ_i, ρ_E	Ice density
ρ, ρ_w	Water density
σ_0	Reference strength
σ_b	Bending strength of ice
σ_c	Crushing (compressive) strength of ice
σ_f	Bending (flexural) strength of ice
σ_t	Tensile strength of ice
τ	Adhesive shear strength, Section 9.2 or duration of loading/unloading cycle, Section 9.4
τ_{mean}	Mean air temperature (24h) in a frost period
ϑ_A	Ice temperature, averaged over the ice thickness
ϕ	Angle of internal friction
ϕ_B	Ice porosity
ϕ_{nC}	Magnitude of the n'th eigenmode at the ice action point

1 Introduction

The present report contains an ice assessment study for the Energy Island Baltic Sea project for the two offshore wind farms (OWF) Bornholm I and II for design of the wind turbines support structures (cylindrical structures). The sites are located in the Danish waters of the Baltic Sea approximately 15 km south-west of the island Bornholm. The ice assessment is based on the MetOcean study provided by DHI [1] for Bornholm I and II OWF, ice observation reports, data from the atmospheric model NORA3, literature, and standards.

1.1 Codes, standards and references

Normative standards:

- IEC International Standard, IEC 61400-3-1 Edition 2019, Wind Energy Generation Systems – Part 3-1: Design Requirements for Fixed Offshore Wind Turbines
- ISO 19906:2019 Petroleum and natural gas industries - Arctic offshore structures
- DNV-ST-0437 Edition 2016-11, Amended in 2021-11 (Loads and site conditions for offshore wind turbines)
- DNV-RP-0175 Edition 2017-12, Amended in 2021-10 (Icing of wind turbines)
- GL IND SERVICE IV-6-7. Rules and Guidelines Industrial Services Part 6- Offshore Installations Chapter7-Guideline for the Construction of fixed Offshore Installations in Ice Infested Waters. Edition June 2005.

A complete list of references can be found in Section 13.

2 Input data

The input data include follow different types of data sets:

- Ice observation reports
- Model data
- Measured data

2.1 Ice observation reports

Yearly ice observation reports [4] are available from the Danish national defence marine department (SOK) since year 1861 for Danish and adjacent waters including the Swedish and German waters. The ice coverage, ice thickness, ice structure, hinderance for ship traffic and other parameters are based on subjective visual inspections for each winter.

Further, ice observations are available Sveriges meteorologiska och hydrologiska institut (SMHI) for the Swedish waters and adjacent waters including the Danish waters, where observations of maximum ice distribution and summary of ice winters for each year can be found in the period 1980 to today and 1970 to today respectively, [8].

Ice observations for Danish waters are also available from Bundesamt für Seeschifffahrt und Hydrographie (BSH). The German Ice Atlas [6] make an overview of the observations in the period 1961 to 2010. Ice coverage, ice thickness, ice structure, and other parameters are presented for typical ice winter years. For the period after 2004/2005 separate ice reports by BSH [3] are available for all winters with sea ice. Ice charts [3] are available for days with sea ice since year 2009.

Common for all ice reports and ice charts are that the observations are based on subjective and generalized observations of ice thickness and type of ice. The records depend on where the observations are made either from onshore stations, vessels, flights and satellites. The observations have historically primarily been made as a service to ship traffic.

2.2 Model data

The model data are based on the NORA3 and ERA5 and have been provided by DHI [1]. The model data parameters delivered are wind speed and direction, water level, surface current speed and direction, seawater temperature and salinity, air temperature and relative humidity. The DHI metocean hindcast data have been calibrated and validated against various measurements' stations, being FINO2 and Arkona buoy measurements ref. Figure 2-2 and Figure 2-3, and the LOT3 and LOT4 measurements provided by Energinet ref. Figure 3-1, ref. [1].

2.2.1 ERA5 model data

ERA5 is an atmospheric model which is the fifth generation ECMWF (European Centre for Medium-Range Weather Forecasts) reanalysis for the global climate ref. Figure 2-1 and weather for the past 8 decades. Data is available from 1940 and onwards. The data set is a reanalysis dataset. Reanalysis combines model data with observations from across the world into a globally complete and

consistent dataset using the laws of physics. ERA5 provides hourly estimates for a large number of atmospheric and land-surface quantities.

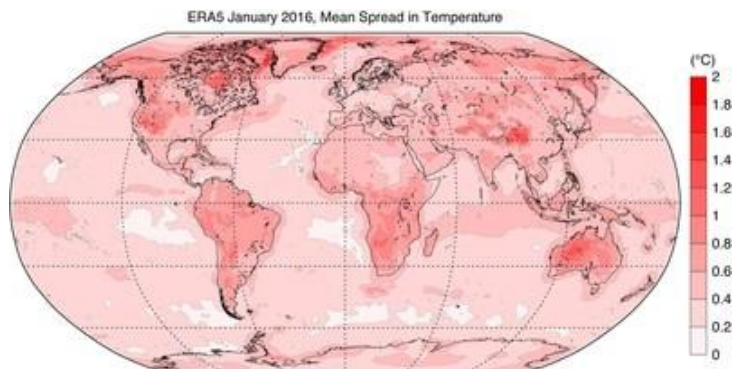


Figure 2-1 ERA5 model data global coverage.

2.2.2 NORA3 model data

The NORA3 atmospheric dataset, made available by The Norwegian Meteorological Institute, is generated using a process called high-resolution atmospheric dynamic downscaling, [9]. This technique refines data from the advanced ERA5 reanalysis dataset provided by the ECMWF. In this process, the NORA3 model acquires boundary values from ERA5 at 6-hour intervals but retains detailed hourly output data, with certain data points saved every third hour. The NORA3 model domain encompasses almost the entire northern expanse of the Atlantic Ocean and boasts a horizontal resolution of 3x3 kilometres, spanning 65 vertical layers of the atmosphere. The NORA3 dataset was validated against measurements from the local EIBS SeaWatch Wind LiDAR Buoys (LOT3 and LOT4) and against FINO2 and Arkona stations, showing a very good agreement between model and measurements.

2.2.3 Data availability

The model data have been delivered by DHI for Bornholm I and II OWF, as hourly values. For the wind and air data time series is delivered for 44-year period, 1979-2022, whereas water level, and surface current speed and direction, seawater temperature and salinity have been delivered for a 25-year period, 1998-2022. The assumed layout of for Bornholm I and II OWF and locations of analysis point and measurement points are shown in Figure 3-1.

The model data include the following data:

- Water level [mMSL]
- Current Speed (surface at 1m depth) [m/s]
- Current direction (surface at 1m depth) [°N- to]
- Water temperature (surface at 1m depth) [°C]
- Water salinity (surface at 1m depth) [PSU]
- Wind speed at 10m [m/s]
- Wind direction at 10m [°N- from]
- Air Temperature at 2m [°C]
- Relative Humidity at 2m [%]

2.3 Measured data

Measured data are used from the following stations:

- FINO2 platform (Figure 2-2)
- Arkona Becken buoy (Figure 2-3)
- Arkona lighthouse (Figure 2-4)
- LiDAR buoys LOT3 and LOT4 (Figure 3-1)

2.3.1 FINO2 platform

The research platform FINO2 was built in 2007 and since 2010 DNV have been awarded the operation and maintenance of FINO2. The platform is stationed at the location 55.01°N, 13.15°E, which is 33 km north of the island Rügen in the southern edge of Kriegers Flak and about 80-100 km from the Bornholm I & II OWFs , see Figure 2-2. The FINO2 platform provides estimates of water temperatures, salinity, Oxygen saturation, chlorophyll, turbidity, current and meteorology.

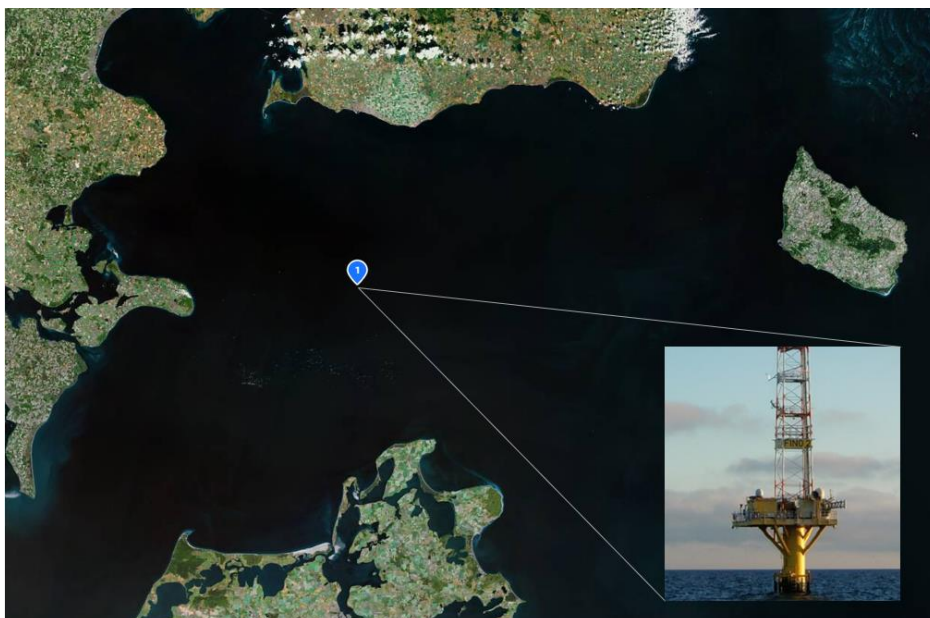


Figure 2-2 – Location of the FINO2 platform, Eniro.

2.3.2 Arkona Becken platform and buoy

The semi-submersible buoy at Arkona Becken was launched in September 2002 by BHS and is stationed at the location 54°53' N, 13°52' E next to the Arkona Becken platform about 50 km from Bornholm I & II OWFs, see Figure 2-3. Arkona Becken measuring station provides hourly estimates for, water temperatures, salinity, Oxygen saturation, chlorophyll, turbidity, current and meteorology.

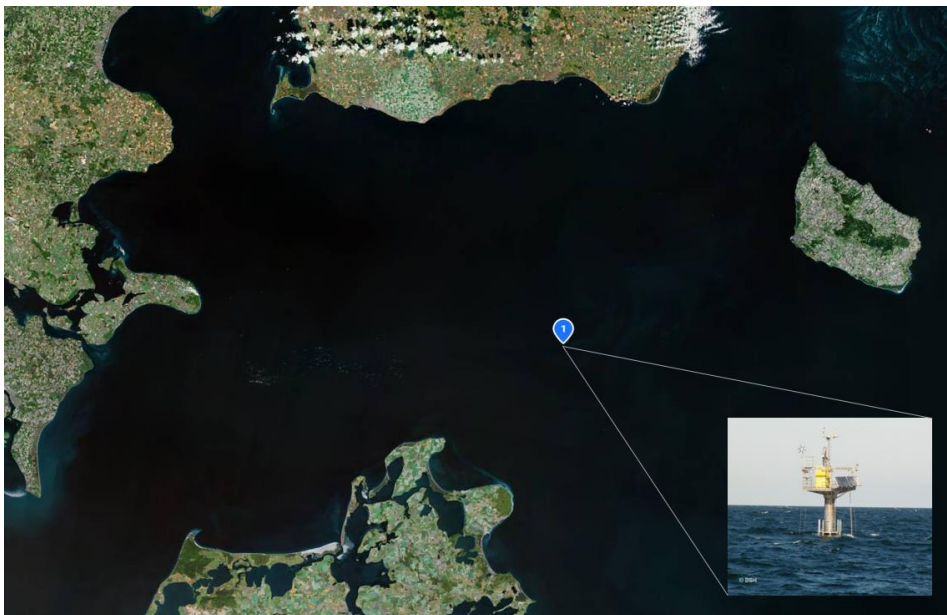


Figure 2-3 – Location of the Arkona Becken measuring station, Eniro.

2.3.3 Arkona Lighthouse

The onshore Arkona Lighthouse has available data since September 1973 by BSH. (Location 54°40' N, 13°25' E, see Figure 2-4) about 80km from Bornholm I & II OWFs. Arkona Lighthouse measuring station provides hourly estimates for a number of meteorological data including air and water temperatures.



Figure 2-4 – Location of the Arkona Lighthouse measuring station, Eniro.

2.3.4 LOT3 and LOT4 air temperature data

The air temperature is measured at the project LiDAR buoys LOT3 and LOT4 (ref. Figure 3-1). A scatter plot between air temperatures of the NORA3 dataset and LOT3 and LOT4 measured data is shown below in Figure 2-5 and Figure 2-6 respectively, both for the period ranging from November 2022 to November 2022. The comparisons show that the model results being in the same order of magnitude and follow a similar trend as the measurements, [1]. The LOT3 and LOT4 data sets does not include many data of negative air temperatures that are relevant for the ice assessment analysis, therefore the NORA3 hindcast data is calibrated against the Arkona Becken Bouy in the next section 2.3.5.

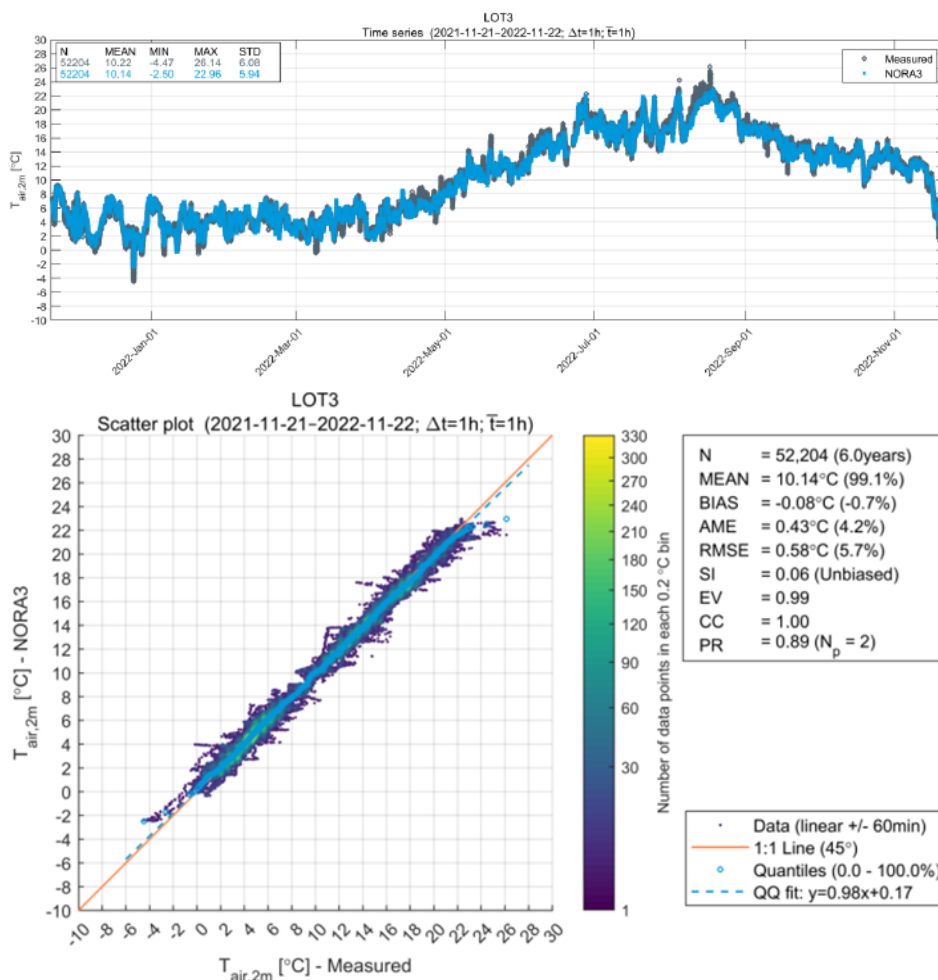


Figure 2-5 Time serial and scatter plot of air temperature data (NORA3 versus LOT3 measurements), [1].

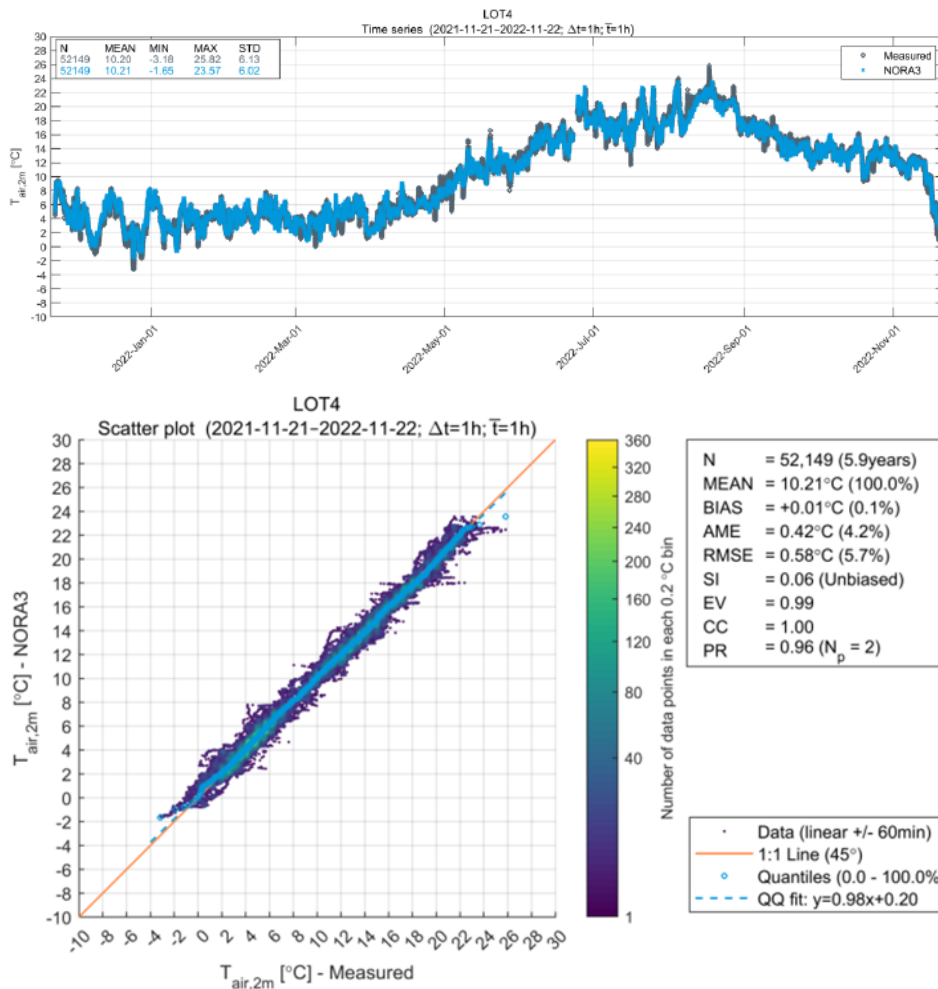


Figure 2-6 Time serial and scatter plot of air temperature data (NORA3 versus LOT4 measurements), [1].

2.3.5 Air temperature calibration

The NORA3 hind cast model data show a tendency of not to correlate for the negative temperatures as illustration in Figure 2-7. The NORA3 negative air temperature data is therefore calibrated against the measured data from Arkona Becken buoy (see location in Figure 2-3). The Arkona Becken buoy is selected for the calibration since the dataset include more air temperature data for periods with negative air temperatures.

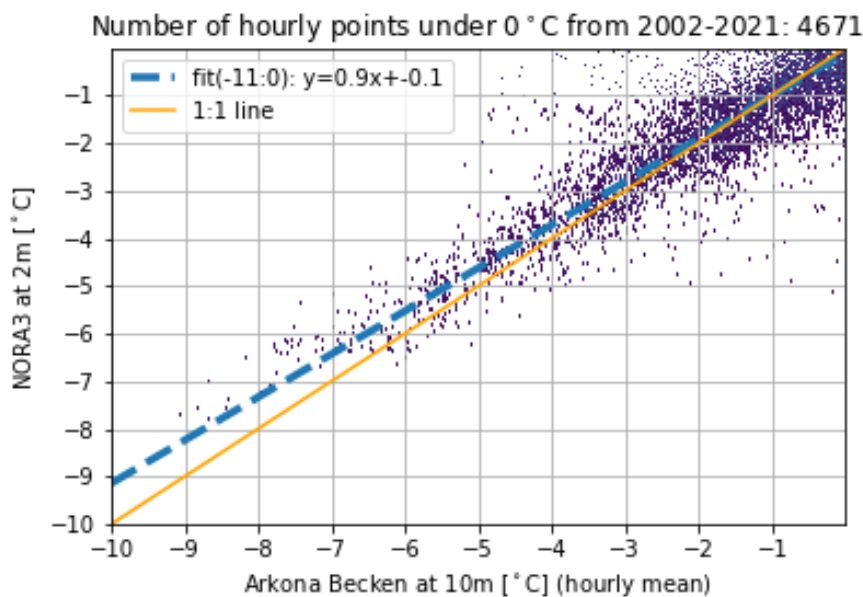


Figure 2-7 Comparison of temperature data below -0.4 °C (NORA3 versus Arkona Becken buoy measurements).

Based upon the comparison of measured and NORA3 data the NORA3 data will be scaled with $T_{Use} = (T_{NORA3} + 0.1)/0.9$

2.3.6 Wind data

The model wind data have been provided by DHI and comes from the NORA3 data model. The data is hourly mean at 10 m height. The output of the model is validated against the local measurement stations LOT3 and LOT4, the FINO2 and Arkona Becken measurement at 10 m. The measured wind speed has been converted by the power law using $\alpha=0.08$ to get the wind speed and direction at 10 mMSL, [1]. A direct comparison between the wind speed at 10 m height of the NORA3 dataset and the two stations LOT3 and LOT4 measurements is shown below in Figure 2-8 and Figure 2-9 respectively, with for the period ranging from January 2021 to November 2021. The NORA3 model captures the wind speed and direction in the region to a satisfying degree, showing a high correlation and is therefore used as it is.

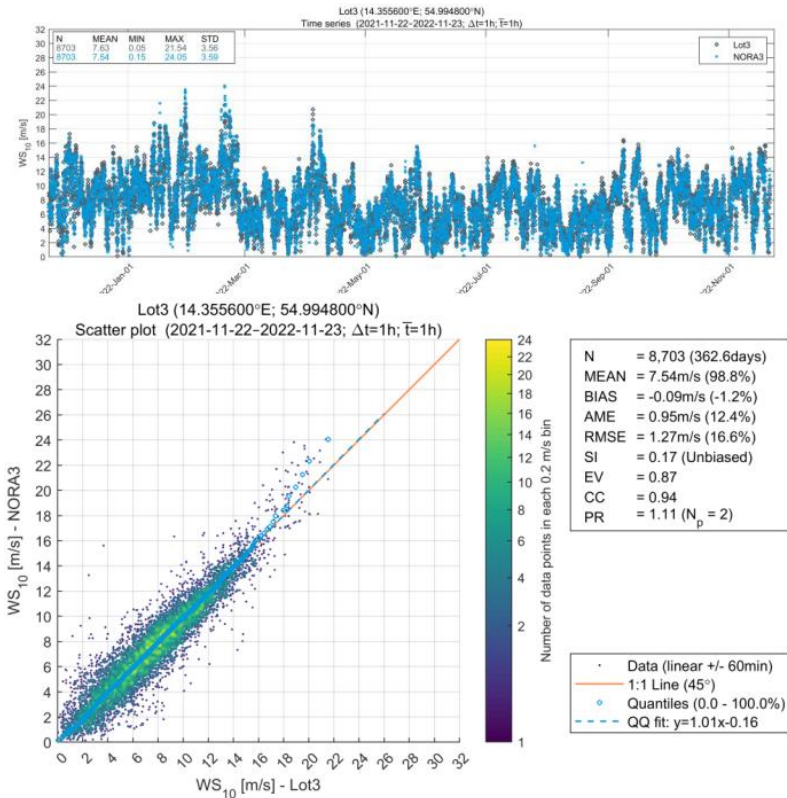


Figure 2-8 Wind speed correlation analysis (NORA3 versus LOT3 measurements), [1].

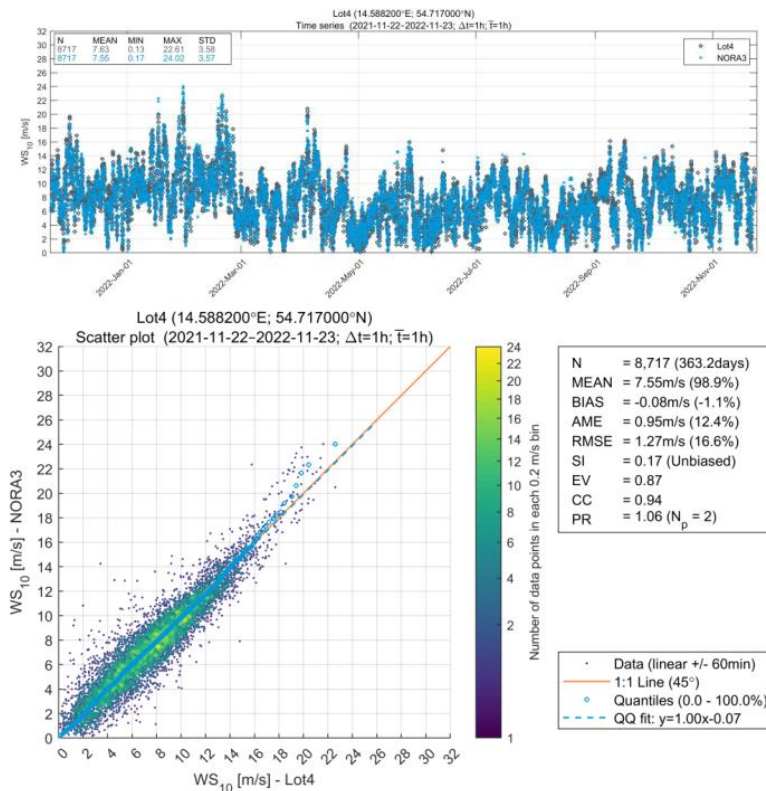


Figure 2-9 Wind speed correlation analysis (NORA3 versus LOT4 measurements), [1].

2.3.7 Current speed data

The surface current speed and direction data have been provided by DHI and comes from DHI 3D hydrodynamic model (HD_{EIBS}) ranging from 1998-2022. The current model data is calibrated and validated against the LOT3 and LOT4 measurements provided by Energinet, see location in Figure 3-1, and the FINO2 and Arkona Becken measuring stations were also used for this purpose, [1]. A comparison between the current speed dataset at 10m below sea surface and the LOT3 and LOT4 measurements data is shown below in Figure 2-10 and Figure 2-11, for the period ranging from January 2022 to June 2022.

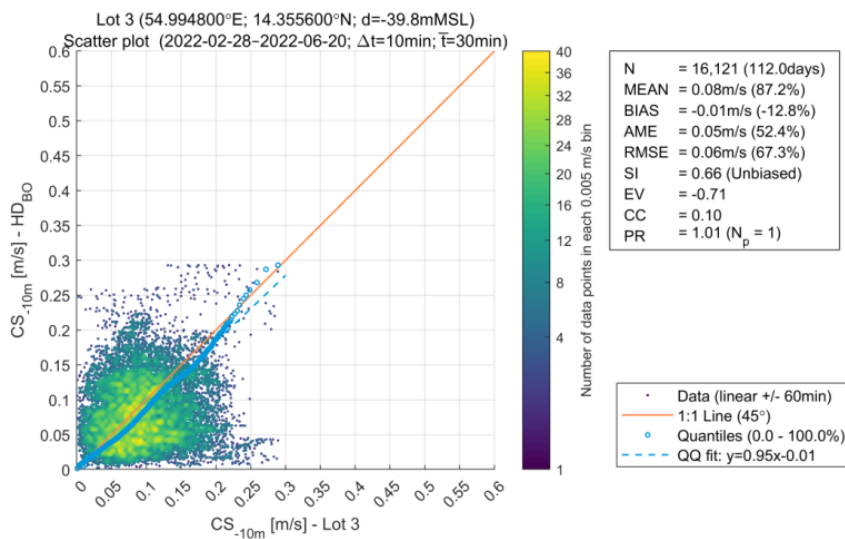


Figure 2-10 Current speed at 10 m depth below sea surface correlation analysis (DHI 3D HD_{EIBS} model versus LOT3 measurements), [1].

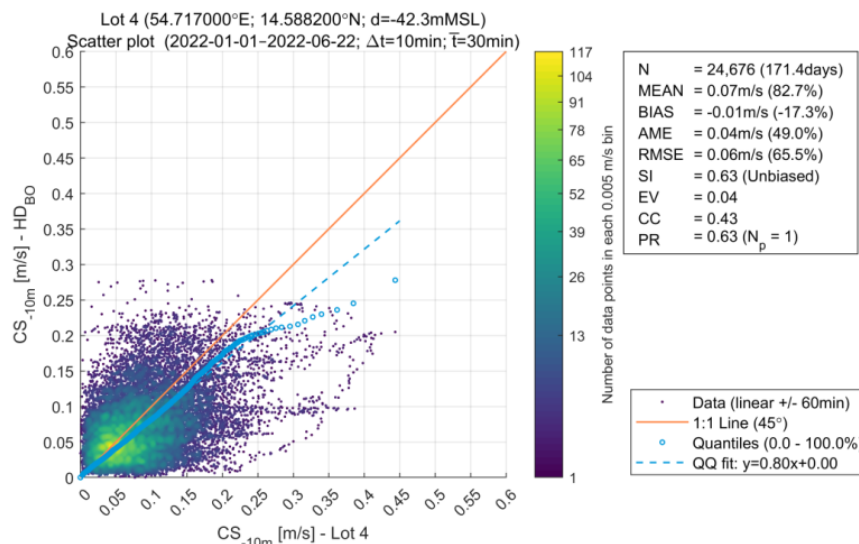


Figure 2-11 Current speed at 10 m depth below sea surface correlation analysis (DHI 3D HD_{EIBS} model versus LOT4 measurements), [1].

A mistiming between the two datasets, is reflected in Figure 2-10 and Figure 2-11. The reason for the poor time correlation is due to the complexity of the current in the Baltic Sea. Though the DHI 3D HD_{EIBS} model results of the surface current data is still considered to represent a realistic picture of the surface current speed and direction therefore is deemed to be acceptable.

3 Project site

For the Energy Island Baltic Sea project, the site of the Bornholm I and II OWF are located in the Danish waters of the Baltic Sea approximately 15 km southwest of the coast of the Danish Island Bornholm, as shown in Figure 3-1. The area of Bornholm I and II OWF is divided into two areas, being Bornholm I toward north and Bornholm II toward south. The water depths at the Bornholm I and II OWF site range from -37 mMSL to -47 mMSL and -34 mMSL to -57 mMSL respectively, see Figure 3-1

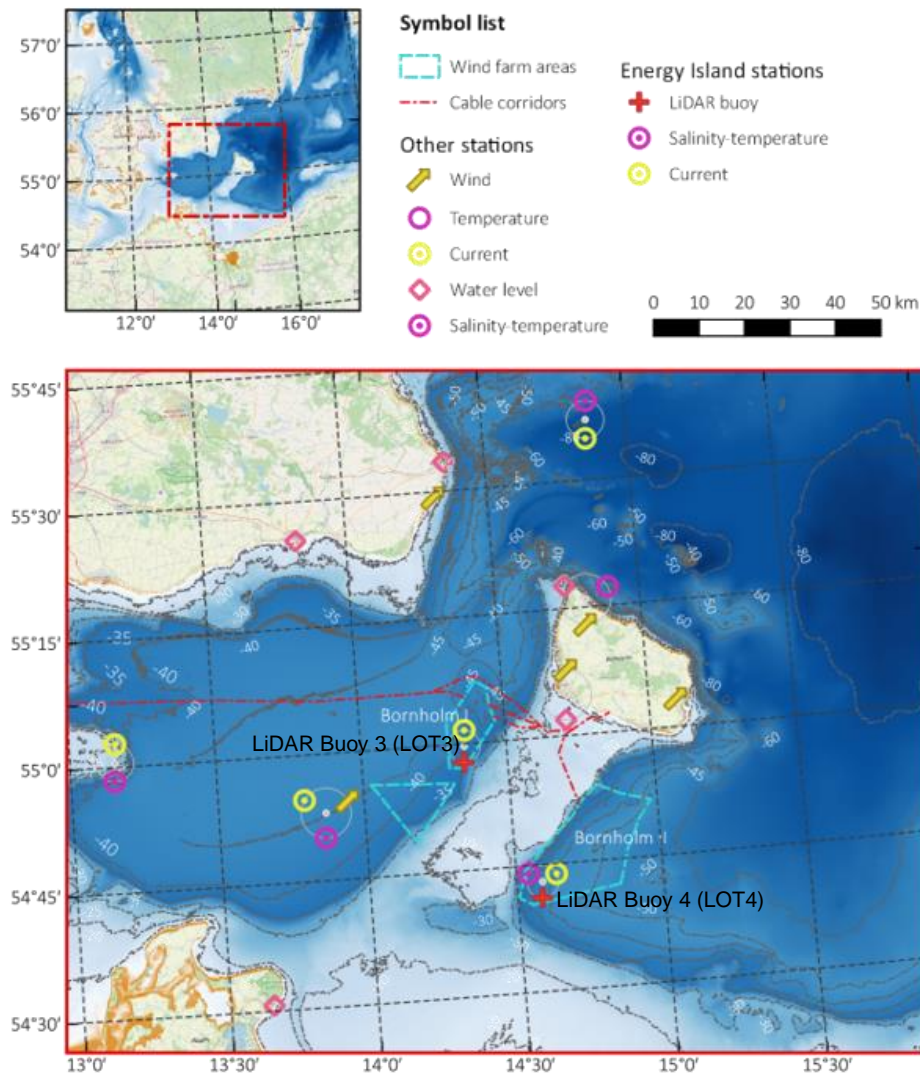


Figure 3-1 Map of assumed layout for Bornholm I and II OWF, Bathymetry and location of measuring stations.

In Figure 3-2 Bornholm I and II OWF surroundings is shown. To the south-west of the site of Bornholm I south OWF, the existing German Arkona Becken and Wikingen OWF's are located, whereas the site of Bornholm I north OWF and Bornholm II OWF, do not have any (existing) close neighbouring OWF, see Figure 3-2.

Towards southwest the distance to the shoreline of Germany (Rügen) is 50-60 km. The distance to the Swedish coast is 50-80 km. Two planned offshore wind farms called Windanker and Wikingen Süd in the German waters will be located at distance of approximately less than 5 km toward south-west of the Bornholm I south OWF. Open water is prevailing in the area around Bornholm I and II OWF for Energy Island Baltic Sea project.

The MetOcean data used for the analysis are generated for coordinates representing the LiDAR Buoy 3 (LOT3) and 4 (LOT4) locations as shown in Figure 3-1. Mentioned above other wind farms exist and are planned near the site of the Bornholm I and II OWF. These wind farms will interfere with ice movements and ice ridge generation, which will affect Bornholm I and II OWF. The foundation structures in OWF's will slow down or stop the ice movements depending on the number of involved structures and the external forces (wind and current). Further blocked ice will increase the tendency of ice ridge generation. The effects for Bornholm I and II OWF is not analysed in the this report.

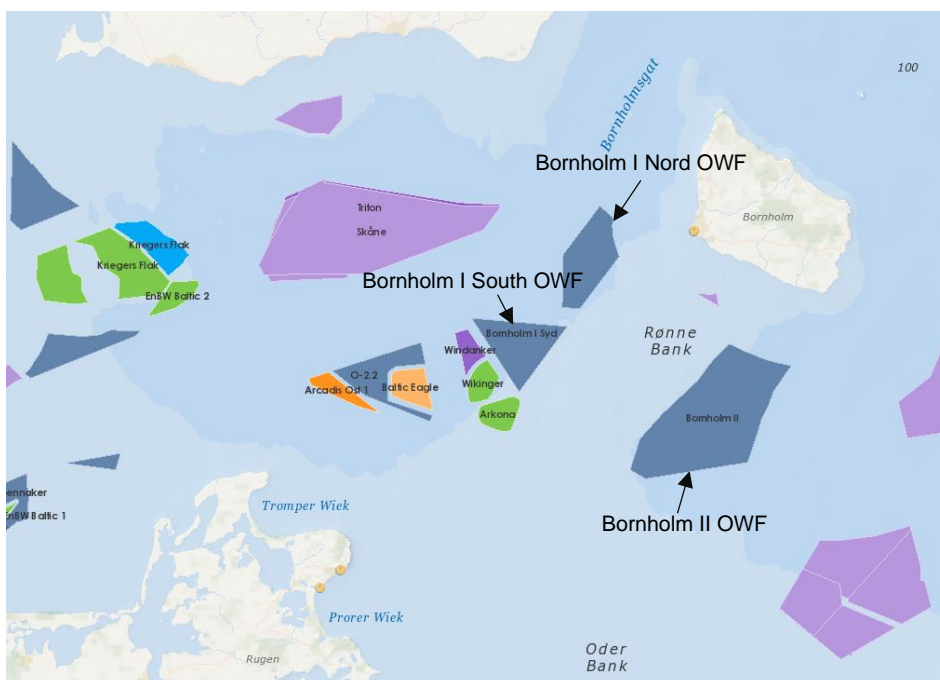


Figure 3-2 Map of Bornholm I and II OWF and the surroundings (www.4coffshore.com, 15-06-2023). Colour description: purple: concept/early planning, grey: development zone, blue: consent authorised, orange: under construction and green: fully commissioned.

4 Sea ice observations

The site of Bornholm I and II OWF are located approximately 15 km from the the Island of Bornholm. In ice winters, ice will preliminary be generated near the coasts and spread to deeper locations over time depending on the severity and length of the ice period. Ice will also be generated in the open waters but will stay for a shorter period due to the water movement.

For the analysis of ice observations, the Bornholm I north and south OWF will in this section be addressed as one Bornholm I OWF, since in the perspective of historical ice observations, these two areas are close and little or no difference in characteristic of ice formation between the two is expected.

The Bornholm I and II OWF areas is located in a region dominated by the inflow from the North Sea to the Baltic Sea and return flow depending on wind direction and level of water in the Baltic Sea. The dominating flow direction is toward west and east. The in/out flow will affect the current, water level temperature and salinity in the region.

Global warming is affecting the ice generation and a clear tendency of reduced ice coverage and frequency is observed since the year 1942. It is found sufficiently conservative to base the ice assessment on the period from year 1979 until 2022. Any reduction in frost days and frequency since year 1979 is not considered.

4.1 General ice observations

Ice formation and ice navigation observations are made by the Danish, German and Swedish authorities for the Danish waters. Observations for the Danish waters are available from the Danish national defence marine department (SOK), where yearly ice observation reports have been made since year 1861, [4].

Observations from German sources are available from Bundesamt für Seeschifffahrt und Hydrographie (BSH). The German Ice Atlas [6] provides an overview of the observations in the period 1961 to 2010. Ice coverage, ice thickness, ice structure, and other parameters are presented for typical ice winter years. For the period after 2004/2005 separate ice reports by BSH [3] are available for all winters with sea ice. Ice charts [3] are available for days with sea ice since year 2009.

Observations from Swedish sources are available from “Sveriges meteorologiska och hydrologiska institute” (SMHI), where observations of maximum ice distribution and summary of ice winters for each year can be found in the period 1980 to today and 1970 to today, respectively [8].

Very severe winters occurred in the years 1940, 1941, 1942 and 1947, but the tendency is that the severity and frequency of ice winters are reduced in the recent years. In light of the general tendency and the global warming it is evaluated that it will be safe to concentrate on the recent 40 years (from year 1979 and onward) when analysing the ice conditions for the Bornholm I and II OWF for the coming 30-40 years. Ice analysis used for reference are however made for different periods and output from these will be included as found appropriate.

In Figure 4-1 the ice volume sum for the German east seacoast (1879-2019) Ref [4] is included to illustrate the severity of the winters since year 1878.

In Figure 4-2 the frost index for Arkona Lighthouse, Bornholm I OWF (1979-2022) are shown to illustrate the severity of the winters since year 1979. The frost index is based on the method as described in Section 5.1.

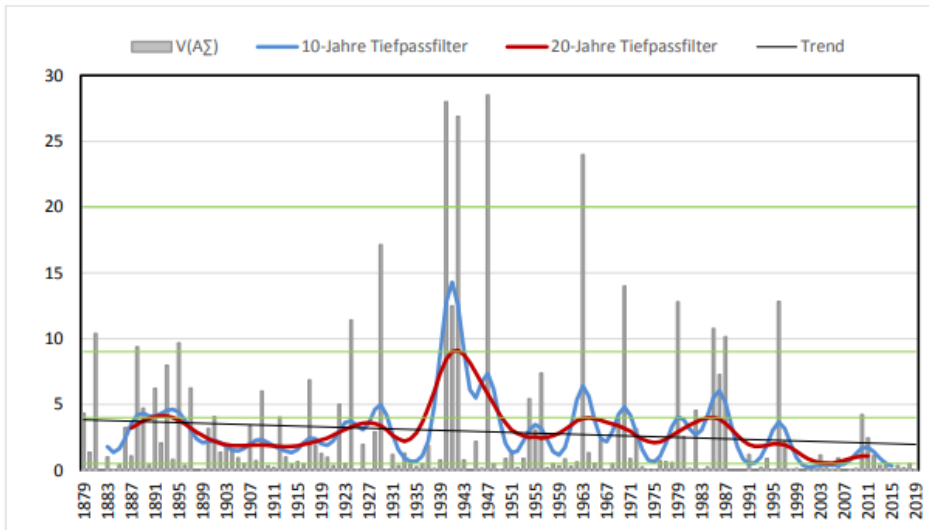


Figure 4-1 German ice volume sum for the German east seacoast (1879-2019) with date (years) on the x-axis and the y-axis is the accumulated areal ice volume (m^2N), where it is the ice thickness m multiplied with the ice concentration N , Ref [3].

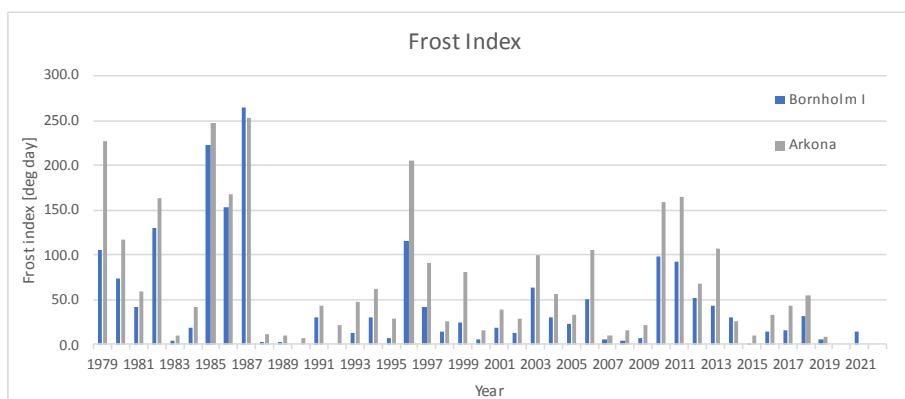


Figure 4-2 Frost Index for Arkona Lighthouse and Bornholm I OWF (1979-2022).

In Figure 4-3 the relative frequency of ice occurrence in the winter period is shown based on German ice observations from year 1965 to 2005. For the Bornholm I and II OWF reference points for Metocean data (LOT3 and LOT4 measuring stations) are located at $54.995^{\circ}N$, $14.356^{\circ}E$ and $54.717^{\circ}N$, $14.588^{\circ}E$ respectively, see blue points. Figure 4-3 shows an ice occurrence with a frequency of 20-30% for both areas, where Bornholm II OWF also borders on to an area with an ice occurrence of 15-20%. This implies that an average occurrence once per 4 years of winters is expected. The frequency of ice occurrence has reduced in the recent years and are estimated to reduce further in the coming years due to the global warming. The amount of ice during ice winters is described in this section.

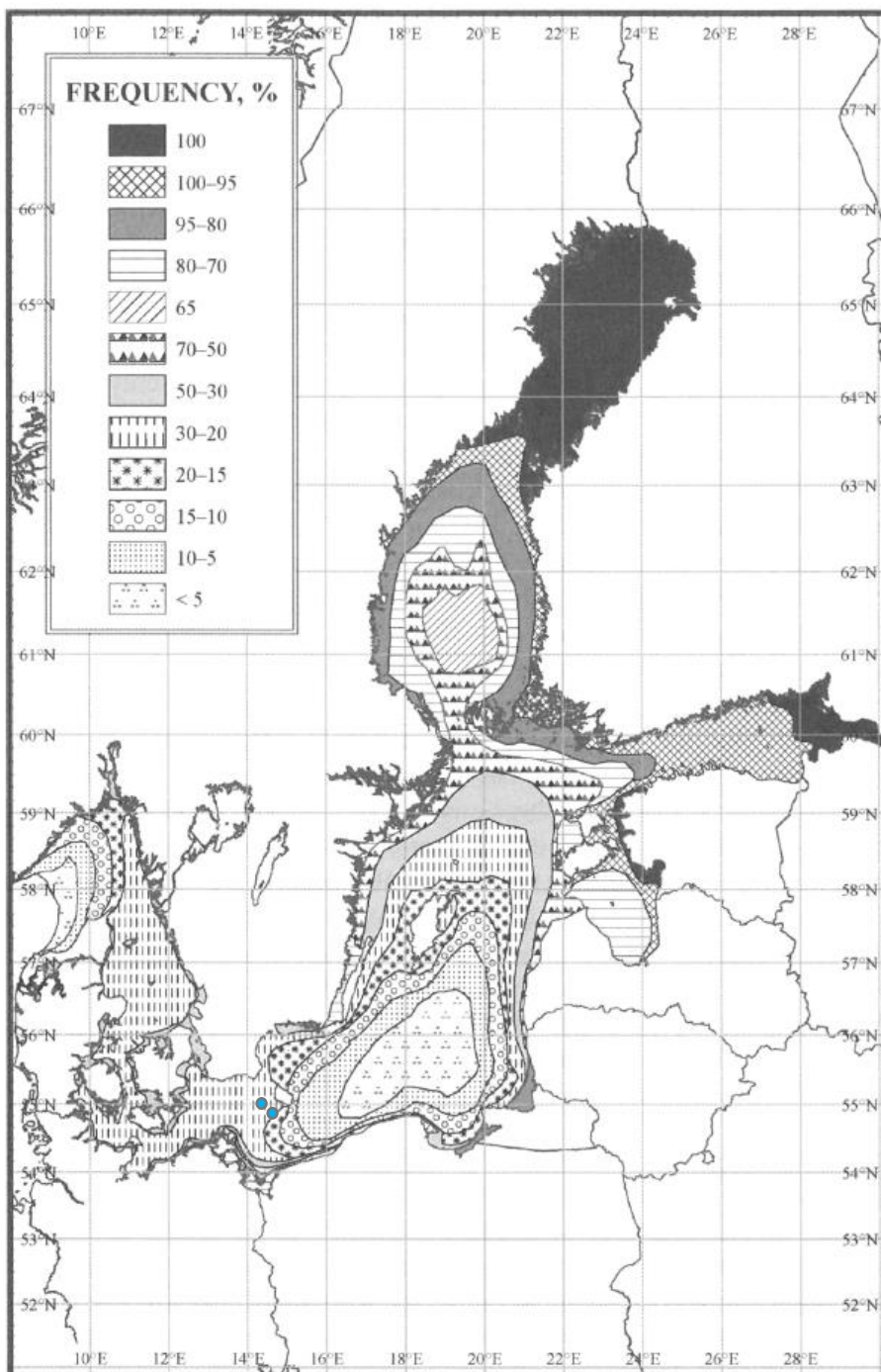


Figure 4-3 Relative frequency of ice occurrence in the period from year 1956 to 2005. Blue dots: Bornholm I and II OWF. Ref. [7] Figure 8.4.

The following ice charts shown in Figure 4-4, Figure 4-5 and Figure 4-6, show the observed ice occurrence in the years 1985, 1986 and 1987 respectively according to the Danish observations, [4].

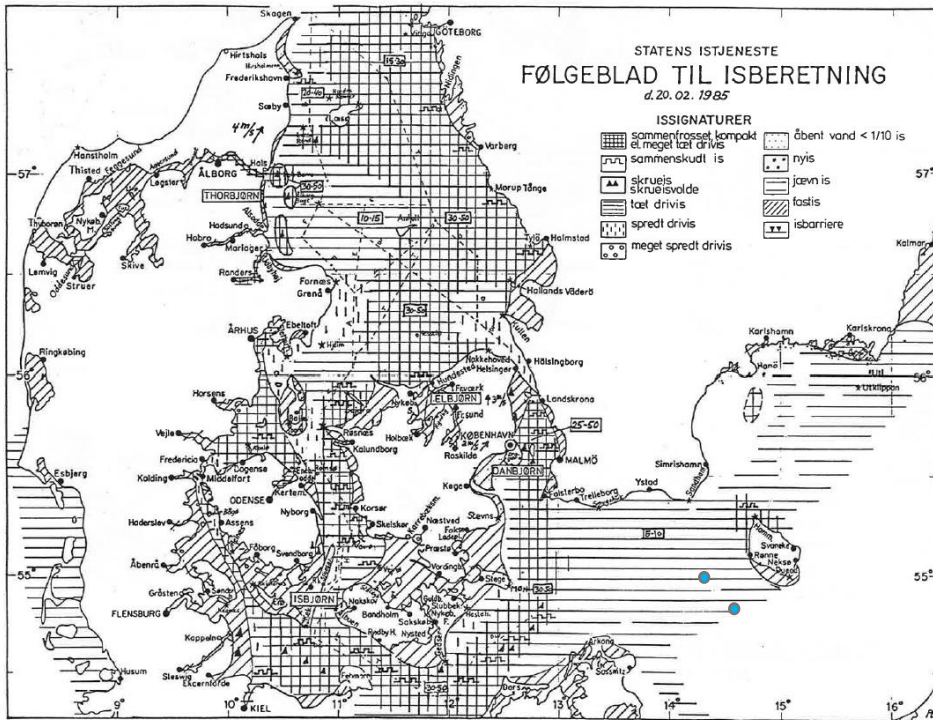


Figure 4-4 Ice observations the 20th of February 1985 ref. [4]. Blue dots: Bornholm I and II OWF.

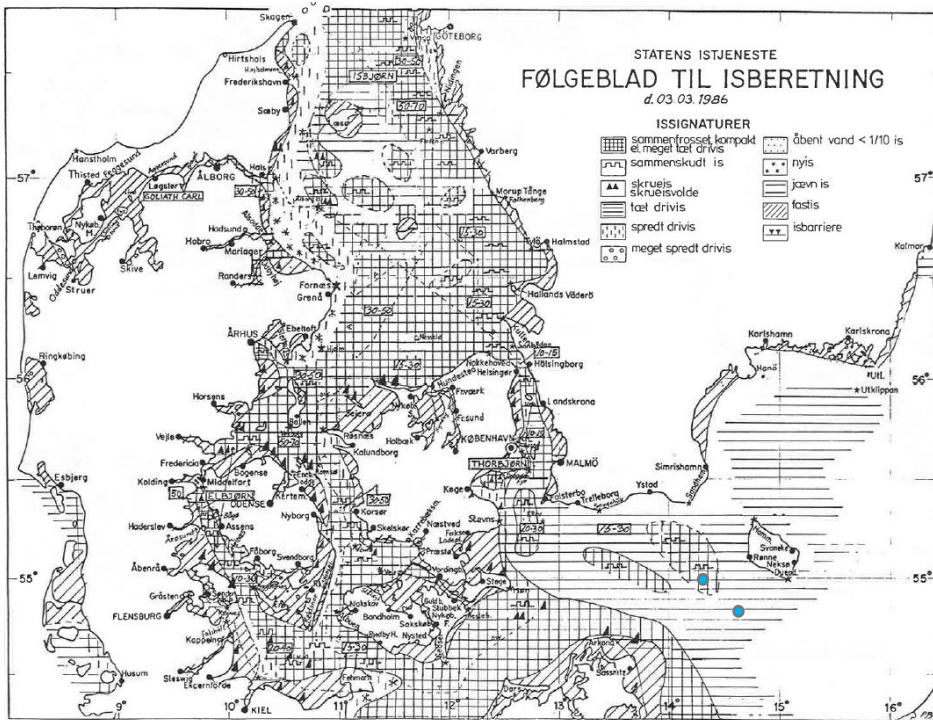


Figure 4-5 Ice observations the 3rd March 1986 ref. [4]. Blue dots: Bornholm I and II OWF.

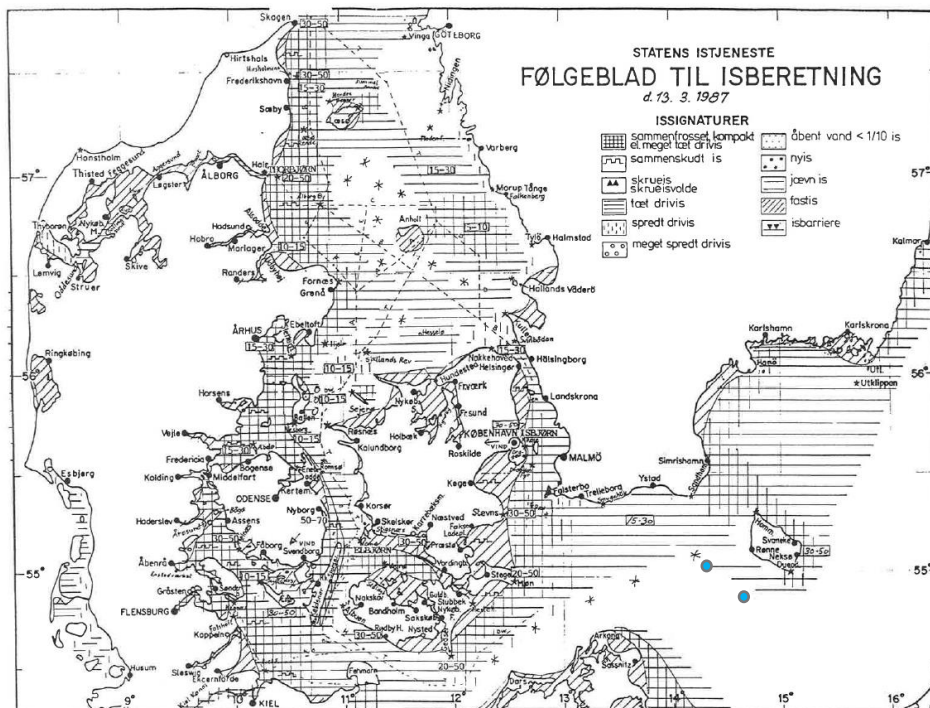


Figure 4-6 Ice observations the 13th March 1987 ref. [4]. Blue dots: Bornholm I and II OWF.

The Danish ice chart on Figure 4-4 show level ice for the 20th of February 1985 for both Bornholm I and II OWF areas, though Bornholm II are just at the edge to open waters. In year 1986 on the 3rd of March, the Danish ice chart on Figure 4-5 shows compact ice and rafted ice for the area of Bornholm I OWF, where level ice is observed in the area of Bornholm II. On the 13th of March in 1987, see Figure 4-6, the Danish ice chart shows a combination of new ice, level ice and open waters in the area of Bornholm I OWF, where Bornholm II OWF is situated in open waters and borders on to registered level ice.

In the following, the relevant German observations [6] of ice occurrence in the very strong ice winter 1986/1987 are described in Table 4-1 and shown in Figure 4-8 to Figure 4-17.

The German ice observations for the period 11.12.1986 – 11.01.1987 shows that the water around and at the Bornholm I and II OWF site is free of ice and therefore for this period ice observations maps will not be presented in this section. The first occurrence of ice in the waters around the Bornholm I and II OWF is seen on the ice observation made the 21.01.1987, which is shown on Figure 4-8. In relation to Table 4-1 describing the very strong ice winter, Figure 4-7 shows an overview of the air temperature for 1987. The German ice observations are considered as governing from Bornholm I and II OWF due to the vicinity to the German observation points and the illustrative and systematic ice charts (Figure 4-8 to Figure 4-17) produced by the German ice observation institute.

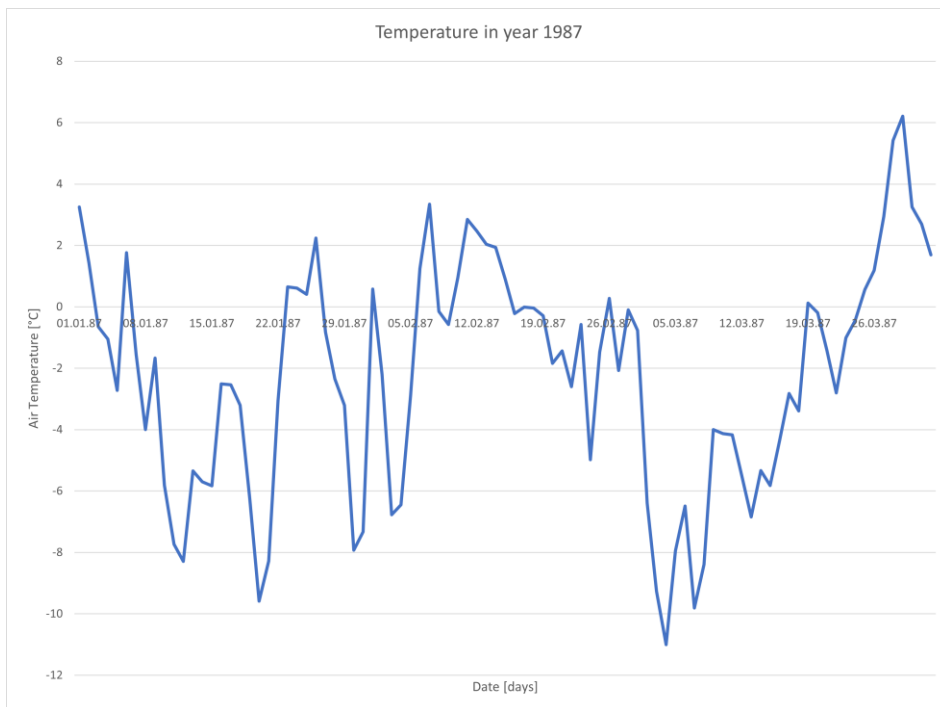


Figure 4-7 Overview of Arkona lighthouse air temperature during winter year 1987.

Table 4-1 Overview of ice distribution in the winter of 1987. Based on German observations.

Date	Illustration	Summary of the ice winter 1987 in the south Baltic Sea
01.01	Figure 4-7	The frost period has started
11.01		Fast ice and new ice have been generated in bay to the right of the city Stralsund.
21.01	Figure 4-8	Compact ice has been generated near the coast stretching from Arkona down to Swinoujscie, where an ice thickness of 20-40 cm has been observed. Rafted ice has occurred south of Arkona. The waters north of Poland and Germany is open, where close to the coast open ice have been observed. There is 5-15 cm of compact ice observed in the Danish straits and 15-30 cm in Køge Bay. New ice has been generated near the coast of Sweden and ridged ice has occurred east of Trelleborg. There is no ice observed in the area of Bornholm I and II OWF.
23.01	Figure 4-7	A short (5 days) melting period has started.
01.02	Figure 4-9	The ice occurrence is still severe with an ice thickness up to 15-30 cm is observed at more locations. Rafting has occurred north of Rostock. Ice ridges are observed south of Arkona and north of Swinoujscie. Open ice is observed in the Danish straits. For the area of Bornholm I and II OWF no ice is observed.
06.02	Figure 4-7	A longer (10 days) melting period has started.
11.02	Figure 4-10	Open water is observed along the German coast from Arkona to Rozewie and south of Sweden. Very open ice is observed west of Arkona and in the Danish straits. Also, for the area of Bornholm I and II OWF is situated in open waters.

16.02	Figure 4-7	A mild freezing period (10 days) has started.
21.02	Figure 4-11	Open water is observed north of Arkona and new ice are generated near the coast of Sweden. Open water and very open ice are observed in the Danish straits. In the area Bornholm I and II OWF no ice is observed.
01.03	Figure 4-7	A severe frost period (20 days) has started.
01.03	Figure 4-12	More new ice is generated near the coast of Sweden and near the coast of Germany. Compact ice is generated in the low water areas in Germany and Denmark. No ice observed in the area of Bornholm I and II OWF.
11.03	Figure 4-13	Compact ice has been generated in larger areas. 10-30 cm compact ice is observed north of Germany and in the Danish straits. Rafting ice has occurred north of Germany and south of Sweden. Hummock ice have formed south of Arkona and east of the coastline of Skåne. The waters north of Poland is open, but compact ice is generated near the coast. Close ice and rafted ice are observed in the area of Bornholm I OWF, having an ice thickness around 10-20 cm. For the area of Bornholm II OWF open ice, new ice and level ice with an ice thickness of 10-15 cm is observed, though no rafted ice.
19.03	Figure 4-7	The melting period has started, and the ice winter has come to an end.
21.03	Figure 4-14	Open water and very open ice are observed north of Germany and in the Danish straits. Formations of level ice is observed south of Bornholm and south of Sweden close ice is found with a thickness of 10-20 cm. Compact ice is still observed in the low water areas, hummock and rafted ice is observed along the of Sweden. In the area of Bornholm I OWF both open waters and level ice with a thickness of 5-30 cm is observed, where for Bornholm II OWF only level ice, with the same thickness, is observed.
01.04		For the observation made on the 01.04.1987 and observations dated later, no ice was observed in the area of the Bornholm I and II OWF.

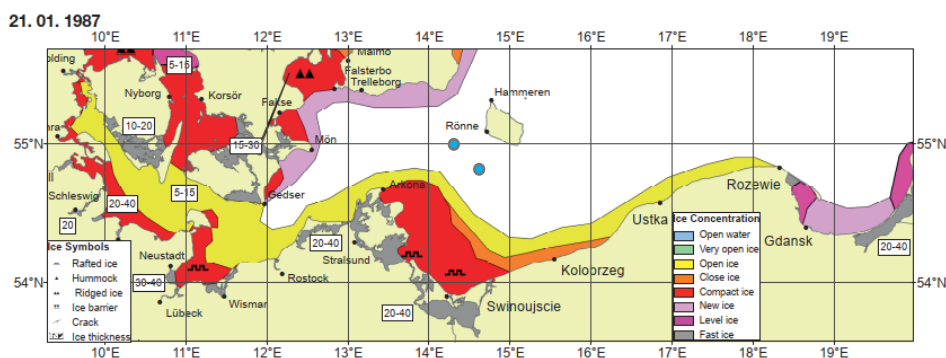


Figure 4-8 Ice conditions in the western and southern Baltic Sea on the 21st of January 1987, [6].
Blue dots: Bornholm I and II OWF.

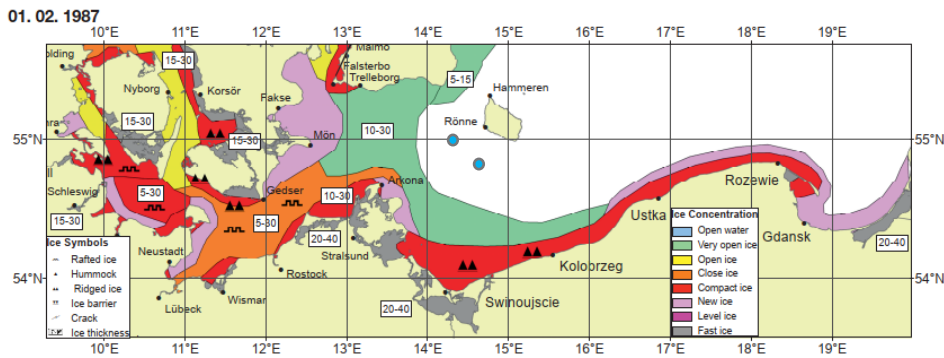


Figure 4-9 Ice conditions in the western and southern Baltic Sea on the 1st of February 1987, [6].
Blue dots: Bornholm I and II OWF.

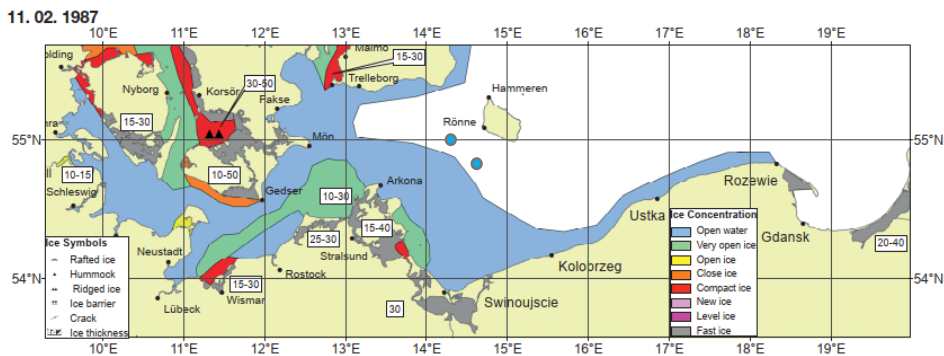


Figure 4-10 Ice conditions in the western and southern Baltic Sea on the 11th of February 1987, [6].
Blue dots: Bornholm I and II OWF.

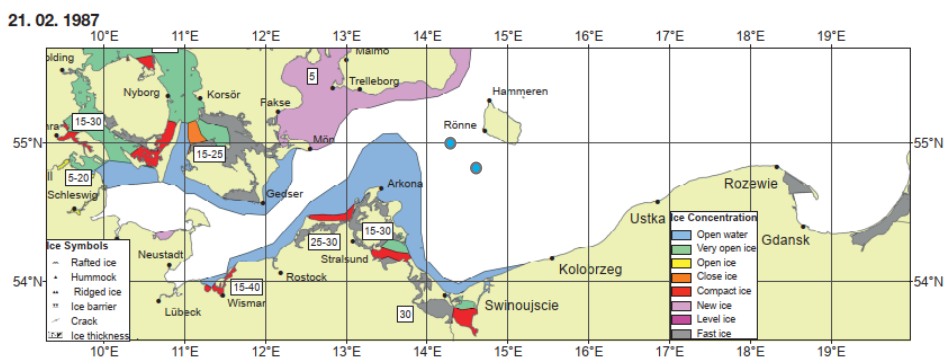


Figure 4-11 Ice conditions in the western and southern Baltic Sea on the 21st of February 1987, [6].
Blue dots: Bornholm I and II OWF.

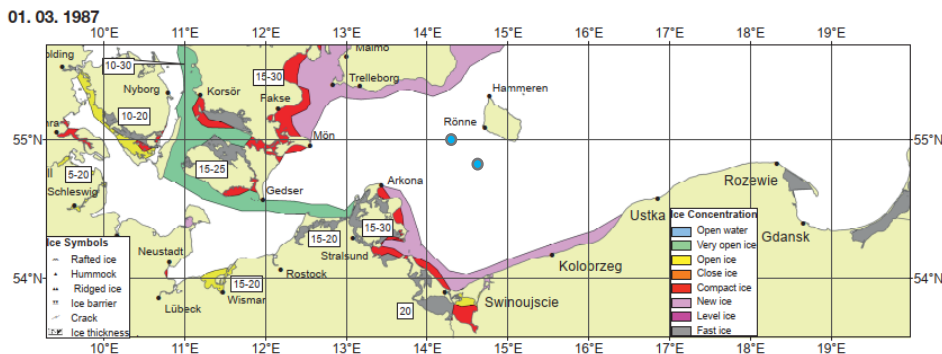


Figure 4-12 Ice conditions in the western and southern Baltic Sea on the 1st of March 1987, [6]. Blue dot: Bornholm I and II OWF.

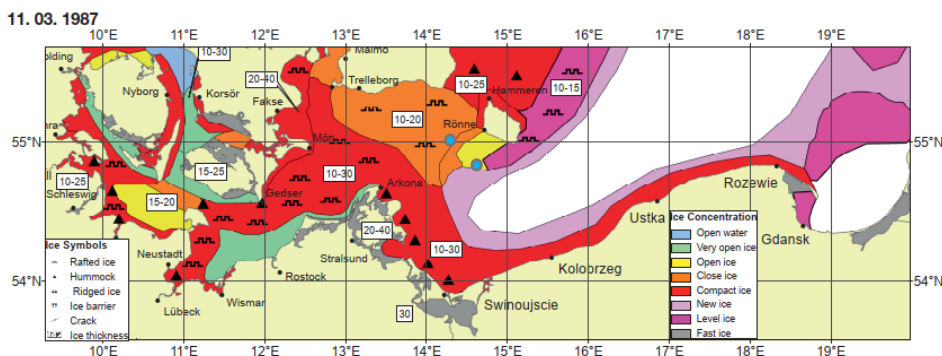


Figure 4-13 Ice conditions in the western and southern Baltic Sea on the 11th of March 1987, [6]. Blue dots: Bornholm I and II OWF.

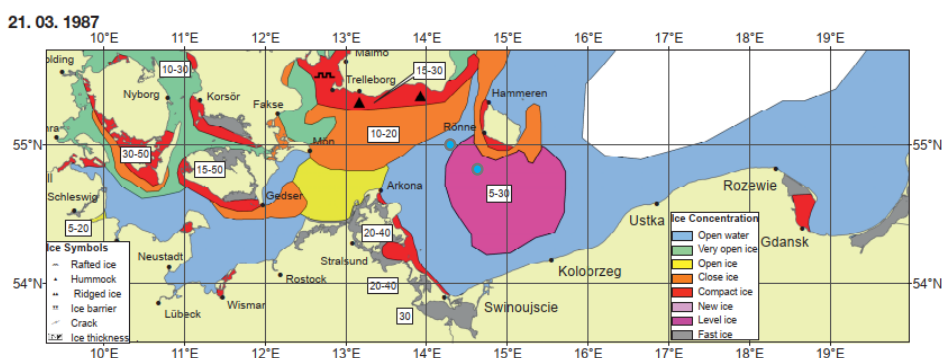


Figure 4-14 Ice conditions in the western and southern Baltic Sea on the 21st of March 1987, [6]. Blue dot: Bornholm I and II OWF.

For comparison with Swedish ice charts, these are shown in Figure 4-15, Figure 4-16 and Figure 4-17 made by SMHI, which shows the observations of maximum ice distribution charts for the years of 1985, 1986 and 1987 respectively, where ice have been present in the area of both Bornholm I and II OWF, [8].

Observations of maximum ice distribution chart shows in relation to the Bornholm I OWF area on Figure 4-15 that level ice with a thickness of 10-20 cm

was registered and for the area of Bornholm I OWF new ice and open waters was observed on the 21st of February 1985. Further, no ice ridges and rafted ice in the area around the Bornholm I and II OWF was observed. The following year 1986 on the 27nd of February, see Figure 4-16, a combination of compact ice with a thickness of 10-20 cm, level ice and open pack ice was observed in the area of Bornholm I OWF. For the site of Bornholm II OWF open pack ice and open waters was observed. Further to the north of Bornholm I OWF rafted ice was observed.

Year 1987 on the 13th of March, the Swedish maximum ice chart on Figure 4-17 shows close and open packed ice in the area of Bornholm I OWF and for the site of Bornholm II OWF level ice and open packed ice observed. To the north and northeast of Bornholm I OWF rafted ice and ice ridges close to the coast of Sweden the same year.

SHMI observations made on the 13th of March 1987, see Figure 4-17, shows in general the same distribution of ice, rafted ice and ridged ice as for the observations made by BHS date 11th of March 1987, see Figure 4-13. Though deviating is the area close to the coast east of Arkona, where rafted ice is observed and no hummock ice.

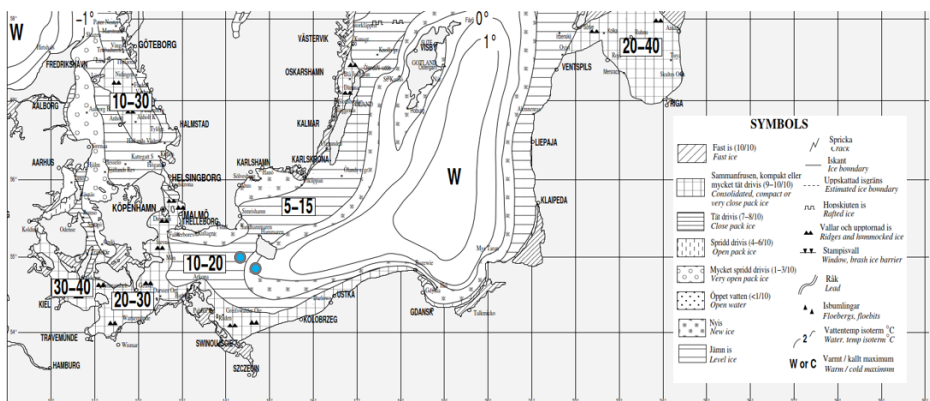


Figure 4-15 Ice conditions in the western and southern Baltic Sea on the 21st of February 1985 by SMHI, [9]. Blue dots: Bornholm I and II OWF.

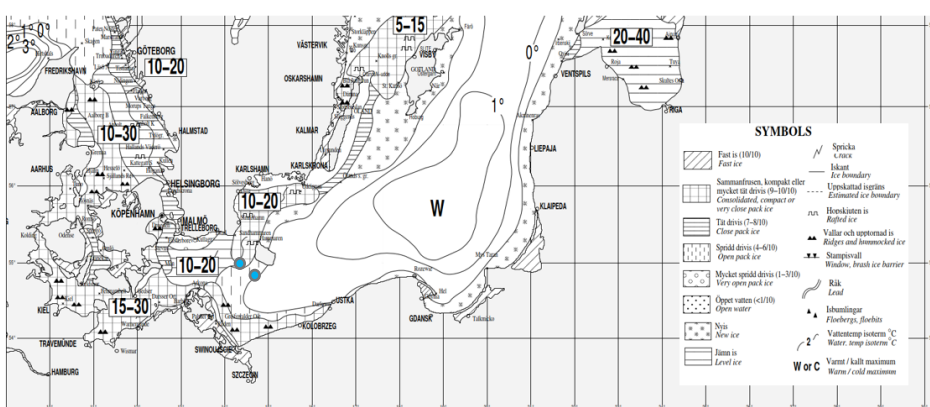


Figure 4-16 Ice conditions in the western and southern Baltic Sea on the 27th of February 1986 by SMHI, [9]. Blue dots: Bornholm I and II OWF.



Figure 4-17 Ice conditions in the western and southern Baltic Sea on the 13th of March 1987 by SMHI, [9]. Blue dots: Bornholm I and II OWF.

The Danish ice observation, previously presented in Figure 4-6, from the 13th of March 1987, can be compared to the German observations on the 11th of March and the 21st of March 1987, shown in Figure 4-13 and Figure 4-14 respectively and to the Swedish observation from the 13rd March 1987 shown in Figure 4-17. The comparison shows that the observation differs as the German and Swedish observations in general agrees showing close ice, level ice and open ice on the 11th and 13rd March in 1987. The German observations show a mix of open water and level ice on the 21st March 1987 in the area of interest. While the Danish ice charts observations shows a combination of new ice, level ice and open waters in the area of Bornholm I OWF, where Bornholm II OWF is situated in open waters and borders on to registered level ice on the 13th March 1987.

Thus, the comparison of the Danish ice charts with the German and Swedish ice charts illustrates the difficulties of estimating the ice occurrence over this large area. Based on the evaluation of the ice winters 1985-1987 it is estimated that the 1/50y ice thickness shall be in the range of 20-30 cm for Bornholm I and II OWF. In Section 5.2 the design 1/50 year ice thickness will be derived for the Bornholm I and II OWF.

4.2 Local ice observations

Local ice observations at strategic spots for the German waters are available for the period 1961-2010. Here the measurement station at Arkona Lighthouse is considered to be the most representative for the Bornholm I and II OWF. Figure 4-18 shows all the German observation spots as well as the relevant Danish observation spots.

The Swedish Ice Atlas made by SMHI [5] have made detailed records of ice thickness distribution for the period of year 1963 to 1979. Here the Baltic Sea and Kattegat have been divided into areas, whereas area 16 will be used for comparison, since this is the area closest to the location of Bornholm I and II OWF, also marked on Figure 4-18. The full figure and table of data for area 16 can be found in Annex A.

Ice observations have been made for the Danish waters at strategic spots each year from year 1861 ref. [4]. The observation points have not been exactly the same for all the years, however the locations as listed below represent the ice

observation locations. For the Bornholm OWF the following observations spots, shown on Figure 4-18, are the most representative:

- Møn Lighthouse
- Rønne
- Hammerodde Lighthouse
- Dueodde Lighthouse
- Arkona Lighthouse
- Area 16

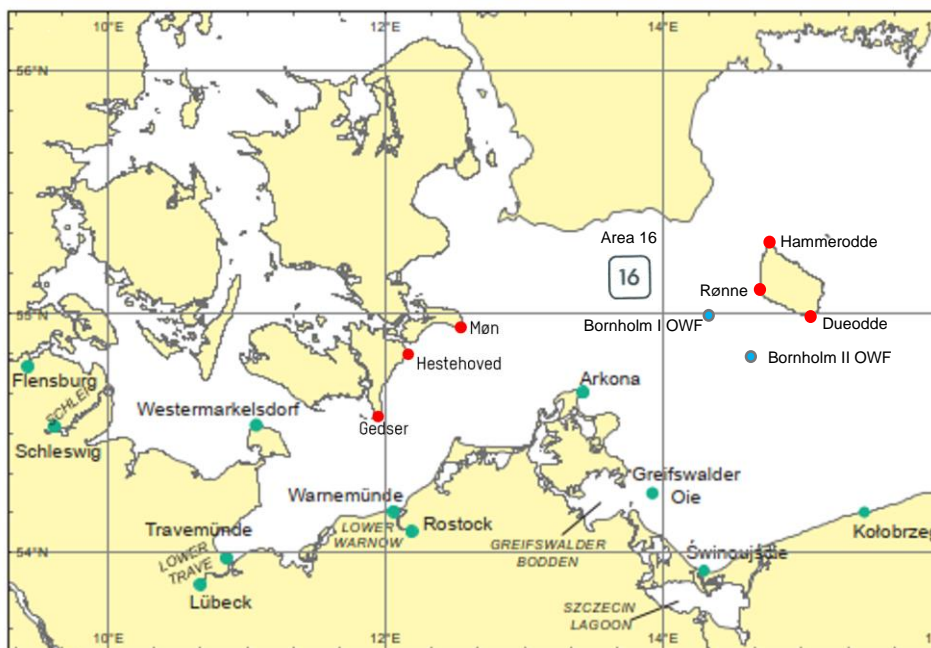


Figure 4-18 Location of ice observation spots near Bornholm I and II OWF. Red dots show Danish observation spots, Green dots show the German observation spots and area 16 represent the south Baltic Sea also marked in the figure. Blue dots: Bornholm I and II OWF.

The main flow direction at the Bornholm I and II OWF site is towards east or west through Øresund and Storebælt. The Danish ice observations has since year 1983 been noted according the general accepted Baltic Sea Ice Code (ASTK), and the ice observations ref. [4] for the Danish observations points are listed in Table 4-2, where Rønne and Dueodde Lighthouse being the observation point closest in relation to Bornholm I and II OWF.

Table 4-2 shows that the largest ice thickness observed is 50 – 70 cm found in the waters close to Hammerodde Lighthouse in the winter 1984-1985 and 1995-1996. The observations from the waters off the coast at Møn Lighthouse, Rønne and Dueodde Lighthouse indicate a maximum ice thickness of 30-50 cm, which was observed the successive winters of 1984-1985, 1985-1986 and 1986-1987, which are considered to be most representative in relation to the Bornholm I and II OWF, see Table 4-3.

Table 4-3 Largest observed ice thickness in the period 1983 - 2019, Ref. [4].

Observation point	Møn Lighthouse, waters outside	Dueodde Lighthouse	Hammerodde Lighthouse	Rønne, water outside
Largest measured ice thickness [cm]	30-50	30-50	50-70	30-50

For the Swedish observations for area 16 the ice thickness distribution is shown in Figure 4-19, where the distribution of different ice thickness is presented in percentage during the winter period, to which presence of ice is expected. For area 16 south of Skåne Figure 4-19 shows that the largest ice thickness reported is 21-30 cm in March.

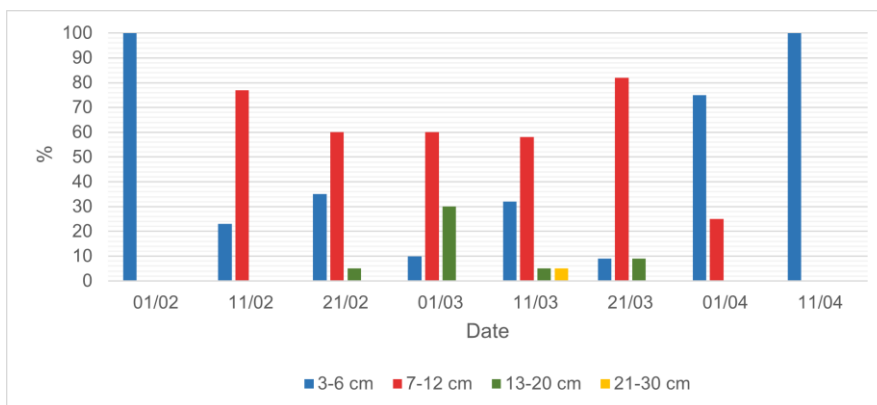


Figure 4-19 Percentage of ice thickness distribution for area 16 during the winter year 1963-1979, [5].

The German ice observations [3] is the result of a statistical evaluation of ice data for a 50-year period. Further, the German observations include a comparison of the three 30-year periods 1961-1990, 1971-2000 and 1981-2010. The data is collected from 14 observation spots along the southern Baltic Sea coast and from offshore waters, hereof 11 observation spots are illustrated on Figure 4-18 (green dots). The dataset consists of digitised German and Polish ice charts.

Similarly, the ice thickness is reported in the German observations [3]. This is illustrated in Figure 4-20, which shows the mean ice thickness for all winters and only for winters with ice as well as the maximum ice thickness.

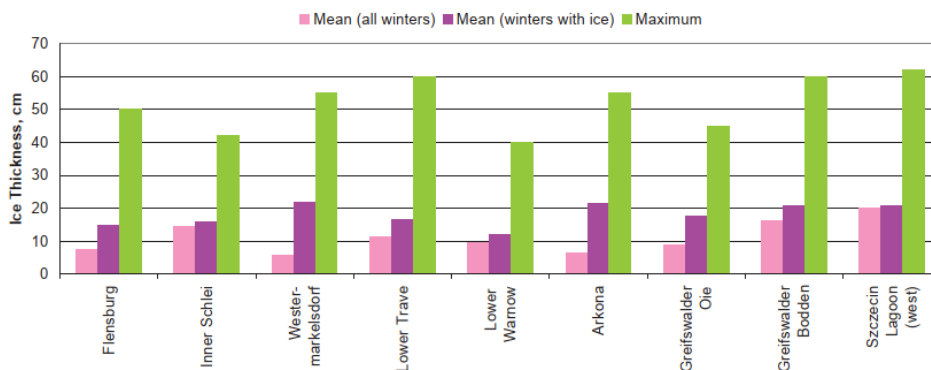


Figure 4-20 Mean and extreme values of ice thickness at coastal for nine (9) observation spots on the southern German Baltic Sea coast during the period 1961-2010 [3].

From Figure 4-20 it is seen that the maximum ice thickness reported at Arkona is approximately 55 cm for the period 1961-2010. This value lies above the interval of 21-30 cm reported by the Swedish observations and the interval of 30-50 cm, which is the maximum reported at Møn Lighthouse, Rønne and Dueodde Lighthouse in the Danish observations.

The Swedish observations of ice thickness is reported for an offshore area (area 16), whereas the Danish and German observations are for near shore locations, which give the difference in ice thickness intervals. The German observations [3] includes a comparison of the ice conditions for the 30-year periods 1961-1990, 1971-2000 and 1981-2010 (Figure 4-21).

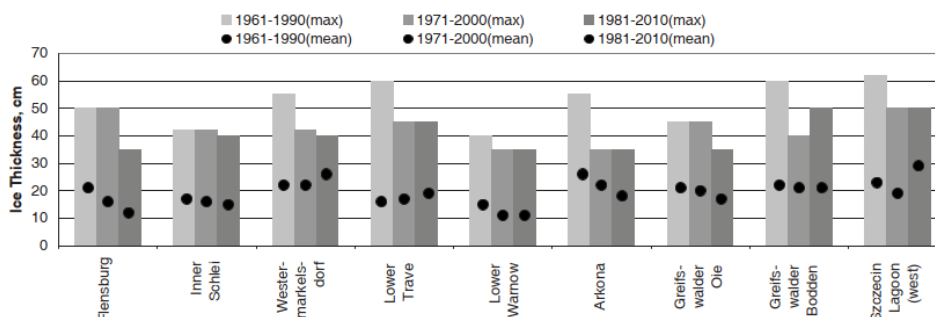


Figure 4-21 Mean ice thickness for winters with ice and extreme values for the ice thickness at observation spots on the southern German Baltic Sea coast ref. [3].

Figure 4-21 shows that the maximum ice thickness of 55 cm observed at Arkona Lighthouse is part of the dataset for the period 1961-1990. Thus, this value is most likely observed in the very severe winter of 1962-1963. For the other 30-year periods, 1971-2000 and 1981-2010, the maximum ice thickness observed was approximately 35 cm which corresponds with the interval of 30 – 50 cm observed at Møn Lighthouse, Rønne and Dueodde Lighthouse, cf. Table 4-3, and are closer in range of the interval of 21-30 cm stated by the Swedish observations, cf. Figure 4-19. It shall be noted that the ice thickness generally is higher near the coast that offshore.

The German observations [3] also includes information on the first and last ice occurrence. The median and extreme values for the beginning and end of the ice occurrence is shown in Figure 4-22 for the different observation spots.

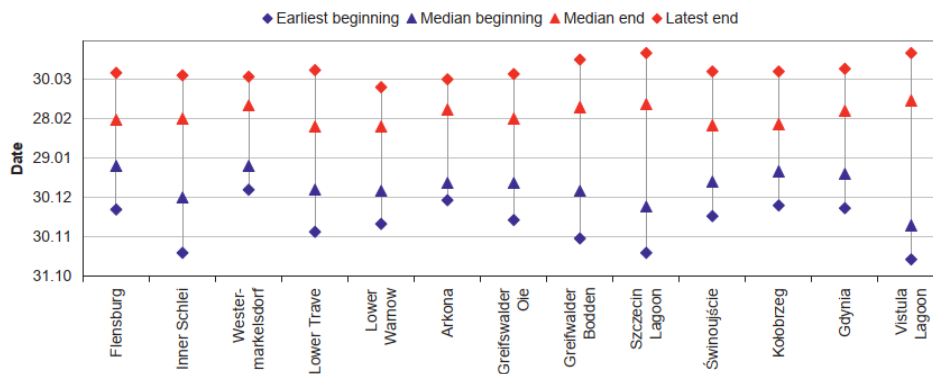


Figure 4-22 Median and extreme values of the beginning and end of ice occurrence at observation spots on the southern German Baltic Sea coast [3].

Figure 4-22 shows that the earliest beginning of ice occurrence at Arkona happens slightly earlier than the 31/12, while the latest end of ice occurrence is reported around the 30/3. These dates are similar to those reported by the Danish observations in [4]. For the Swedish observations shown in Figure 4-19, the presence of ice expected starts at the 01/02 and ends at the 11/04. It can according Figure 4-13 to Figure 4-17 be seen that for Bornholm I and II OWF the maximum ice thickness is observed the period from middle of February to middle of March. This is considered typical for the location.

Though the Swedish observations covers a large area, whereas the Danish and German observations are for specific locations, which may explain the difference in beginning and end of ice occurrences. As mentioned in relation to the ice thickness, it should be taken into account that the extreme values reported by the German observations might be for winter of 1962-1963 and not be applicable for comparison with the Danish and Swedish observations. However, the comparison between the three 30-year datasets only shows a weak trend of an earlier occurrence for the extreme value of the earliest ice occurrence, while no trend was observed for the extreme value of the latest ice occurrence. Thus, the German, Danish and Swedish observations are considered to be comparable. The ice observations are primarily made from onshore stations where the ice thickness and ice deformation will be more severe compared to an offshore locations.

4.3 Observed types of ice

From the ice observations presented in Table 4-2 it can be seen that the following ice types are observed:

- Hummocked or ridged ice
- Compacted slush or shuga, or compacted brash ice
- Rafted ice

The latter two types of ice are observed more times and for more days for the majority of the included observation stations. Since the ice is moving around, it cannot be ruled out the ice ridges will occur at Bornholm I and II OWF. Further the ice maps included in Section 4.1 also include signatures for rafted ice observations close to Bornholm I and II OWF.

Ice ridges due to blocking effects in the wind farm or neighbouring windfarms may also occur as described in Section 10.

4.4 Climate change effects

Climate change effects (increased average global temperature) affect the ice occurrence in the Baltic Sea. A tendency of reduced frost index, ice thickness and ice coverage can be observed in more data sets, e.g., in the Danish ice observation reports [4]. For the frost index at the Bornholm I and II OWF Figure 4-23 shows how the average frost index is diminished since year 1980. A considerable scatter is seen in the dataset due to the random nature of ice winters.

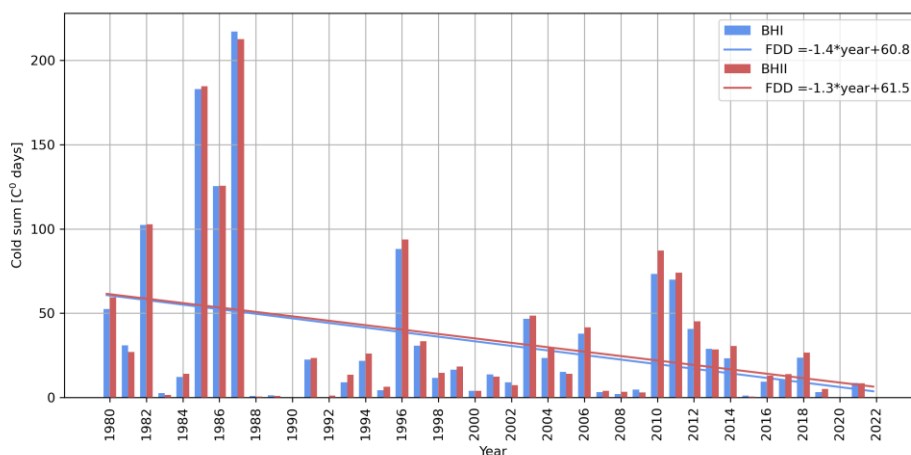


Figure 4-23 Frost index and trend for the Bornholm I and II OWF site for the years 1980-2022.

According to the German Climate Atlas [122] made by the Deutscher Wetterdienst, DWD, concerning climate change effects for Germany, the average temperatures during winters have been analysed since year 1881 until year 2022 and estimated until year 2100 based on the different emission scenarios. Figure 4-24 and Figure 4-25 shows the measured and predicted temperatures for a low emission Intergovernmental Panel on Climate Change (IPCC RCP2.6) scenario and a high emission (IPCC RCP8.5) scenario respectively. Both estimates predict that future winters in the future will be warmer, on average, than the winters in the past 40 years.

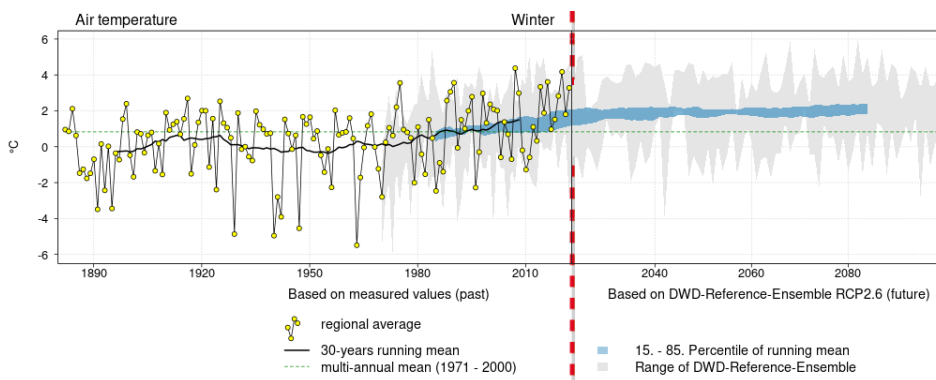


Figure 4-24 Average winter temperatures for the period 1881-2022 and estimates for a low emission scenario, (IPCC) RCP2.6, until year 2100 [122].

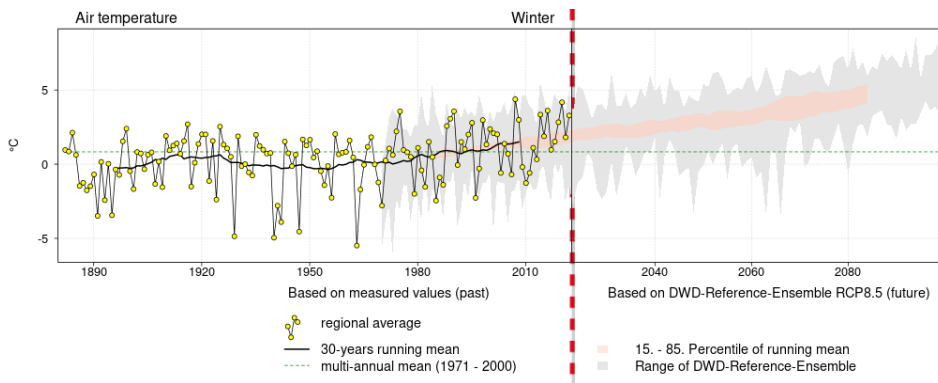


Figure 4-25 Average winter temperatures for the period 1881-2022 and estimates for a high emission scenario, (IPCC) RCP8.5, until year 2100 [122].

DMI [118] has estimated the number of frost days in the period until year 2100 as shown in Table 4-4.

Table 4-4 Estimated number of future frost days for the given year according to DMI, [118].

Estimate for year	1990	2050	2100
Frost days [day/year]	85 (+/- 8)	61 (+/- 7)	29 (+/- 5.3)

Due to the scatter of ice winters, it is not considered safe to use the tendency of the recent ice winters to predict the future frost index. It is conservatively selected to base the design frost index analysis on the winters since year 1980 for Bornholm I and II OWF.

Climate changes are as well described in the Metocean report [1] section 9 based on the analysis by IPCC, as summarized the following section.

According to IPCC, the change in surface wind in the Medium Term (including year 2055) as predicted by the climate models, does not show a clear trend, and the climate models show a low agreement (i.e. a large scatter) in their predictions.

According to IPCC, the change in sea surface temperature in the Medium Term (including year 2055) will amount to 1.4 °C (median) with a variation between 0.3 °C (5 percentile) and 2.6 °C (95 percentile) and the climate models show a robust agreement.

According to IPCC, future changes in salinity will depend on changes in the wind patterns over the Baltic Sea region, river runoff from the Baltic Sea catchments, and mean sea level rise relative to the seabed of the sills in Danish straits. Due to the large uncertainty in projected changes in wind fields over the Baltic Sea region, freshwater supply from the catchments, and global sea level rise, salinity projections show a large variation. Ensemble studies that consider all potential drivers predict no significant changes in ensemble mean salinity. Among climate models, no systematic changes were projected for either the

saline-induced stratification or the overturning circulation in the Baltic Sea when considering all drivers of salinity changes, including wind, river runoff, and global sea level rise.

4.4.1 Gulf Stream weakening.

The Gulf Stream System is considered to provide 2-5 degree higher temperatures in the Baltic region compared to expected temperature based on the latitude. The system is also known as the Atlantic Meridional Overturning Circulation (AMOC) Figure 4-26, has weakened by 15 percent in recent decades. This is likely due to an influx of cool freshwater from melting ice sheets in the Arctic region that reduces ocean salinity and thus the density of the water, which inhibits the sinking, thus weakening the flow of the Gulf Stream System. The heat transfer by the Gulf Stream is considered to be the main driver for a milder climate in the northern Europe than expected for the given latitude.

The complexity of the Atlantic meridional overturning circulation (AMOC) system and uncertainty over levels of future global heating make it impossible to forecast the date of any collapse for now. It could be within a decade or two, or several centuries away.

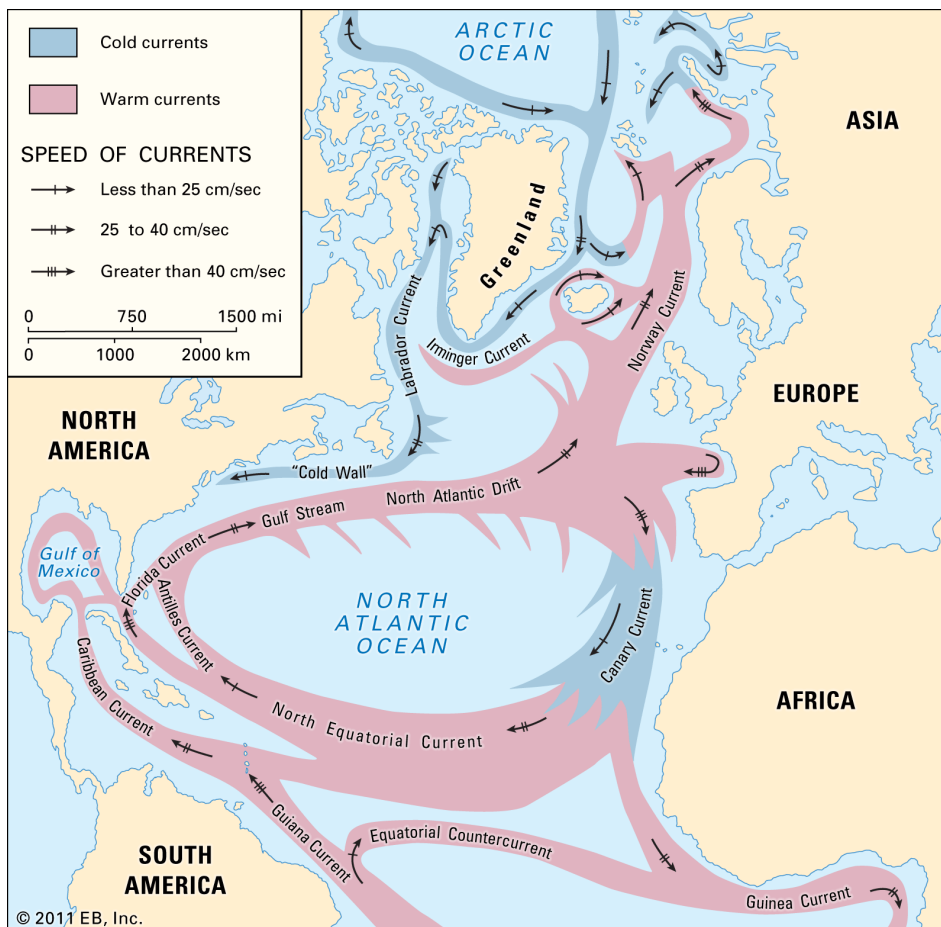


Figure 4-26 Illustration of the North Equatorial current (Britannica)

5 Frost index and ice occurrence

5.1 Frost index

As a basis for the design for ice loads, the frost index K according ISO 19906 [103] will be used. The frost index is derived from the frost days - defined as the actual accumulated number of days for a winter, where the 24h average air temperature is below the freezing temperature of the water.

$$K = \left| \sum (T_a - T_f) \right| \text{ for } T_a < T_f \quad (4.1)$$

Where:

K : Frost index summarized in a winter period (deg. days)

Where:

T_a : The daily average air temperature [$^{\circ}\text{C}$ day]

T_f : The freezing temperature of the underlying water [$^{\circ}\text{C}$ day]

In which the sum is made only over the days for which the air temperature is less than the freezing temperature of the water. T_f is -0.4 $^{\circ}\text{C}$ calculated from salinity,

The frost index exhibit variability from year to year and may be represented by its probability distribution.

The frost index with return period T_R in units of years is defined as the $(1/T_R)$ quantile in the distribution of the frost index, i.e., it is the frost index which probability of exceedance in one year is $1/T_R$. It is denoted $K(T_R)$ and is expressed as

$$K(T_R) = a * \ln\left(\frac{1}{T_R}\right) + b \quad (4.2)$$

Where:

$K(T_R)$: Frost index for return period T_R (deg. days)

a : Slope of frost index distribution (-)

b : Offset of frost index distribution (-)

As a comparison and reference for the frost index analysis for the Bornholm I and II OWF project, the frost index for Arkona onshore Lighthouse is used. The frost index is based on formulae (4.1)

For the Bornholm I and II OWF project data for 40+ years are generated from the data set described in Section 2.2.3. The frost index for Bornholm I and II

OWF are shown in Figure 5-1 and compared with the average data for Arkona lighthouse for the same period. The Arkona is a land station and therefore expected to be colder.

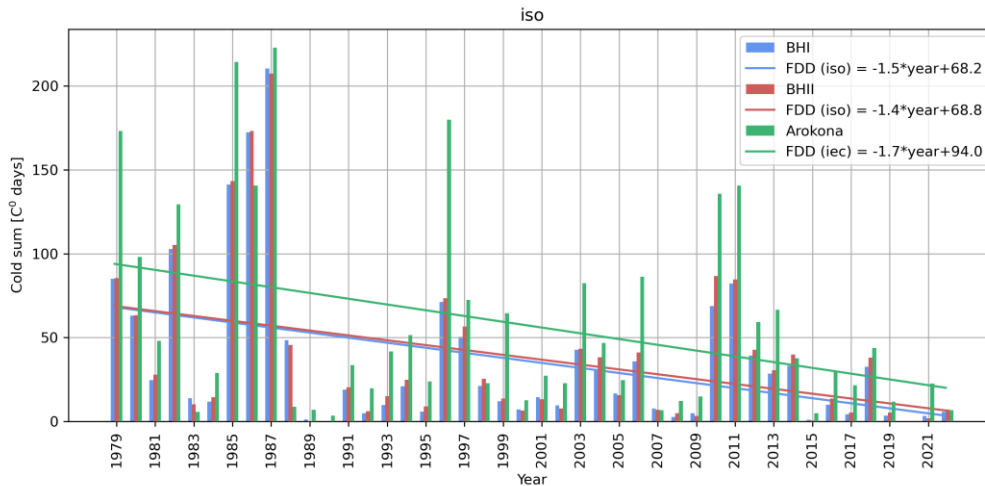


Figure 5-1 Frost index for Bornholm I and II OWF Arkona Lighthouse from year 1979 to 2021.

Based on the frost index in Figure 5-1 the frost index distribution for Bornholm I and II OWF and Arkona Lighthouse is presented in Figure 5-2 where the data is arranged according to the probability of occurrence formulae (4.2).

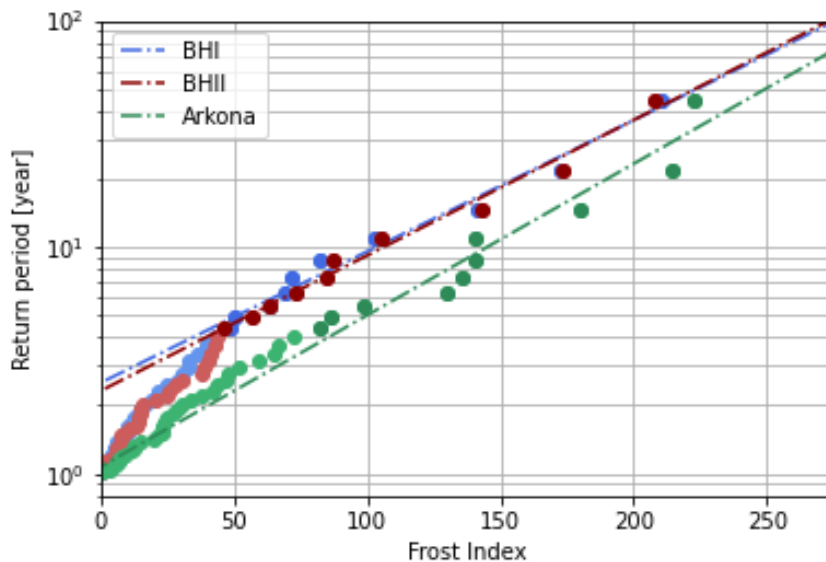


Figure 5-2 Return period plot of frost index for Bornholm I and II OWF and Arkona Lighthouse. Only the 10 coldest winters is used for the extreme analysis. Marked with a darker colour.

According to Figure 5-1 and the derived trend lines the following frost indexes are found:

Table 5-1: Frost index and return period for BHI, BHII and Arkona Lighthouse for comparison.

Return period	Frost Index BHI [deg. days]	Frost Index BHII [deg. days]	Frost Index Arkona [deg. days]
5	51	56	100
50	224	223	250
100	276	273	295

5.2 Ice thickness (50-year return period)

According to ISO 19906 [103] and Annex D.3 IEC 61400-3-1 [102] the ice thickness, t , at the end of a frost period may be estimated as:

$$t = 0.032\sqrt{0.9K - 50} \quad (4.3)$$

Where the ice thickness, t , has a unit of metres and the frost index according to formulae (4.2), K , has a unit of days deg. It shall be noted that the formula (4.3) applies for both open and closed waters.

Based on analysis [105] of sea ice occurrence in open waters in Denmark in the winters from year 1941 to 1942, it was found that the formula (4.3) leads to a too conservative design ice thickness for open waters. On this basis it is suggested to modify the formula for ice thickness for Bornholm I and II OWF:

$$t_{open} = 0.024\sqrt{0.9K - 50} \quad (4.4)$$

For reference and as an alternative to the above formula (4.4) the sea ice thickness can be calculated according the Lebedev formula (4.5) specified by: "National Snow and Ice Data Center (NSIDC)". The Lebedev formula (4.5) derives the sea ice thickness, t , based on the frost index, K ref. formula (4.2), as follows:

$$t = 0.0133 * K^{0.58} \quad (4.5)$$

The key conclusion of the analysis [105] is shown in Table 5-4.

Table 5-2 Estimated and observed sea ice thickness for Kriegers Flak (west of Bornholm) ref. [105].

The ice thickness calculated according to equation (4.3), (4.4) and (4.5).

Winter Year	Frost Index	Calculated ice thickness			Observed max ice thickness	Observed ice thickness of fast ice
		(4.3) m	(4.4) m	(4.5) m		
1941-42	495	0.64	0.48	0.49	-	0.48 but 0.40 in semi-open waters
1978-79	220	0.39	0.29	0.30	0.40	0.21-0.30
1984-85	275	0.45	0.34	0.35	0.15-0.50	0.15-0.30
1985-86	190	0.35	0.26	0.28	0.20-0.30	0.15-0.30
1986-87	265	0.44	0.33	0.34	0.30-0.50	0.15-0.30 (Danish source) 0.10-0.20 (Swedish source)

It is found that the modified equation (4.4) for open waters (factor 0.024) and the NSIDC estimate ref. equation (4.5) of the sea ice thickness compare better to the observed sea ice thickness for open waters than equation (4.3).

Based on the above formulas the ice thickness can be calculated for Arkona Lighthouse for reference as shown in Table 5-3. The ice thickness with one-year return period is considered as zero.

Table 5-3 Estimated ice thickness for Arkona onshore Lighthouse.

Arkona - data 1979-2019				
Return period	5	50	100	y
Frost Index	100	250	295	deg days
Ice thickness, closed waters, eq. (4.3)	0.2	0.42	0.47	m
Ice thickness, open waters, (factor 0.024), eq (4.4)	0.15	0.32	0.35	m
Ice thickness (NSIDC) eq. (4.5)	0.19	0.33	0.36	m

For Bornholm I and II OWF the same analysis leads to the sea ice thickness as shown in Table 5-4.

Table 5-4 Estimated ice thickness for Bornholm I and II OWF respectively. The bold is the value used in the summary Table 5-1.

Bornholm I/II OWF - data 1979-2019				
Return period	5	50	100	y
Frost Index	51/56	224/233	276/273	deg days
Ice thickness, closed waters, eq. (4.3)	0/0.01	0.39/0.39	0.45/0.45	m
Ice thickness, open waters, (factor 0.024), eq. (4.4)	0/0.01	0.3/0.29	0.34/0.34	m
Ice thickness (NSIDC) eq. (4.5)	0.13/0.14	0.31/0.31	0.35/0.34	m

From Table 5-3 it can be seen that BHI and BHII are almost identical. They are very close located, which therefor make sense. Is does not make sense to differentiate between the two locations regarding ice thickness. Compared with the data from Arkona Lighthouse Table 5-4 BHI/II are a couple of centimetres lower. Which is to be expected since Arkona Lighthouse is a land station.

5.3 Ice occurrence distribution

Observation of ice occurrence have been made carefully by the Swedish Meteorological and Hydrological Institute, SMHI, for the period 1963 to 1979 ref. [5]. The observations summarise and generalise the ice conditions over 17 years for strategic locations in the Swedish waters. The observation point Area 16 (ref. Annex A) is located close to the Bornholm I and II OWF with quite identical conditions for ice generation. The average ice cover and days with ice has changed significantly over the period 1963-2019 and a reduction of ice cover frequency is seen. To evaluate the difference for the two periods the extent of ice cover and the number of days with ice have been analysed for two periods: 1963-1979 and 1979-2019. This analysis was conducted by averaging the ice extent from Table 4-3 for each of the two periods, this gives a reduction factor of 0.5 of ice occurrence (Table 5-5).

Table 5-5 Ice floe thickness distribution based area 16 [5] (with 0.5 reduction factor).

Ice floe thickness				
Center	Range		Hours in	Occurrence
[cm]	[cm]	[cm]	25 years	
3.00	0.00	5.00	934	40.20%
6.75	5.00	9.50	1214	52.27%
12.00	9.50	15.50	160	6.87%
18.75	15.50	24.50	13.5	0.58%
30.00	24.50	-	1.9	0.08%
			Total: 2322	

It is noted that the ice thickness of 30 cm with a recurrence of 1.9 hours/25 years in Table 5-5 is conservative considering this is close to the 50-year ice recurrence.

The ice speed distribution as shown in Table 5-6 is based on data for the wind and current speed and direction over the years 1979-2021 for the winter months (January-April) and have been determine as described in Section 5.5.

Table 5-6 Bornholm I & II OWF - Ice floe speed distribution.

Bornholm I OWF - Ice floe speed				Bornholm II OWF - Ice floe speed			
Center	Range		Occurrence	Center	Range		Occurrence
[m/s]	[m/s]	[m/s]	[%]	[m/s]	[m/s]	[m/s]	[%]
0.010	0.00	0.02	0.84%	0.010	0.00	0.02	0.84%
0.030	0.02	0.04	2.52%	0.030	0.02	0.04	2.73%
0.050	0.04	0.06	4.06%	0.050	0.04	0.06	4.19%
0.070	0.06	0.08	5.34%	0.070	0.06	0.08	5.39%
0.090	0.08	0.10	6.34%	0.090	0.08	0.10	6.31%
0.125	0.10	0.15	18.31%	0.125	0.10	0.15	19.66%
0.175	0.15	0.20	17.55%	0.175	0.15	0.20	19.93%
0.225	0.20	0.25	14.53%	0.225	0.20	0.25	15.39%
0.275	0.25	0.30	10.90%	0.275	0.25	0.30	9.86%
0.325	0.30	0.35	7.19%	0.325	0.30	0.35	5.94%
0.375	0.35	0.40	4.52%	0.375	0.35	0.40	3.73%
0.450	0.40	0.50	4.68%	0.450	0.40	0.50	3.59%
0.550	0.50	0.60	1.95%	0.550	0.50	0.60	1.44%
0.650	0.60	0.70	0.79%	0.650	0.60	0.70	0.67%
0.750	0.70	0.80	0.24%	0.750	0.70	0.80	0.20%
0.850	0.80	0.90	0.14%	0.850	0.80	0.90	0.12%
0.950	0.90	1.00	0.07%	0.950	0.90	1.00	0.02%
1.125	1.00	1.25	0.01%	1.125	1.00	1.25	0.00%
1.375	1.25	1.50	0.00%	1.375	1.25	1.50	0.00%
1.750	1.50	2.00	0.00%	1.750	1.50	2.00	0.00%
2.200	2.00	2.40	0.00%	2.200	2.00	2.40	0.00%

The ice floe thickness distribution and ice floe velocity distribution according to Table 5-5 and Table 5-6 shall for the detailed design simulations (ref. Section 12) of combined wind and ice load be split in the wind turbine operational modes: idling, strong misalignment and power production depending on wind turbine related criteria as listed below:

- Idling (or strong misalignment) (usual damping estimate say 2 % for 1 mode)
- $U_{wind} < 4$ m/s (No production)
- Downtime power production (failures) (Typically assumed to 2 % of time but to be updated for detailed design based on WTG design and grid connection)
- Downtime power production ($U_{wind} > 25$ m/s) (not actual)
- Downtime power production (icing turbine). This could be estimated to 2-4 % of situations with significant ice
- Strong misalignment (say $> 45^\circ$)
- Power production (usual damping estimate say 7% for 1 mode)

5.4 Ice floe size

It is a common practice to use a 2 km diameter ice floe size in open Danish waters including the open waters southern of Denmark. According to the ice observations as listed in Table 4-2 ice floes of this size or bigger has been observed in ice winters. The observations points are located on land and may not represent the open water location at Bornholm I and II OWF correctly. To follow the normal Danish practice the ice floe size for Bornholm I and II OWF area is specified to: 2 km in diameter.

5.5 Free ice floe speed

Sea ice movement and speed is mainly driven by wind forces from wind blowing over the ice supplemented by the current in the upper water layers. When the ice floes meet structures, they will be stopped, or the speed will be reduced depending on the external forces and the blocking effect ref. [123].

In the following section only the free flow ice speed will be analysed. The resulting ice speed shall be evaluated based on the pattern of blocking structures at or near the wind farm.

As an estimation of the free ice floe speed (in the absence of any structures) can be calculated as a vector summation from 2.5% of the wind speed, $U_{w,10m}$, (10 m above the water (see [102])) and the surface current speed, U_c (1 m below the water). See the equation below, [123].

$$\vec{V}_{ice} = U_c + 0.025 \vec{U}_{w,10m} \quad (4.6)$$

The free ice floe speed of the actual thickness <30 cm is not considered to be affected by the thickness of the ice.

The free ice floe movement analysis is based on the four winter months of January to April as this is where sea ice is expected in the area.

In the following pages illustrations of the estimated ice floe probability and floe movement pattern are presented. The following can be concluded for the ice floe movement in the area of the Bornholm I and II OWF:

- The dominant wind direction is from west to east (cold air). The secondary wind direction is from east.
- The dominant current direction is toward east and west (approximately). This is as expected based on the in and out flow from the Baltic Sea.
- The ice movements are dominated by the wind forces.
- The dominant ice floe direction is toward east, and a secondary direction is toward west (approximately).
- When the wind speed increases the ice floe direction gets clearly governed by the wind direction. At low wind speed the ice floe direction is also affected by the sea current direction.

In Figure 5-3 and Figure 5-4 the probability of ice floe speed for the four winter months January-April is shown for Bornholm I and II OWF

respectively with input data from the years 1998-2022 based on the current and wind speed.

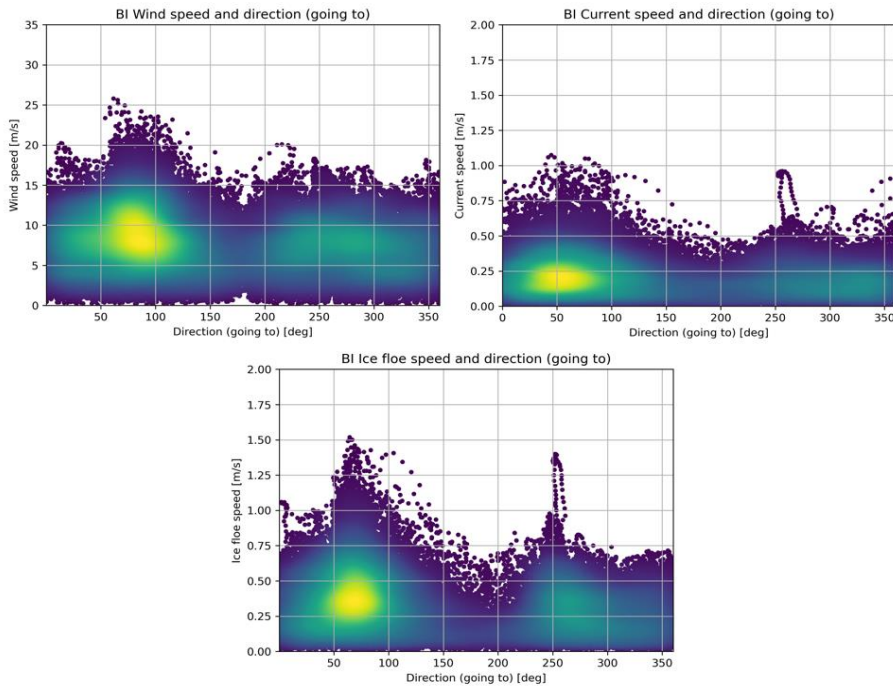


Figure 5-3 Bornholm I OWF: Directional distribution of current, wind and ice movements (all toward directions) for the 4 winter months (January-April) in the period 1998-2022. The colour indicates the concentration of the occurrences (blue: low, yellow: high).

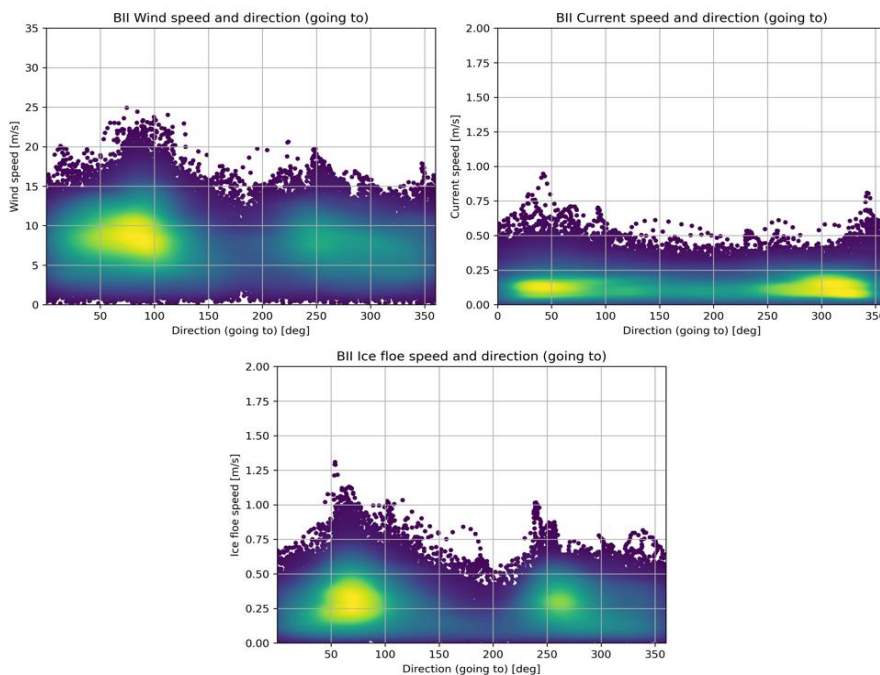


Figure 5-4 Bornholm II OWF: Directional distribution of current, wind and ice movements (all toward directions) for the 4 winter months (January-April) in the period 1998-2022. The colour indicates the concentration of the occurrences (blue: low, yellow: high).

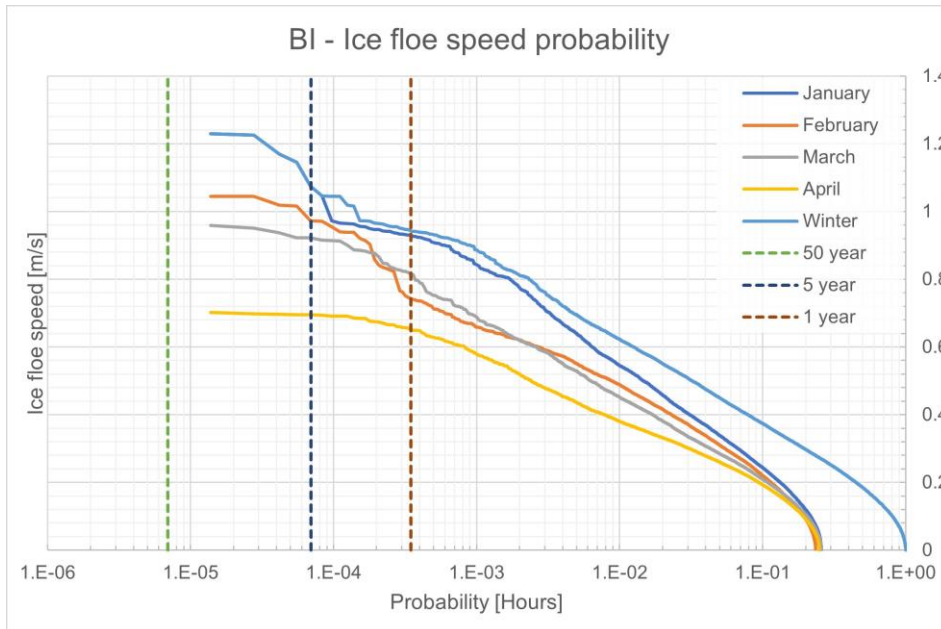


Figure 5-5 Bornholm I OWF: Probability of ice floe speed. Data for the period 1998-2022 (January-April). $1h/1y = 1/(4*30*24) = 3.47*10^{-4}$.

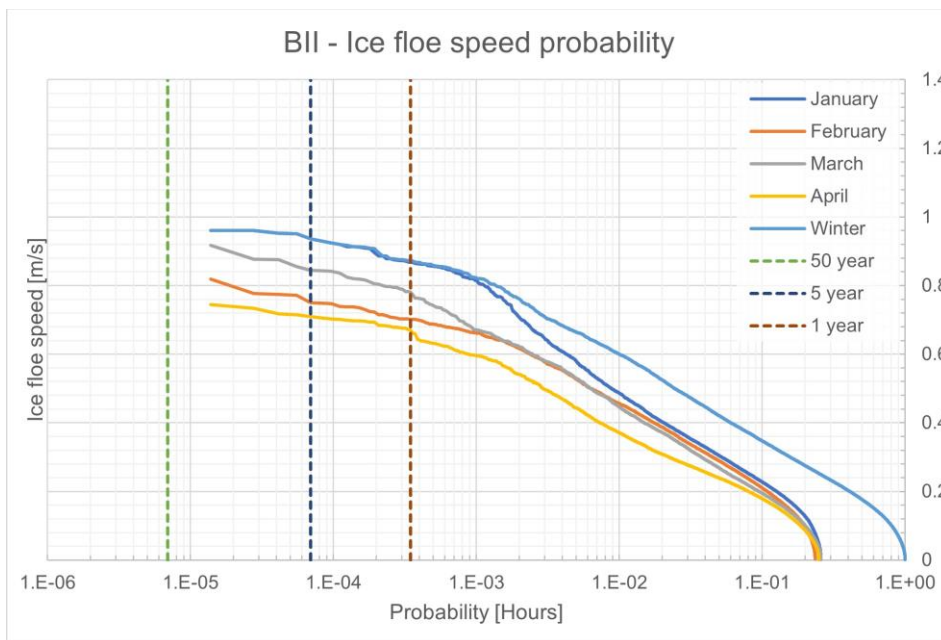


Figure 5-6 Bornholm II OWF: Probability of ice floe speed. Data for the period 1998-2022 (January-April). $1h/1y = 1/(4*30*24) = 3.47*10^{-4}$.

In Table 5-7 and Table 5-8 the free ice floe speed is listed versus the wind speed at 10 m for Bornholm I and II OWF respectively.

Table 5-7 Bornholm I OWF – Free ice floe speed vs. wind speed at 10 m based on hourly data 1998-2022 (January-April).

Ice Floe speed vs. Wind speed, Bornholm I OWF, 1/1/1998 - 31/12/2022, Months: January - April																													
Speed	Wind	0	2	4	6	8	10	12	14	16	18	20	22	24	26	28	30	32	34	36	38	40	42	44	46	48	50	Numbers	Occurance
Ice Floe Bin [m/s]		2	4	6	8	10	12	14	16	18	20	22	24	26	28	30	32	34	36	38	40	42	44	46	48	50			
0.00	0.02	75	132	124	131	76	37	15	10	4	0	0	0	0	0	0	0	0	0	0	0	0	0	0	0	0	604	0.84%	
0.02	0.04	176	395	355	355	263	151	79	22	17	5	1	0	0	0	0	0	0	0	0	0	0	0	0	0	0	1819	2.52%	
0.04	0.06	236	597	610	620	428	261	132	30	9	6	2	1	0	0	0	0	0	0	0	0	0	0	0	0	0	2932	4.06%	
0.06	0.08	301	756	736	767	621	427	158	53	24	6	2	1	1	1	1	1	1	1	1	1	1	1	1	1	1	3853	5.34%	
0.08	0.10	266	829	933	944	708	518	261	79	20	10	7	1	1	1	1	1	1	1	1	1	1	1	1	1	1	4577	6.34%	
0.10	0.15	596	2045	2811	2695	2386	1453	800	231	126	39	21	4	1	1	1	1	1	1	1	1	1	1	1	1	1	13208	18.31%	
0.15	0.20	363	1521	2527	2891	2433	1561	833	328	126	50	17	7	4	4	4	4	4	4	4	4	4	4	4	4	4	12661	17.55%	
0.20	0.25	202	916	1901	2529	2126	1456	792	369	127	48	9	7	2	2	2	2	2	2	2	2	2	2	2	2	2	10484	14.53%	
0.25	0.30	95	431	1103	1867	1799	1238	822	318	107	58	21	5	2	2	2	2	2	2	2	2	2	2	2	2	2	7866	10.90%	
0.30	0.35	37	196	620	1131	1347	824	580	272	124	37	17	1	0	0	0	0	0	0	0	0	0	0	0	0	0	5186	7.19%	
0.35	0.40	21	99	297	628	845	618	407	223	71	36	15	1	0	0	0	0	0	0	0	0	0	0	0	0	0	3261	4.52%	
0.40	0.50	9	74	218	433	846	798	524	313	110	41	10	2	0	0	0	0	0	0	0	0	0	0	0	0	0	3378	4.68%	
0.50	0.60	11	24	58	110	259	337	345	166	72	16	6	2	0	0	0	0	0	0	0	0	0	0	0	0	0	1406	1.95%	
0.60	0.70	0	12	17	37	82	140	141	75	31	28	5	1	0	0	0	0	0	0	0	0	0	0	0	0	0	569	0.79%	
0.70	0.80	0	0	1	9	33	39	41	29	11	7	2	1	0	0	0	0	0	0	0	0	0	0	0	0	0	173	0.24%	
0.80	0.90	0	0	0	2	14	29	32	14	6	3	3	1	0	0	0	0	0	0	0	0	0	0	0	0	0	104	0.14%	
0.90	1.00	0	0	0	3	6	11	24	2	5	0	1	2	0	0	0	0	0	0	0	0	0	0	0	0	0	54	0.07%	
1.00	1.25	0	0	0	0	0	5	5	0	0	0	0	0	0	0	0	0	0	0	0	0	0	0	0	0	0	10	0.01%	
1.25	1.50	0	0	0	0	0	0	0	0	0	0	0	0	0	0	0	0	0	0	0	0	0	0	0	0	0	0	0	0.00%
1.50	2.00	0	0	0	0	0	0	0	0	0	0	0	0	0	0	0	0	0	0	0	0	0	0	0	0	0	0	0	0.00%
2.00	2.40	0	0	0	0	0	0	0	0	0	0	0	0	0	0	0	0	0	0	0	0	0	0	0	0	0	0	0	0.00%
	Numbers	2388	8027	12311	15152	14272	9903	5991	2534	990	390	139	37	11	11	11	11	11	11	11	11	11	11	11	11	11	11	72145	
	Occurance	3.31%	11.13%	17.06%	21.00%	19.78%	13.73%	8.30%	3.51%	1.37%	0.54%	0.19%	0.05%	0.02%	0.02%	0.02%	0.02%	0.02%	0.02%	0.02%	0.02%	0.02%	0.02%	0.02%	0.02%	0.02%	0.02%	100.00%	

Table 5-8 Bornholm II OWF – Free ice floe speed vs. wind speed at 10 m based on hourly data 1998-2022 (January-April).

Ice Floe speed vs. Wind speed, Bornholm II OWF, 1/1/1998 - 31/12/2022, Months: January-April		0		2		4		6		8		10		12		14		16		18		20		22		24		Numbers	Occurrence
		Speed	Wind	Ice Floe	Bin [m/s]																								
0.00	0.02	86	177	135	109	52	28	12	12	5	1	0	0	0	0	0	0	0	0	0	0	0	0	0	0	0	605	0.84%	
0.02	0.04	262	530	470	359	203	99	27	27	12	4	2	0	0	0	0	0	0	0	0	0	0	0	0	0	1968	2.73%		
0.04	0.06	359	816	735	558	311	146	61	61	28	8	2	0	0	0	0	0	0	0	0	0	0	0	0	0	3024	4.19%		
0.06	0.08	351	989	957	752	457	261	82	82	29	8	5	1	0	0	0	0	0	0	0	0	0	0	0	0	3892	5.39%		
0.08	0.10	360	1060	1172	926	618	295	87	87	30	6	0	1	0	0	0	0	0	0	0	0	0	0	0	0	4555	6.31%		
0.10	0.15	656	2201	3393	3313	2526	1388	515	515	108	66	15	2	1	0	0	0	0	0	0	0	0	0	0	0	14184	19.66%		
0.15	0.20	249	1260	2729	3603	3246	2173	861	861	182	47	26	5	1	0	0	0	0	0	0	0	0	0	0	0	14382	19.93%		
0.20	0.25	83	455	1534	2555	2789	2093	1073	1073	358	108	37	12	4	0	0	0	0	0	0	0	0	0	0	0	11101	15.39%		
0.25	0.30	19	199	715	1431	1760	1409	919	919	438	151	44	21	5	1	0	0	0	0	0	0	0	0	0	0	7112	9.86%		
0.30	0.35	8	75	275	780	996	772	743	743	378	170	60	19	10	1	0	0	0	0	0	0	0	0	0	0	4287	5.94%		
0.35	0.40	3	39	142	405	669	552	432	432	273	120	35	16	2	1	0	0	0	0	0	0	0	0	0	0	2689	3.73%		
0.40	0.50	1	10	80	265	522	674	531	531	288	126	52	35	3	0	0	0	0	0	0	0	0	0	0	0	2587	3.59%		
0.50	0.60	0	4	15	75	170	267	308	308	112	49	17	16	6	0	0	0	0	0	0	0	0	0	0	0	1039	1.44%		
0.60	0.70	0	1	3	15	87	106	100	100	58	71	30	7	3	0	0	0	0	0	0	0	0	0	0	0	481	0.67%		
0.70	0.80	1	0	1	2	15	48	29	29	17	12	11	2	3	0	0	0	0	0	0	0	0	0	0	0	141	0.20%		
0.80	0.90	2	1	0	0	6	20	35	35	13	2	0	3	2	0	0	0	0	0	0	0	0	0	0	0	84	0.12%		
0.90	1.00	0	0	0	0	0	0	7	7	5	0	0	1	1	0	0	0	0	0	0	0	0	0	0	0	14	0.02%		
1.00	1.25	0	0	0	0	0	0	0	0	0	0	0	0	0	0	0	0	0	0	0	0	0	0	0	0	0	0	0.00%	
1.25	1.50	0	0	0	0	0	0	0	0	0	0	0	0	0	0	0	0	0	0	0	0	0	0	0	0	0	0	0.00%	
1.50	2.00	0	0	0	0	0	0	0	0	0	0	0	0	0	0	0	0	0	0	0	0	0	0	0	0	0	0	0.00%	
2.00	2.40	0	0	0	0	0	0	0	0	0	0	0	0	0	0	0	0	0	0	0	0	0	0	0	0	0	0	0.00%	
	Numbers	2440	7817	12356	15148	14427	10331	5822	5822	2334	949	336	141	41	3	0	0	0	0	0	0	0	0	0	0	0	72145		
	Occurrence	3.38%	10.84%	17.13%	21.00%	20.00%	14.32%	8.07%	8.07%	3.24%	1.32%	0.47%	0.20%	0.06%	0.00%	0.00%	0.00%	0.00%	0.00%	0.00%	0.00%	0.00%	0.00%	0.00%	0.00%	0	100.00%		

In Table 5-9 and Table 5-10 the free ice floe speed versus the ice floe direction is listed for Bornholm I and II OWF respectively.

Table 5-9 Bornholm I OWF – Free ice floe speed vs. ice floe direction based on hourly data 1998-2022 (January-April).

Ice floe direction (going to) vs. ice floe speed, Bornholm I OWF, 1/1/1998 - 31/12/2022, Months: January - April		1998-2022 (January-April)												Total							
Ice floe direction [deg]	Ice floe speed [m/s]	0.00	0.02	0.04	0.06	0.08	0.10	0.15	0.20	0.25	0.30	0.35	0.40	0.50	0.60	0.70	0.80	0.90	1.00	Numbers	Occurrence
-7.5	7.5	29	87	145	178	210	726	963	837	731	491	330	361	215	146	40	43	19	5	5556	7.70%
7.5	22.5	21	87	118	157	232	710	848	870	639	455	341	271	80	62	21	9	5	1	4927	6.83%
22.5	37.5	22	91	123	206	214	677	728	718	527	314	202	180	53	25	3	0	0	0	4083	5.66%
37.5	52.5	30	76	127	170	188	584	611	641	557	316	177	165	23	12	0	0	0	0	3677	5.10%
52.5	67.5	25	66	126	144	200	596	602	596	458	342	177	65	12	1	0	0	0	0	3410	4.73%
67.5	82.5	24	73	126	152	210	598	611	555	316	153	61	39	12	1	0	0	0	0	2931	4.06%
82.5	97.5	24	81	115	174	210	592	581	406	235	120	53	38	16	1	3	0	0	0	2649	3.67%
97.5	112.5	28	68	136	155	170	613	569	356	239	142	59	69	29	6	4	1	0	0	2644	3.66%
112.5	127.5	23	78	114	149	166	529	540	405	300	191	110	120	37	8	10	6	1	0	2787	3.86%
127.5	142.5	30	83	133	160	197	536	520	543	450	382	221	298	120	32	17	4	0	0	3726	5.16%
142.5	157.5	26	74	124	132	180	554	470	454	490	390	291	410	218	49	7	1	0	0	3870	5.36%
157.5	172.5	26	85	118	154	191	523	494	350	305	230	167	205	45	9	5	0	0	0	2907	4.03%
172.5	187.5	23	83	117	151	184	481	384	296	162	104	52	51	15	1	0	0	0	0	2104	2.92%
187.5	202.5	33	79	100	165	190	448	319	231	125	71	21	26	5	0	0	0	0	0	1813	2.51%
202.5	217.5	24	68	140	146	178	455	314	188	156	74	31	32	12	1	0	0	0	0	1819	2.52%
217.5	232.5	24	74	138	149	148	410	324	225	141	63	36	41	2	0	0	0	0	0	1775	2.46%
232.5	247.5	31	65	120	164	185	447	327	255	139	75	46	52	6	0	0	0	0	0	1912	2.65%
247.5	262.5	21	68	97	160	164	451	406	242	167	115	70	32	27	0	0	0	0	0	2020	2.80%
262.5	277.5	26	66	126	166	185	500	332	238	148	72	41	30	15	0	0	0	0	0	1945	2.70%
277.5	292.5	26	61	110	150	195	435	336	252	145	66	37	31	3	1	0	0	0	0	1848	2.56%
292.5	307.5	24	82	106	160	191	478	396	290	209	106	57	41	2	0	0	0	0	0	2142	2.97%
307.5	322.5	20	68	137	161	204	524	534	338	268	185	117	125	48	18	4	0	0	0	2751	3.81%
322.5	337.5	26	71	109	171	184	601	657	527	413	282	191	288	162	66	21	9	13	1	3792	5.26%
337.5	352.5	18	85	127	179	201	740	795	671	546	447	373	408	249	130	38	31	16	3	5057	7.01%
	Numbers	604	1819	2932	3853	4577	13208	12661	10484	7866	5186	3261	3378	1406	569	173	104	54	10	72145	
	Occurrence	0.84%	2.52%	4.06%	5.34%	6.34%	18.31%	17.55%	14.53%	10.90%	7.19%	4.52%	4.68%	1.95%	0.79%	0.24%	0.14%	0.07%	0.01%	100.00%	

Table 5-10 Bornholm II OWF – Free ice floe speed vs. ice floe direction based on hourly data 1998-2022 (January-April).

Ice floe direction (going to) vs. Ice floe speed, Bornholm II OWF, 1/1/1998 - 31/12/2022, Months: January - April																		Occurrence			
Ice floe speed [m/s]	Direction [deg]	0.00	0.02	0.04	0.06	0.08	0.10	0.15	0.20	0.25	0.30	0.35	0.40	0.50	0.60	0.70	0.80	0.90	1.00	Numbers	Occurrence
7.5	-7.5	22	87	123	159	205	666	702	602	470	303	208	209	126	63	36	15	4	4000	5.54%	
7.5	22.5	21	95	123	157	197	573	608	498	278	173	95	65	34	9	1	1	0	2928	4.06%	
22.5	37.5	20	89	107	162	165	450	422	277	177	89	63	25	7	0	0	0	0	2053	2.85%	
37.5	52.5	31	91	115	126	132	350	399	263	184	107	59	25	0	0	0	0	0	1882	2.61%	
52.5	67.5	21	87	120	135	141	338	347	233	142	52	10	10	0	0	0	0	0	1636	2.27%	
67.5	82.5	35	61	111	129	132	377	324	134	43	21	7	14	1	0	0	0	0	1389	1.93%	
82.5	97.5	22	87	130	130	145	343	246	101	31	13	6	4	0	0	0	0	0	1258	1.74%	
97.5	112.5	26	85	140	155	127	310	214	103	46	22	5	4	2	0	0	0	0	1239	1.72%	
112.5	127.5	23	79	141	162	140	433	290	147	103	34	14	12	0	0	0	0	0	1578	2.19%	
127.5	142.5	27	81	122	172	158	538	380	236	158	95	69	76	13	5	0	0	0	2130	2.95%	
142.5	157.5	28	92	138	163	195	598	612	428	311	230	178	223	82	1	0	0	0	3279	4.55%	
157.5	172.5	32	76	119	196	205	720	731	662	581	399	366	417	143	40	4	0	0	4691	6.50%	
172.5	187.5	22	78	123	190	236	816	825	724	562	326	259	206	53	23	2	0	0	4445	6.16%	
187.5	202.5	30	87	151	199	267	831	845	719	352	165	90	63	5	0	0	0	0	3804	5.27%	
202.5	217.5	16	92	144	171	220	774	804	552	251	156	58	17	2	0	0	0	0	3257	4.51%	
217.5	232.5	24	75	136	206	203	708	855	578	302	211	85	34	3	1	0	0	0	3421	4.74%	
232.5	247.5	23	82	124	150	221	678	784	620	327	164	70	51	3	1	0	0	0	3298	4.57%	
247.5	262.5	27	83	113	163	210	719	719	639	378	158	70	37	13	0	0	0	0	3329	4.61%	
262.5	277.5	34	76	135	155	206	707	698	633	348	153	61	41	4	0	1	0	0	3252	4.51%	
277.5	292.5	25	78	142	164	209	647	660	473	316	98	42	46	1	0	0	1	0	2902	4.02%	
292.5	307.5	25	74	122	188	213	621	694	563	319	171	116	95	13	7	0	2	1	3224	4.47%	
307.5	322.5	26	66	99	150	217	650	706	548	383	283	181	197	82	50	11	3	2	3654	5.06%	
322.5	337.5	23	83	124	164	219	675	740	693	536	413	285	320	186	97	37	29	4	4628	6.41%	
337.5	352.5	22	84	122	146	192	662	777	675	514	451	292	396	266	184	49	33	3	4868	6.75%	
Numbers		605	1968	3024	3892	4555	14184	14382	11101	7112	4287	2689	2587	1039	481	141	84	14	72145		
Occurrence		0.84%	2.73%	4.19%	5.39%	6.31%	19.66%	19.93%	15.39%	9.86%	5.94%	3.73%	3.59%	1.44%	0.67%	0.20%	0.12%	0.02%	100.00%		

In Table 5-11 and Table 5-12 the misalignment of wind vs. ice floe directions are listed for Bornholm I and II OWF respectively.

Table 5-11 Bornholm I OWF – Ice floe speed vs. misalignment wind/ice directions based on hourly data 1998-2022 (January-April).

Misalignment between Wind direction vs. ice floe direction for various wind speed bins, Bornholm I OWF, 1/1/1998 - 31/12/2022, Months: January - April																												
Wind speed [m/s]	0	2	4	6	8	10	12	14	16	18	20	22	24	26	28	30	32	34	36	38	40	42	44	46	48	50	Numbers	Occurance
Misalignment [deg]	2	4	6	8	10	12	14	16	18	20	22	24	26	28	30	32	34	36	38	40	42	44	46	48	50			
-180	79	145	168	178	119	91	70	19	18	4	1	0	0	0	0	0	0	0	0	0	0	0	0	0	0	892	1.24%	
-165	76	173	174	146	120	107	83	30	14	8	0	0	1	1	0	0	0	0	0	0	0	0	0	0	0	932	1.29%	
-150	87	185	210	167	142	120	96	42	15	3	3	0	0	0	0	0	0	0	0	0	0	0	0	0	0	1070	1.48%	
-135	90	195	213	172	160	124	78	44	23	19	2	2	2	2	2	2	2	2	2	2	2	2	2	2	2	1124	1.56%	
-120	76	191	223	237	170	178	106	54	24	13	4	2	0	0	0	0	0	0	0	0	0	0	0	0	0	1278	1.77%	
-105	70	208	298	305	253	186	129	58	47	11	6	5	1	1	1	1	1	1	1	1	1	1	1	1	1	1577	2.19%	
-90	99	226	362	431	332	234	174	80	39	32	7	2	1	1	1	1	1	1	1	1	1	1	1	1	1	2019	2.80%	
-75	106	294	404	540	475	313	257	125	35	30	11	2	2	2	2	2	2	2	2	2	2	2	2	2	2	2594	3.60%	
-60	101	298	483	605	592	407	300	133	51	25	9	0	1	1	1	1	1	1	1	1	1	1	1	1	1	3005	4.17%	
-45	128	413	526	654	666	424	234	154	92	23	6	2	0	0	0	0	0	0	0	0	0	0	0	0	0	3322	4.60%	
-30	135	492	715	838	826	473	329	142	42	22	5	1	1	1	1	1	1	1	1	1	1	1	1	1	1	4021	5.57%	
-15	128	582	964	972	848	516	306	116	39	19	3	0	0	0	0	0	0	0	0	0	0	0	0	0	0	4493	6.23%	
0	140	624	1161	1311	1049	714	368	134	52	11	7	0	0	0	0	0	0	0	0	0	0	0	0	0	0	5571	7.72%	
15	133	709	1173	1484	1335	891	418	151	63	26	12	0	0	0	0	0	0	0	0	0	0	0	0	0	0	6395	8.86%	
30	131	596	1262	1628	1376	964	584	206	74	19	17	2	0	0	0	0	0	0	0	0	0	0	0	0	0	6859	9.51%	
45	144	544	965	1467	1522	1050	702	347	102	29	9	6	1	1	1	1	1	1	1	1	1	1	1	1	1	6888	9.55%	
60	119	442	768	1224	1410	986	600	227	65	21	13	5	0	0	0	0	0	0	0	0	0	0	0	0	0	5880	8.15%	
75	103	368	597	808	977	774	432	136	53	26	10	5	0	0	0	0	0	0	0	0	0	0	0	0	0	4289	5.94%	
90	81	322	491	639	587	455	212	89	33	12	3	2	0	0	0	0	0	0	0	0	0	0	0	0	0	2926	4.06%	
105	89	268	338	449	424	316	160	73	33	3	0	0	0	0	0	0	0	0	0	0	0	0	0	0	0	2153	2.98%	
120	59	198	286	333	348	242	143	52	23	9	5	1	1	1	1	1	1	1	1	1	1	1	1	1	1	1700	2.36%	
135	68	227	198	235	226	129	84	42	11	13	4	0	0	0	0	0	0	0	0	0	0	0	0	0	0	1237	1.71%	
150	78	171	184	177	167	89	68	46	19	11	0	0	0	0	0	0	0	0	0	0	0	0	0	0	0	1010	1.40%	
165	68	156	148	152	148	120	58	34	23	1	2	0	0	0	0	0	0	0	0	0	0	0	0	0	0	910	1.26%	
Numbers	2388	8027	12311	15152	14272	9903	5991	2534	990	390	139	37	11	11	11	11	11	11	11	11	11	11	11	11	11	11	72145	
Occurance	3.31%	11.13%	17.06%	21.00%	19.78%	13.73%	8.30%	3.51%	1.37%	0.54%	0.19%	0.05%	0.02%	0.02%	0.02%	0.02%	0.02%	0.02%	0.02%	0.02%	0.02%	0.02%	0.02%	0.02%	0.02%	0.02%	100.00%	

Table 5-12 Bornholm II OWF – Ice floe speed vs. misalignment wind/ice directions based on hourly data 1998-2022 (January-April).

Misalignment between Wind direction vs. Ice floe direction for various wind speed bins, Bornholm II OWF, 1/1/1998 - 31/12/2022, Months: January - April																										
Wind speed [m/s]	0	2	4	6	8	10	12	14	16	18	20	22	24	26	28	30	32	34	36	38	40	42	44	46	48	50
Misalignment [deg]	2	4	6	8	10	12	14	16	18	20	22	24	26	28	30	32	34	36	38	40	42	44	46	48	50	Occurrence
	Numbers																									
-180	39	71	75	63	29	36	2	4	3	0	0	0	0	0	0	0	0	0	0	0	0	0	0	0	322	
-165	43	90	64	69	37	19	4	6	1	1	0	0	0	0	0	0	0	0	0	0	0	0	0	0	334	
-150	65	111	68	66	29	25	20	4	4	1	0	0	0	0	0	0	0	0	0	0	0	0	0	0	393	
-135	64	107	73	73	49	27	13	6	6	2	0	0	0	0	0	0	0	0	0	0	0	0	0	0	420	
-120	67	113	119	123	69	58	27	7	6	3	1	0	0	0	0	0	0	0	0	0	0	0	0	0	593	
-105	69	168	185	179	139	95	43	27	20	15	0	0	0	0	0	0	0	0	0	0	0	0	0	0	940	
-90	87	227	233	272	208	145	82	43	23	19	8	0	0	0	0	0	0	0	0	0	0	0	0	0	1347	
-75	113	317	385	414	364	224	153	73	26	9	10	3	0	0	0	0	0	0	0	0	0	0	0	0	2091	
-60	121	422	583	682	520	406	256	134	70	21	16	8	2	0	0	0	0	0	0	0	0	0	0	0	3241	
-45	157	557	779	1003	813	578	470	213	110	43	16	7	0	0	0	0	0	0	0	0	0	0	0	0	4746	
-30	146	706	1162	1287	1018	735	475	216	76	37	14	4	0	0	0	0	0	0	0	0	0	0	0	0	5876	
-15	180	788	1500	1652	1590	1026	461	123	32	14	4	1	0	0	0	0	0	0	0	0	0	0	0	0	7371	
0	194	776	1584	1838	1821	1348	686	305	91	19	4	0	0	0	0	0	0	0	0	0	0	0	0	0	8666	
15	182	766	1491	1962	1987	1498	819	394	191	60	31	13	1	0	0	0	0	0	0	0	0	0	0	0	9395	
30	166	631	1186	1792	1878	1456	866	364	141	42	19	1	0	0	0	0	0	0	0	0	0	0	0	0	8542	
45	132	509	930	1450	1586	1257	746	247	69	31	8	4	0	0	0	0	0	0	0	0	0	0	0	0	6969	
60	129	407	595	947	1113	744	396	101	33	9	8	0	0	0	0	0	0	0	0	0	0	0	0	0	4482	
75	103	263	442	535	550	325	145	23	16	7	2	0	0	0	0	0	0	0	0	0	0	0	0	0	2411	
90	75	208	276	266	276	117	62	18	10	2	0	0	0	0	0	0	0	0	0	0	0	0	0	0	1310	
105	76	160	191	157	117	69	32	10	6	0	0	0	0	0	0	0	0	0	0	0	0	0	0	0	818	
120	75	121	143	103	78	49	25	5	11	1	0	0	0	0	0	0	0	0	0	0	0	0	0	0	611	
135	60	103	112	92	61	28	15	4	3	0	0	0	0	0	0	0	0	0	0	0	0	0	0	0	478	
150	51	97	111	61	53	35	19	3	0	0	0	0	0	0	0	0	0	0	0	0	0	0	0	0	430	
165	46	99	69	62	42	31	5	4	1	0	0	0	0	0	0	0	0	0	0	0	0	0	0	0	359	
Numbers	2440	7817	12356	15148	14427	10331	5822	2334	949	336	141	41	3	0	0	0	0	0	0	0	0	0	0	0	72145	
Occurrence	3.38%	10.84%	17.13%	21.00%	20.00%	14.32%	8.07%	3.24%	1.32%	0.47%	0.20%	0.06%	0.00%	0.00%	0.00%	0.00%	0.00%	0.00%	0.00%	0.00%	0.00%	0.00%	0.00%	0.00%	100.00%	

6 Climate properties

Climate and ice properties relevant for estimating sea ice load are based on general available information for the southern part of the Baltic Sea and project specific data [1]. Air properties can be found in Table 6-1. Water level information's can be found in Figure 6-1, Figure 6-2 and Table 6-2.

6.1 Air properties

Table 6-1 Air properties [1]. Data from NORA3 except Air density which is standard values in the region.

Parameter	Units	Mean	Min	Max
Air temperatures normal	(°C)	8.7/8.8	-13.0/-12.1	24.6/25.4
Air density	(kg/m ³)	1.25	1.17	1.38
Relative humidity	(%)	83.6/83.5	33.1/31.8	100/100

6.2 Water levels and tidal range

The principal cause of water level fluctuation is meteorologically induced surge associated with surface wind forcing and response to atmospheric pressure fluctuations.

The water level distribution is based on data as described in Section 2.3.7. The used input data for the water level analysis represent the 4 winter months (January – April) for the years 1979-2021. For the one-year return period of still water level the fluctuation is found to be: $+1.07 + |-1.02| = 2.09$ m. ref. Figure 6-1 and Figure 6-2.

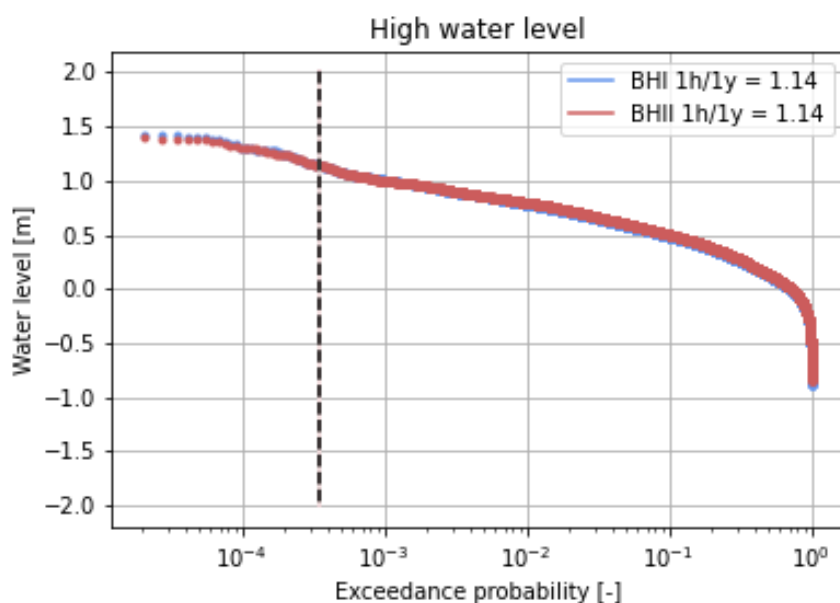


Figure 6-1 Exceedance probability (hourly) of high water level January to April, 1979-2021. Events: 117136. Probability 1h/1y: $1/(4 \cdot 30 \cdot 24) = 3.5 \cdot 10^{-4}$

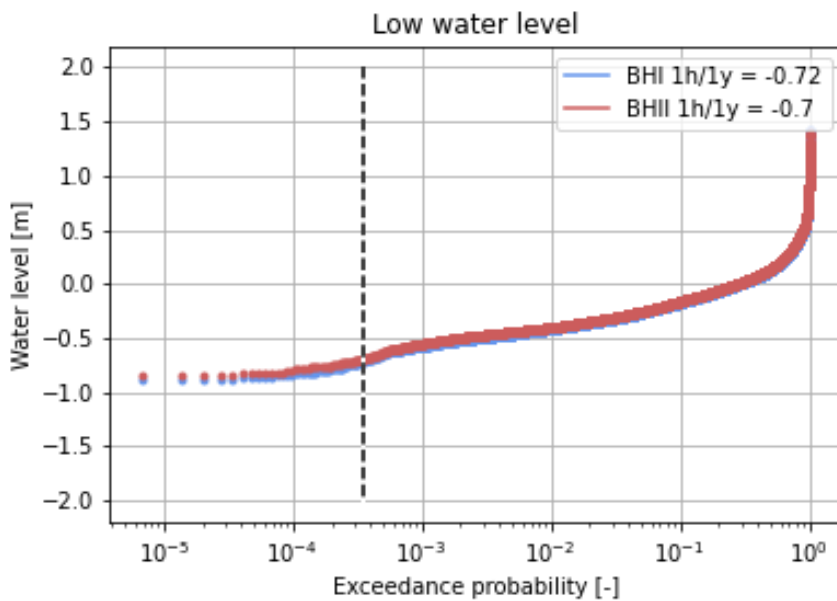


Figure 6-2 Exceedance probability (hourly) of low water level for January to April, (4 months) 1979-2021. Events: 117136. Probability 1h/1y: $1/(4 \cdot 30 \cdot 24) = 3.5 \cdot 10^{-4}$

In Table 6-2 the average daily mean water variation for the winter months is shown.

Table 6-2 Water level values for the winter months (January to April).

Parameter	BHI Level mMSL	BHII Level mMSL
Average high water level	+0.1 [m]	+0.09 [m]
Mean	0.00	0.00
Average low water level	-0.11 [m]	-0.11 [m]

6.2.1 Sea level rise due to climate changes.

Sea level rise due to climate changes are described in the Metocean report [1] section 9 based on the Intergovernmental Panel on Climate Change (IPCC).

According to IPCC, the sea level rise in Northern Europe will amount to between 0.0m (5 percentile) and 0.5m (95 percentile) with a median of 0.25m in year 2055.

6.3 Temperature

Design water temperature: $-5^{\circ}\text{C} < T_{sea,design} < 20^{\circ}\text{C}$

Freezing point temperature of sea water (8.5 PSU): -0.45°C

6.4 Salinity

FINO2 measurement station has salinity probes at various depths. The average salinity at a 2m depth during the winter months is 8.5 PSU, which is equivalent to 0.85%. The same salinity is applicable for Bornholm I & II OWF which is confirmed by short term measurements at Bornholm II OWF.

6.5 Seawater and ice density

Seawater density variation: 1003-1013 kg/m³

Seawater typical density [104]: 1007 kg/m³

The sea ice density depends on salinity, temperature, and the age of the ice. Typical values are in range of 912 kg/m³ to 925 kg/m³ [104]. For the west Baltic sea the value of 920 kg/m³ can be used as an average value [104].

7 Ice properties

Ice properties as described in this section are defined according to ISO 19906 [103]. The properties can be used to determine the ice strength if the required information about: Ice brine volume, Porosity, Poisson ration and Young's modulus is available. In the present document alternative guidelines to determine the ice strength based on measurements is described in Section 8.

7.1 Ice brine volume

The ice brine volume v_b [ppt] of enclosed saline brine influences porosity and density of sea ice. Typical brine volumes are in the range of 20 to 100 ppt, depending on salinity, temperature, type, and age of the ice. From salinity and ice temperature, v_b can be estimated by:

$$v_b = 41.64 S_B^{0.88} |\vartheta_A|^{-0.67} \quad (6.1)$$

Where:

S_B : Bulk salinity after completed ice growth [ppt].

ϑ_A : Ice temperature, averaged over the ice thickness [°C].

See Section 1.3.2.4. of [104].

7.2 Porosity

Naturally grown sea ice contains various inclusions and irregularities which lead to a porosity ϕ_B [ppt] of typically 3 to 20 ppt, approximately described by:

$$\phi_B = 19.37 + 36.18 S_B^{0.91} |\vartheta_A|^{-0.69} \quad (6.2)$$

Where S_B und ϑ_A are as defined under Section 7.1.

See Section 1.3.2.5. of [104].

7.3 Poisson ratio

Poisson ratio of sea ice [111] and [103]: 0.33

Range: 0.3 – 0.35

7.4 Young's modulus

Effective elasticity ref. ISO 19906 A.8.2.8.9 [103]

$$E_f = 5.31 - 0.436 v_b^{0.5} \quad (6.3)$$

E_f : is the effective elastic modulus

v_b : is the brine volume fraction

With an ice salinity of 2% and an ice temperature of -3 °C the recommended effective elasticity modulus is: 2.7 GPa

Local range: 2 GPa – 4 GPa

7.5 Ice friction coefficient

The friction coefficient is usually described as static friction coefficient μ_s and dynamic friction coefficient μ_d . The dynamic friction coefficient has usually been considered to be a constant but newer investigations, Nakazawa et al (1993) [106] and Frederking & Barker (2002) [107] have shown that μ_d is strongly dependent upon the velocity between the structure and the ice. The velocity estimate shall include the eventual velocity of the structure due to structural deflection. The following estimate may be proposed:

$$\mu_d = 2 \mu_{d0}, 1 \text{ m/s} \leq V_{ice} \Leftrightarrow \mu_d = \mu_{d0} (2 - \log V_{ice}), 10^{-3} \text{ m/s} < V_{ice} < 1 \text{ m/s}$$

where μ_{d0} is a constant depending on the structure surface, see Table 7-1.

Table 7-1 Friction coefficients between ice and structures.

Surface of structure	Static friction coefficient μ_s	Dynamic friction factor μ_{d0}	Dynamic friction coefficient μ_d		
			0.01	0.1	1
Ice velocity (m/s)	-	-	0.01	0.1	1
Concrete	0.3	0.05	0.20	0.15	0.1
New uncoated steel	0.3	0.03	0.12	0.09	0.06
Painted steel	0.25	0.02	0.08	0.06	0.04
Corroded steel	0.45	0.05	0.20	0.15	0.1
Ice-ice	<0.1	<0.1	0.1	<0.1	<0.1

8 Ice strength

Ice strength depend on the ice breaking mechanism and can be divided into:

- Bending (flexural) strength,
- Tensile strength and
- Crushing (compressive) strength

These are basic properties of sea ice used in any analytical or empirical model. Approximation methods to calculate these values are given in ISO 19906 [103], however due to difficulties to determine the ice properties, the ice strength properties for the project are derived from tests and measurements as described in the following section.

8.1 Bending strength

According to ISO 19906 [104] the bending (flexural) strength σ_f [MPa] of saline ice can be approximated from:

$$\sigma_f = 1.76 * e^{-5.88 \sqrt{\frac{v_b}{1000}}} = 1.76 * e^{-0.19 \sqrt{v_b}} \quad (7.1)$$

Where:

v_b : Brine volume [ppt] ref. Section 7.1

Typical values for σ_f are in range of 0.5 to 2 MPa.

The bending strength is according to ISO 19906 specified on the basis of the brine contents related to sea ice temperature and salinity – see above. But the difficulties of determining these parameters and the variation of the ice temperature and salinity gives such large scatter that the procedure gives unreliable results. Therefore, a more robust estimate is suggested. This originates from the ice design basis applied for Danish Belt crossing projects as shown in Table 8-1. The results are reasonably consistent with the rough estimates which may be found from ice temperature/salinity estimates.

Table 8-1 Ice Design Basis applied for Great Belt and Øresund Links [110].

Return period (years)	5	10	50	100	500	700	1000	1320
K_{max} (-°C 24 hours)	170	245	410	480	665	700	721	744
σ_c (MPa) (no account to snow)	1.00	1.50	1.90	2.00	2.25	2.30	2.35	2.40
σ_f (MPa)	0.25	0.39	0.50	0.53	0.60	0.61	0.62	0.64
h (m)	0.33	0.42	0.57	0.63	0.75	0.77	0.78	0.80
$h r_u$	0.33	0.63	1.08	1.26	1.69	1.77	1.83	1.92
$h^2 r_f$	0.04	0.07	0.16	0.21	0.34	0.36	0.38	0.41

Where:

σ_c : the crushing strength of the ice (MPa)

σ_f : the bending strength of the ice (MPa)

h : calculated ice thickness $h = 0.032 (0.9 K_{max} - 50)^{0.5}$ (m)

K_{max} : frost index = the sum of the 24-hour average temperature (in °C) during the frost period (<0°C).

Based on the design values as listed in Table 8-1 the following distribution of the bending strength vs. frost index can be found as shown in Figure 8-1.

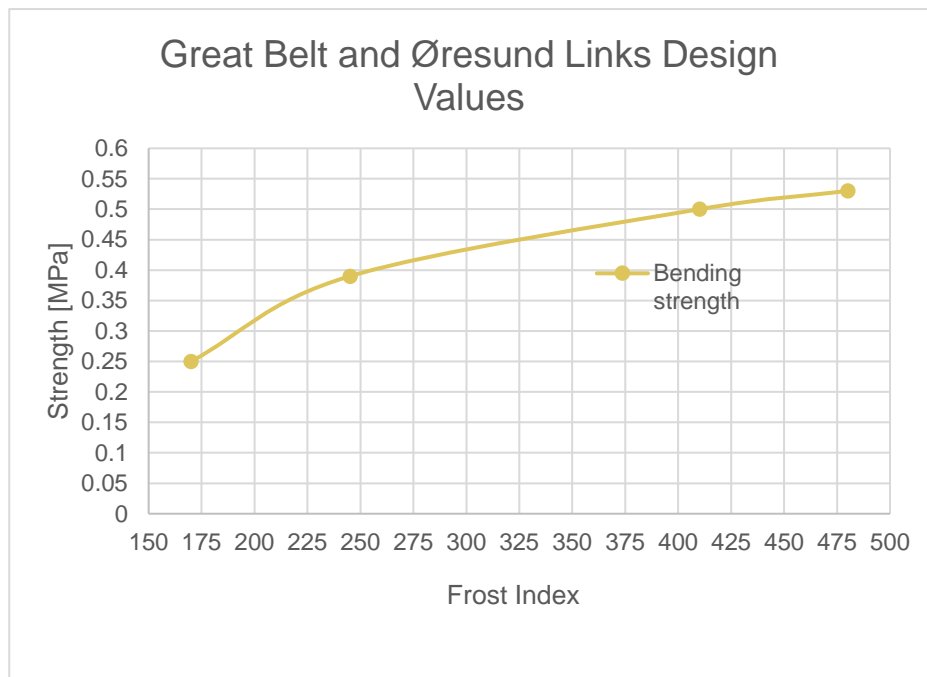


Figure 8-1 Bending strength vs. frost index (dots for Frost Index of 170, 245, 410 and 480) ref. Table 8-1.

For the Bornholm I and II OWF projects the frost indexes of 224/223 and 276/273 are estimated for the 1/50y and 1/100y return periods for Bornholm I & II OWF respectively ref. Section 5.2 hence the bending strength of $\sigma_{f,50y} = 0.36/0.35$ MPa and $\sigma_{f,100y} = 0.42/0.41$ MPa can be applied ref. Figure 8-1 for Bornholm I & II OWF. Due to limited documentation of the reduced bending strength for lower frost indexes and smaller ice floe thickness the bending strength is generally set to minimum 0.30 MPa for all ice thickness estimated for Bornholm I and II OWF.

8.2 Tensile strength

According to ISO 19906 [104] the tensile strength σ_t [Mpa] of saline ice can be approximated from:

$$\sigma_t = \left(1 - \sqrt{\frac{v_b}{v_0}}\right)^2 \cdot \sigma_0 + S \quad (7.2)$$

Where:

v_b : Brine volume [ppt] as given in Section 7.1.

v_0 : Reference volume between 100 and 142 ppt; for calculation purposes a value of 142 ppt should be used.

σ_0 : Reference strength 2.5 Mpa.

S: Security surcharge; S=0.4.

Typical values are in range of 0.5 to 3 Mpa.

Due to the difficulties to determine the brine volume, reference volume, reference strength and security surcharge an alternative method is suggested below.

According to the formulas of ISO 19906 [103] the tensile strength is about 10-20% lower than the bending strength. However due to the scatter of measured ice strength it is recommended using the same strength values for tensile and bending.

The tensile strength can conservatively be assumed to be equal to the bending strength from section 8.1 e.g., 0.36/0.35 MPa and 0.42/0.41 MPa for respectively the 1/50y and the 1/100y return period events for Bornholm I & II OWF.

8.3 Ice strength coefficient

According to ISO 19906 [104] the compression strength over a structure can be expressed by the ice strength coefficient C_R [MPa] of saline ice and can be approximated from:

$$C_R = 2700 \cdot \varepsilon^{1/3} \cdot \phi_B^{-1} \quad (7.3)$$

Where:

ε : Strain rate, typically $\varepsilon = 10^{-3} \text{ s}^{-1}$, depending on the rate of interaction (ice drift velocity)

ϕ_B : Ice porosity as given in Section 7.2

Typical values for σ_c are in range of 0.5 and 12 MPa.

Due to difficulties of estimating the ice porosity, methods to estimate the ice strength coefficient based on experiments are included below.

As the ice load models in ISO 19906 [103] are only representative for locations with heavy ice each year, the ISO 19906 [103] estimate has to be modified for Bornholm I and II OWF, with only heavy ice around every 5 - 8 years or less. According to ISO 19906 [103] the ice strength coefficient is determined by the return period of ice occurrence. This has been described for areas with severe ice coverage but not for the Bornholm I and II OWF area. To cover the gap

reference is made to Gravesen and Kärna (2009) [105]. The main conclusion yields $C_R^{SB} = 1.0$ MPa for South Baltic compared to $C_R^{NB} = 1.3$ MPa for the North Baltic for a 5 years return period.

Based on similar frost indexes and ice coverage for the South Baltic Sea compared to the Bornholm I and II OWF area it is considered safe to use the conclusion of the reference [105] for Bornholm I and II OWF. For a lower return period (1-2 years) Figure 8.2 show a CR value of 0.64 MPa, 0.98 MPa and 1.05 MPa for return period 1, 50 and 100 years respectively. The conventionally used compliance and velocity safety factors of 1.2 and 1.11 respectively are to be applied. With applied safety factors used leads to $0.64 * 1.2 * 1.11 = 0.85$ MPa which is considered suitable for Bornholm I and II OWF.

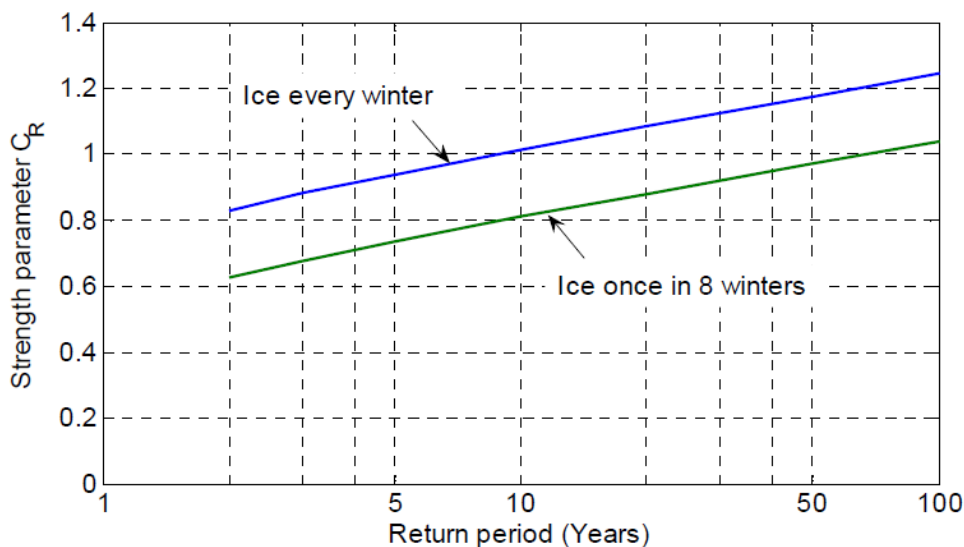


Figure 8-2 Two modes for ice strength coefficient C_R as function of the return period. [105] Figure 5.

The evaluation of the ice strength coefficient can be further supported by the measured Norströmsgrund data as illustrated in Figure 8-3.

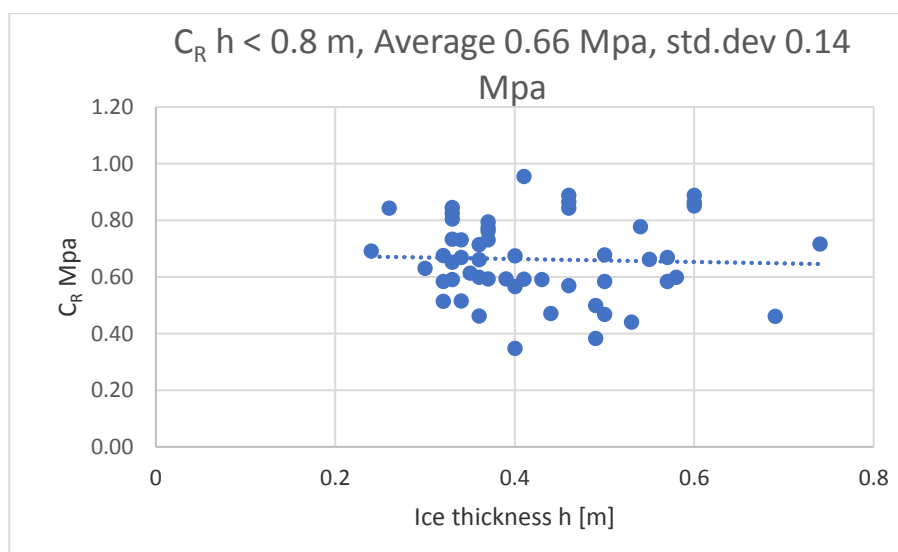


Figure 8-3 C_R values based on measured Norströmsgrund data on overall load for ice thickness $h < 0.8$ m [120].

By considering the Norströmsgrund data (Figure 8-3) and [120] creating the basis for ISO 19906 [103] it cannot be recommended to apply a C_R design value of less than 0.85 MPa for an extreme load and no less than 0.66 MPa for the average load.

According to ref. [105] both laboratory data and field data show that ice loads acting on a vertical structure will increase if the compliance of the structure increases. Accordingly, it can be concluded that the apparent ice strength will increase if the waterline displacement u_w is higher than 0.5 % of the ice thickness [105]. A generalised empirical curve shown in Figure 8-4 is proposed for narrow monopile foundations that are a common option for offshore wind turbines. The compliance parameter γ_s shown in Figure 8-4 is used as a multiplication factor on the ice strength coefficient - C_R .

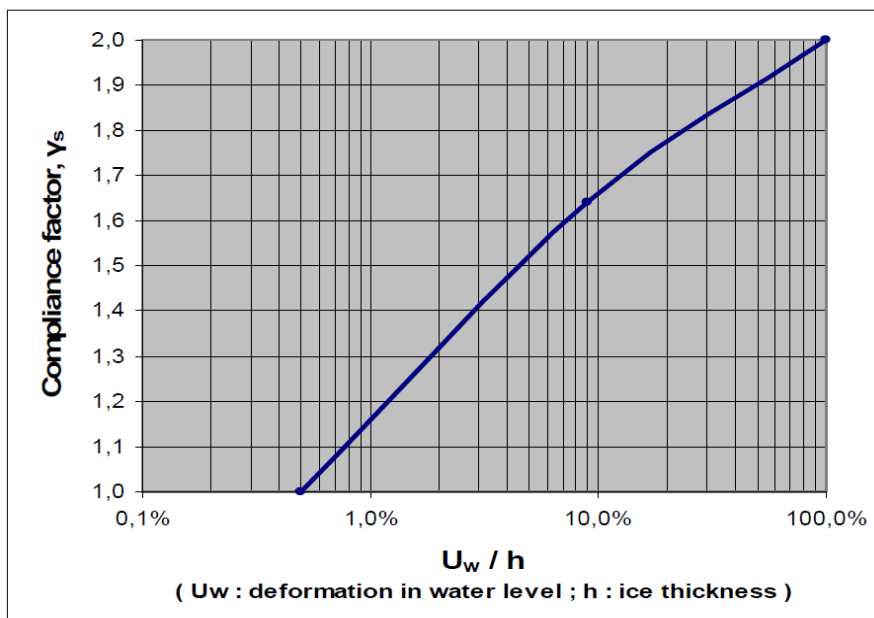


Figure 8-4 Compliance factor γ_s versus relative deformation in water level for quasistatic ice load (Gravesen and Kärna (2009)) Ref. [105].

The ice strength coefficient shall be multiplied with the compliance factor ref. Figure 8-4 or the load model shall include the ice strength coefficient amplification related to the dimension of the structure and the water level variation.

Three different ice crushing phenomena may occur, depending on the ice speed ref. Figure 8-4. Low ice speed below 0.04-0.05 m/s may lead to intermittent crushing. Moderate ice speed in the range of 0.04 m/s to 0.1 m/s may lead to frequency lock-in depending on the structural response. Higher ice speed of more than 0.05 – 0.1 m/s will lead to continuous brittle crushing. For more details refer to ISO 19906 [103].

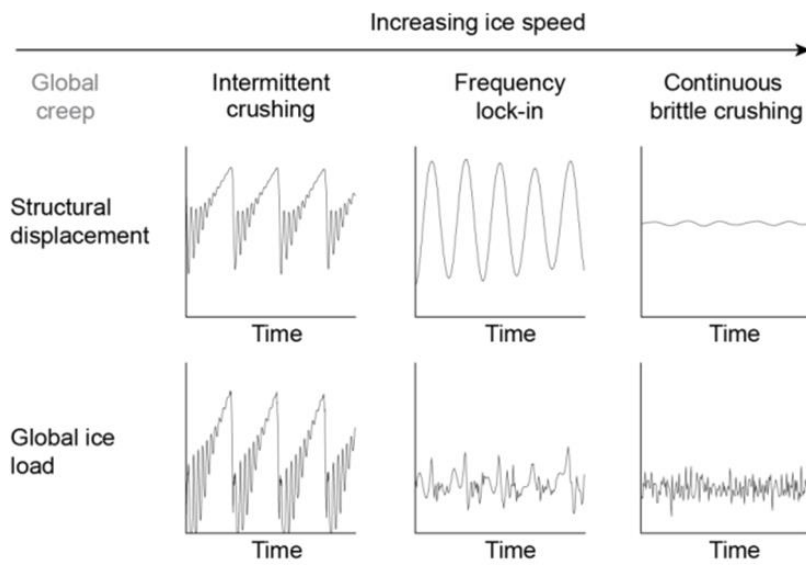


Figure 8-5 Illustration of various ice crushing mechanisms depending on ice floe speed. Intermittent crushing and frequency lock-in may occur up to about 0.05 m/s ice floe speed.

9 Ice loads

9.1 Horizontal ice loads

Calculation of ice loads are not fully standardised. For this reason, the main sections of the relevant standards, extensions and notes are included below.

ISO 19906 [103] A.8.2.4.3.2 includes a rational design method for calculation of horizontal ice loads from crushing ice based on field measurements now implemented in IEC 61400-3-1 [102] D.4.4.

Ice strength coefficient can be estimated based on measured and calibrated ice load data.

The global horizontal crushing ice load is calculated as:

$$F_G = p_G * w * h \quad (8.1)$$

Where:

p_G : is a value of the external global pressure (MPa),

w : is the width of the structure (m),

h : is the thickness of the ice sheet (m)

Data obtained from full-scale measurements in Cook Inlet, the Beaufort Sea, the Baltic Sea and Bohai Bay have been used to determine upper bound action values for scenarios where a first-year or multi-year sheet ice acts against a vertical structure. The data have also been used to analyse how the ice thickness and the width of the structure influence the global ice action. Based on these studies, the global ice pressure can be determined from equation (8.2). The formula for p_G is according to ISO 19906 [103]:

$$p_G = C_R \left[\left(\frac{h}{h_1} \right)^n \left(\frac{w}{h} \right)^m + f_{AR} \right] \quad (8.2)$$

Where:

p_G : is a value of the external global pressure (MPa),

w : is the width of the structure (m),

h : is the thickness of the ice sheet (m), $h_1=1$ m

m, n : n are the empirical exponents to take account of the size effect.
 $m = -0.16$,
 $n = -0.50 + h/5$ for $h < 1.0$ m and $n = -0.30$ for $h \geq 1.0$ m,

C_R : is the ice strength coefficient, in MPa (in different ice regimes)

f_{AR} : is an empirical term for

$$f_{AR} = e^{\frac{-w}{3h}} \sqrt{1 + 5 \frac{h}{w}} \quad (8.3)$$

If $w/h > 5$ the term f_{AR} can be disregarded.

Observations of ice interactions on relatively narrow lighthouse structures (structures width < ~2m, ice thickness < ~1m) in the north Baltic Sea support the inclusion of the f_{AR} term (8.3) in the formula (8.2).

The ice strength coefficient C_R can be derived according to Section 8.3.

According to ISO 19906 [103] one should combine a safe estimate of the (1/50-1/100year) ice thickness with $C_{R(1/1y)}$ and a 1/1year ice thickness with a 1/100year C_R value. However, for Bornholm I and II OWF there is no ice thickness for 1/1year so this combination is not relevant.

9.2 Vertical ice loads

According to IEC 61400-3 [102] D.4.5 the vertical load in case of fluctuating water level with a fast ice cover frozen to the support structure is limited either by the shear strength at adhesion to the support structure surface, V_τ , or by the bending strength if the ice is broken in a ring around the support structure, V_b . The lower of the two alternatives is decisive and should be used.

$$V_\tau = A\tau \quad (8.4)$$

Where:

τ : is the adhesive shear strength (MPa)

$A = \pi Dh$: is the contact surface for a circular vertical support structure (m²).

D : is the diameter (m)

h : is the ice thickness (m)

The adhesive shear strength τ can be set to:

0.8 MPa for steel – freshwater ice,

0.3 MPa for steel – saline ice, or to

1 MPa for concrete – saline ice

$$V_b = 0.6A\sqrt{\sigma_b\rho g\Delta z} \quad (8.5)$$

Where:

A : is the contact surface (m²).

σ_b : is the bending strength of ice, not less than 0.26 σ_c (MPa).

ρ : is the water density (kg/m³).

g : is the gravitational acceleration(m/s²).

Δz : is the water level difference (m).

Note that ice can grow between braces in multi-legged structures.

9.3 Local ice pressures

According to IEC 61400-3 [102] Section D.4.4.4 the support structure should be designed for the following local ice pressure:

$$p_{C,local} = \sigma_c \left(1 + \frac{5h^2}{A_{local}} \right)^{0.5} < 20 \text{ MPa} \quad (8.6)$$

Where:

- $p_{C,local}$ is the characteristic local ice pressure for use in design against moving ice (MPa)
- σ_c Is the characteristic crushing strength for local ice pressure. $\Sigma_c = 1.2$ MPa is suggested (MPa).
- h is the characteristic thickness of the ice (m)
- A_{local} is the local area considered (m²)

9.4 Dynamic ice loads

The wind turbine should be checked for dynamic effects from ice loading. When assessing whether dynamical effects can occur, and how often, it is often necessary to consider ice mobility, floe sizes, ice concentration, misalignment between ice drift- and wind-direction, as well as ice types. In particular, conclusions cannot be based on information on ice concentration alone.

It can be helpful to note that if the appropriate type of mobile ice is present at a site, frequency lock-in is almost always possible since the ice speeds required are usually small, e.g., of the order of 0.1 m/s. Although frequency lock-in is possible due to the factors above, it does not necessarily occur all the time: An assessment of this can be made based on the homogeneity of the ice. As a further guidance, frequency lock-in does normally not occur for ice concentrations below 7/10. All relevant ice speeds, in combination with durations and ice thicknesses, should be considered. Below some simplified equations are given for dynamic load simulation which can be used if statistical data, sufficiently advanced numerical models, or measurements are not available.

The criterion for susceptibility to frequency lock-in for the ice acting on a single point is:

$$\xi_n \leq \frac{\phi_{nC}^2}{4\pi f_n M_n} \cdot h \cdot \theta \quad (8.7)$$

where:

- f_n is the n 'th eigenfrequency [Hz],
- M_n is the modal mass of the n 'th eigenmode in [kg],
- ξ_n is the damping of the n 'th eigenmode as a fraction of critical damping [s],
- ϕ_{nC} is the magnitude of the n 'th eigenmode at the ice action point,
- h is the ice thickness [m], and
- θ is a coefficient with the suggested value of $40 \cdot 10^6$ kg/m·s.

Thus, the design procedure for analysing frequency lock-in consists of the following steps:

- a) Solve the eigenvalues and modes of vibration.
- b) Identify the modes that could be susceptible to frequency lock-in using the criterion above: i.e., if a mode's damping is smaller than or comparable to the right-hand side of equation (8.7), it could be susceptible to frequency lock-in.
- c) Calculate the dynamic response.

Simplifying forcing functions:

The simplified forcing function from Figure 9-1 can be used for determination of response of the vertical structure under frequency lock-in vibrations. The frequency $f = 1/T$, of the forcing function corresponds to the frequency of one of the susceptible natural modes with a natural frequency below 10 Hz, as derived from equation (8.7). The maximum force H_{max} , as well as the amplitude $\Delta H = H_{max} - H_{min}$, can be assumed constant. The peak values can be determined according to equation (8.6). The forcing function should be long enough to assure a steady-state response of the structure. The amplitude ΔH depends on the vibrational modes of the structure and on the ice velocity. It can be expressed as a fraction q , of the maximum force H_{max} . The amplitude ΔH should be scaled so that the velocity response at the waterline is 1.4 times the highest ice velocity. This should assure conservative results in terms of the structural response.

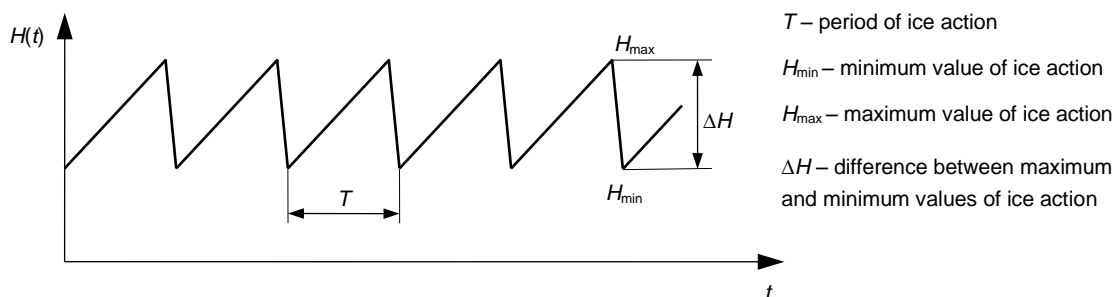


Figure 9-1 Ice load history for frequency lock-in conditions.

A cone at the waterline can reduce the magnitude of ice-induced vibrations relative to the analogous vertical structure. However, structures with narrow cones at the waterline can still experience ice-induced vibrations. The vibrations are enhanced when stable ice rubble does not form on the front face of the cone. The time history for this kind of ice action is presented in Figure 9-2. The dynamic response of the structure excited by this random forcing function is less than for an analogous structure due to frequency lock-in on an analogous vertical structure.

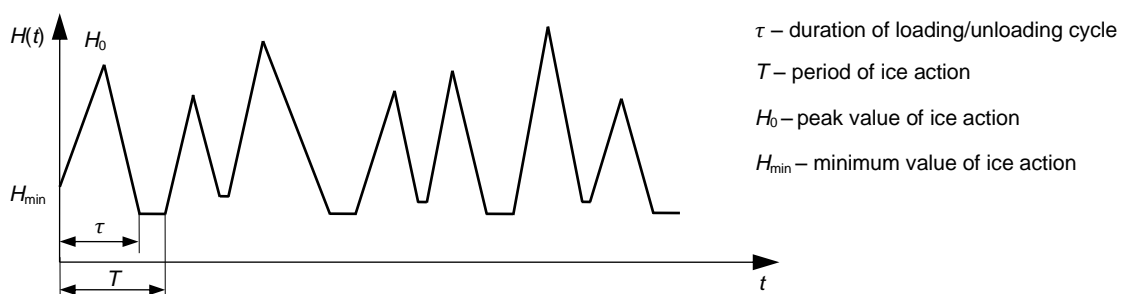


Figure 9-2 Time history of horizontal force component of ice load acting on a conical structure.

The time-varying action, $H(t)$, is a function of several parameters, including the width of the structure, slope angle and the frictional actions involved.

The dynamic behaviour of ice introduced vibrations are further described in the guidelines from ISO 19906 [103] Section A.8.2.6.1.1, A.8.2.6.1.2 and A.8.2.6.1.3, that are included in the following.

A.8.2.6 Dynamic ice actions

A.8.2.6.1 Dynamic actions on vertical and near-vertical structures

A.8.2.6.1.1 General

Ice-induced vibration is observed for practically all vertical and near-vertical fixed structures exposed to moving ice conditions, such as production platforms in Cook Inlet, the Bohai Sea and the Sea of Okhotsk and lighthouses and light piers in the Baltic Sea. Severity of observed ice-induced vibration varies significantly depending on structural properties and ice conditions.

Ice-induced vibration is observed when the ice fails predominantly by crushing. Figure A.8-30 illustrates the three primary modes of interaction in terms of the ice action, $F(t)$, and the corresponding structural displacement at the ice action point, $u(t)$. These loading traces are typical for vertical and near-vertical piles or multi-legged structures. The dynamic ice-structure interaction process is influenced significantly, but not exclusively, by the ice velocity and the waterline displacement of the structure. As a result, the three modes are not necessarily observed for all structures. In general, all three dynamic ice-structure interaction modes are observed for narrow vertical structures. For wide structures, intermittent crushing has been observed in severe ice conditions^[186]. The processes involved in these three modes of interaction are described in A.8.2.6.1.2.

The structural response in the three primary modes of interaction is important primarily for FLS design. The challenge for FLS design is to determine the combinations of ice drift velocities and ice properties for which each of the three modes can be expected to develop. Guidance for determining velocity ranges associated with frequency lock-in can be found in References [187], [188] and [189]. One aspect of this process is the potential decrease in the load borne by the ice as the ice velocity relative to the structure increases^{[188][189]}.

Frequency lock-in can cause resonant loading and can contribute significantly to fatigue accumulation in structures. This dynamic loading state can cause low-cycle fatigue in steel structures and can also cause liquefaction in the soil foundation. Vibrations can also affect topsides structures, such as flare booms, see 15.1.1.3. The vulnerability of structures to frequency lock-in is addressed in A.8.2.6.1.4.

Once the expected modes of interaction are identified for a structure, the structural response can be determined:

- based on ice action data from a similar structure in similar ice conditions;
- using prescribed force-time histories applied to finite-element or other types of structural dynamics models;
- using numerically-generated loading based on a knowledge of ice mechanics applied to finite-element or other types of structural dynamics models.

In the case of intermittent crushing, the ice action peaks can also be important for ULS design.

When ice action data from other structures are applied, it is emphasized that the dynamic interaction problem is strongly non-linear which puts stringent requirements on the similarity. With numerically-generated loading it is emphasized that different theories regarding the development of ice-induced vibration can result in different predictions. Prescribed force-time histories are given in A.8.2.6.1.3 for intermittent crushing and in A.8.2.6.1.5 for frequency lock-in.

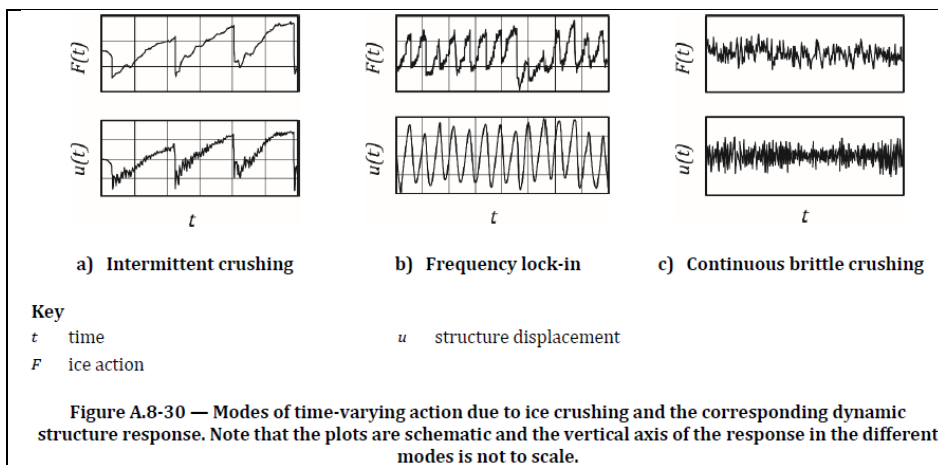


Figure 9-3 ISO 19906 [103] Section A.8.2.6.1.1 Dynamic ice actions.

A.8.2.6.1.2 Time-varying interaction processes

Intermittent ice crushing, depicted in Figure A.8-30 a), can arise if a compliant structure is exposed to actions from slowly moving ice. The interaction involves load build-up and unloading phases.

During the loading phase, the ice action increases and ice edge contact increases due to local crushing and ductile deformations. The velocity of the structure at the waterline is approximately the ice velocity. Elastic energy accumulates in the structure until local brittle ice failure occurs at the edge of the contact area, which spreads quickly to the entire loaded contact area. During the subsequent ice crushing phase, the structure springs back as the elastic energy of the structure is dissipated in ice crushing and converted into kinetic energy. The responses for the dominant structural modes tend to decay before the next cycle starts.

The structure displacement and ice action time histories at the waterline typically display a sawtooth pattern, growing linearly prior to a rapid unloading phase. A double-stroke waveform has also been observed in full-scale data^[190], with the translational and tilting modes of the superstructure both contributing to the process.

Frequency lock-in, depicted in Figure A.8-30 b), can occur at intermediate ice speeds, with typical speeds for Baltic Sea structures ranging from 0,04 m/s to 0,1 m/s. In this case, the ice failure frequency in crushing adapts to one of the lowest natural frequencies of the structure. Particularly for circumstances with low structural and foundation damping, structural response can be amplified significantly due to resonant behaviour. The period between subsequent sudden ice crushing failures and the amplification depends on the ice properties, the ice velocity and the dynamic properties of the structure. Similar to intermittent crushing, frequency lock-in exhibits alternating phases of ductile loading and brittle unloading.

For frequency lock-in, the motion of the structure is close to sinusoidal while the time history of the ice action depends on the characteristics of both the ice and the structure. Based on field experience, structures with a lowest natural frequency in the range of 0,4 Hz to 10 Hz have experienced frequency lock-in when the total structural damping (as a fraction of critical) has been low.

Continuous brittle crushing, Fig. A.8-30 c) shows typical records of the ice action and the structural displacement response at ice velocities well above the maximum velocity for which frequency lock-in occurs. In this case, both the ice action and the response of the structure are random. The response of the structure can be calculated in the frequency domain using the power spectral density for the random ice action.

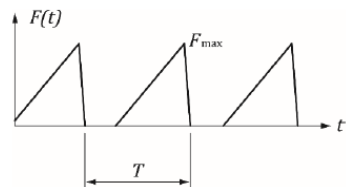
Figure 9-4 ISO 19906 [103] Section A.8.2.6.1.2 Time-varying interaction process.

A.8.2.6.1.3 Dynamic response to intermittent crushing

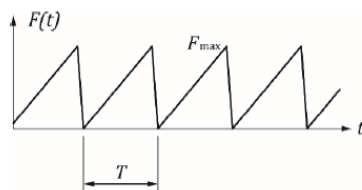
Figure A.8-31 shows idealized time histories of ice actions that can arise due to intermittent crushing. The ice action build-up and failure cycle period, T , of the ice action is much longer than the longest natural period of the structure. The time history shown in Figure A.8-31 a) can also arise from an ice spalling failure mode where the period, T , of the ice action is longer than the duration of the loading/unloading cycle.

General-purpose FE software can be used to calculate the response of the structure due to these assumed repeating ice actions. The peak action, F_{max} , can be determined by the method described in A.8.2.4.3 as the static global ice action, F_G . For an FLS analysis, the period, T , can be assumed to decrease linearly with increasing ice velocity until a velocity is reached at which frequency lock-in is expected to develop. The number of load cycles can be estimated by dividing the ice movement distance at each ice thickness by the static deflection of the structure for the ice thickness in question.

The dynamic analysis is focused on effects of the decaying oscillations of the structure following unloading. As a result, it is often sufficient to determine the response to a single loading cycle.



a) Period of ice action greater than duration of loading/unloading cycle



b) Period of ice action equal to duration of loading/unloading cycle

Key

t time F_{max} maximum value of ice action
 F ice action T period of ice action

NOTE Both F_{max} and T can vary randomly

Figure A.8-31 — Idealized time histories of the ice action due to intermittent crushing

Figure 9-5 ISO 19906 [103] Section A.8.2.6.1.3 Dynamic response to intermittent crushing.

Loads from shock impact of a large ice floe should be checked with a transient load approach as suggested below.

$$H(t) = kUt \quad \text{for } t \leq \frac{H_d}{kU}$$

$$H(t) = \begin{cases} 0 \\ \text{or } H_d \end{cases} \quad \text{for } t > \frac{H_d}{kU} \quad (8.8)$$

Where:

U is the impact velocity,
 t is the time,
 k is the stiffness of the structure at the waterline.

Recommendations for detailed design:

Above formulas represents a simplified safe methodology to assess dynamic ice loads.

For a nearby project called Baltic 2 (Kriegers Flak D) a more advanced methodology was applied:

For cone structures ice load time series were produced based on ice model tests time series from a research project, see Gravesen et al (2003) [110]. It was realised that the corresponding ice model tests results for vertical structures were not reliable probably due to a to large model ice flexibility.

For vertical structures a model calibrated based on ice field tests is required.

Kärna (2008) [112] developed an integrated stochastic model of ice load and turbine dynamics. The results from this model have been applied for vertical structures in Baltic 2 as illustrated in Kärna et al (2010) [113] and in Gravesen, Helkjaer and Kärna (2011) [114] The key assumption is a stochastic ice crushing load as sketched in Figure 9-6 below:

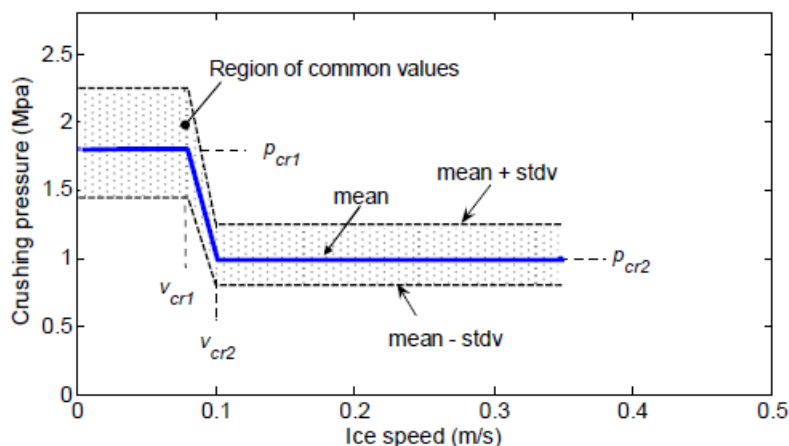


Figure 9-6 Mean value of the full-thickness ice pressure as a function of relative ice speed (ice speed relative to foundation speed)[112].

For Kriegers Flak DK a model developed by Hayo Hendrikse was used for monopiles without cones, see Willems and Hendrikse (2019) [116].

But in addition to the required more advanced modelling of ice crushing, it is important to understand that the ice field measurements are showing relative few periods with lock-in between the ice load and the structure vibrations. So there exist in practice not the stationary conditions assumed in the simplified models proposed in the standards. This aspect is important for the design because it means that ice fatigue loads are overestimated if the simplified models are used for detailed design.

It is proposed that both the extreme ice loads as well as the fatigue ice loads are estimated by a dynamic ice load simulation including the structural and damping conditions of the structure loaded by an advanced ice load like in the

models from Kärna and Hendrikse. Account to lack of stationary lock-in should be included.

Reference is also made to the comments in Annex D. Here it is discussed when the wind turbine is idling (mainly due to $U_{nacelle}$ less than 4 m/s, but account should also be given to other events without power production or with a high misalignment between wind direction and ice drift direction). This is because the 1 mode damping then usually is assumed to be say 2% instead of saying 7 % for 1 mode oscillations when the wind turbine is in operation (due to aerodynamic damping).

The conditions are further complicated by that the maximum ice forces from ice floes of importance for mainly fatigue occurs for $V_{ice} < 0.1$ m/s. But with that low incident velocity at least vertical structure has a large resistance so the ice floes are stopped after a limited penetration and few force oscillations. This occurs even though a certain amount of ice rubble behind the design ice floe can give a limited contribution to increased penetration and more oscillation on the ice force. Rough estimates of potential scenarios are mentioned in Section 4.5.

10 Ice ridges

Ice ridges generated by the nearshore effect or ice packing are expected to occur in ice winters. It is further found relevant to evaluate the ice ridge generation by the blocking effect from the wind turbine foundations in the wind farm and eventual neighbouring wind farms.

In general, ice engineering is based on few field measurements typically made in regions with severe sea ice. In the best case the standards include estimates of characteristic values, the uncertainties to these and the actual probability are not defined. For the Bornholm I and II OWF region, the sea ice occurrence is moderate, and the ice parameters shall be selected based on these less consistent design parameters. For ice ridge design this includes selection of: basic ice thickness and assumed thickness of consolidated layer, assumed ice floe maximum size, etc.

The selected characteristic parameters for the ridge design are found in accordance with recommendations in ISO 19906 [103].

The estimated ice ridge properties are based on ice analysis for wind farms located in the south-western part of the Baltic Sea ref. [119]. The ice conditions in this area are considered similar to the area at Bornholm I and II OWF.

Bornholm I and II OWF will be located near other offshore wind farms and more will be added in the future, see Figure 10-1. The wind farm is assumed to be exposed to ice ridge creation from any direction.

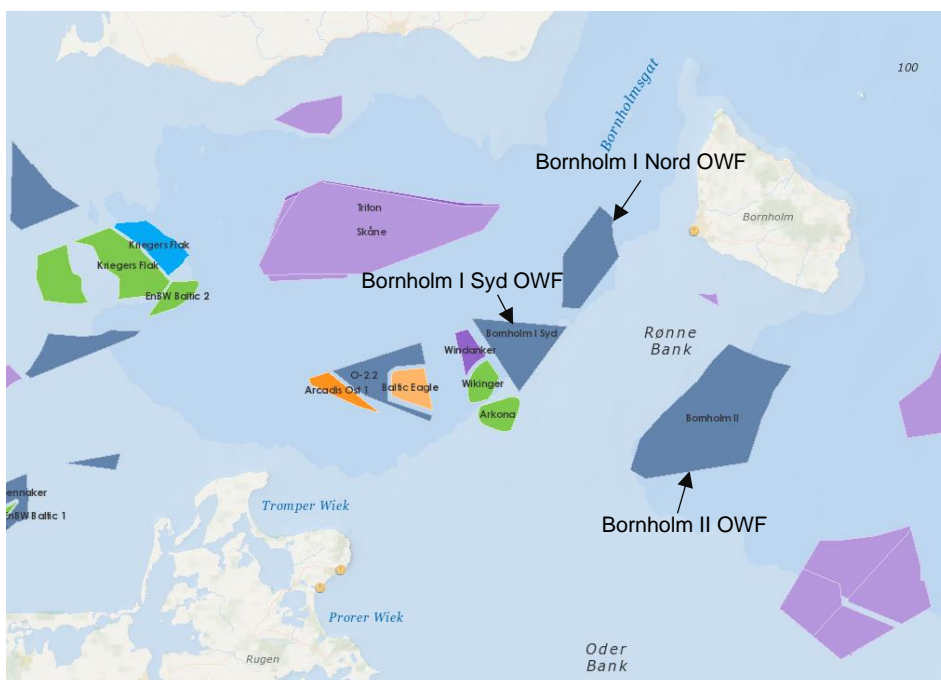


Figure 10-1 Planned offshore windfarms near Bornholm I and II OWF (www.4coffshore.com, 15-06-2023). Colour description: purple: concept/early planning, grey: development zone, blue: consent authorised, orange: under construction and green: fully commissioned.

It can be assumed that a substantial number of foundations will add to the generation of ice ridges no matter of the direction of the ice movement in the

Bornholm I and II OWF. When neighbouring windfarms are built, the blocking effects from a large number of additional foundations shall be included.

10.1 Ice ridge generation pressure

The ice ridge generation pressure can be derived from ISO 19906 [103] Section A.8.2.4.6 which include an equation (A.8-65) for ice ridge generation pressure. It shall be commented that the ice ridge generation method of ISO 19906 [103] is based on ice thickness of 1 m and above. For the Bornholm I and II OWF projects the ice thickness is less 0.15 m – 0.35 m and it is not verified that the method can be used directly for the actual case.

A general expression for the ridge-building action is given by Formula (A.8-65):

$$p_D = R h^{1,25} D^{-0,54} \quad (\text{A.8-65})$$

where

- p_D is the ridge-building action per unit width, expressed in meganewtons per metre;
- h is the thickness of the ice sheet acting on the thicker ice feature, expressed in metres;
- D is the width of the thicker ice feature, expressed in metres;
- R is a coefficient, see Figure A.8-21.

Figure 10-2 Ridge building equation ref. ISO 19906 [103].

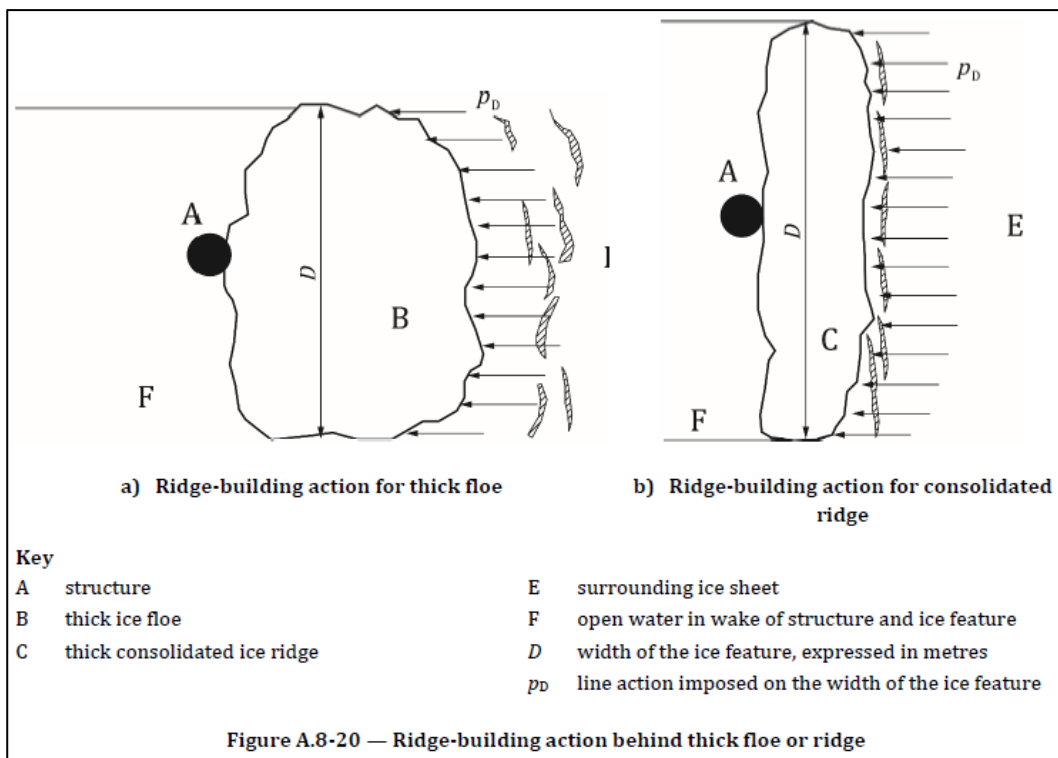


Figure 10-3 Ridge building action illustration ref. ISO 19906 [103].

10.2 Design loads for ice ridge

The ice ridge loads can be calculated according to ISO 19906 [103] Section A.8.2.4.5.1 equation A.8-49.

An accurate, theoretical determination of the actions caused by ice ridges is difficult. An upper bound estimation of the horizontal action caused by a FY ridge, F_R , can be obtained as given by Formula (A.8-49):

$$F_R = F_c + F_k \quad (\text{A.8-49})$$

where

F_c is the action component due to the consolidated part of the ridge;

F_k is the keel action component.

Since the volume of the sail is small compared to that of the keel, the effects of the ridge sail can be neglected in the case of FY ridges. The action component, F_c , can be determined, as an estimate, using instructions given in A.8.2.4.3 for parameters of the consolidated layer of an ice ridge, or A.8.2.4.4 for sloping structures by substituting h_c for h .

Figure 10-4 Ridge loads ref. ISO 19906 [103].

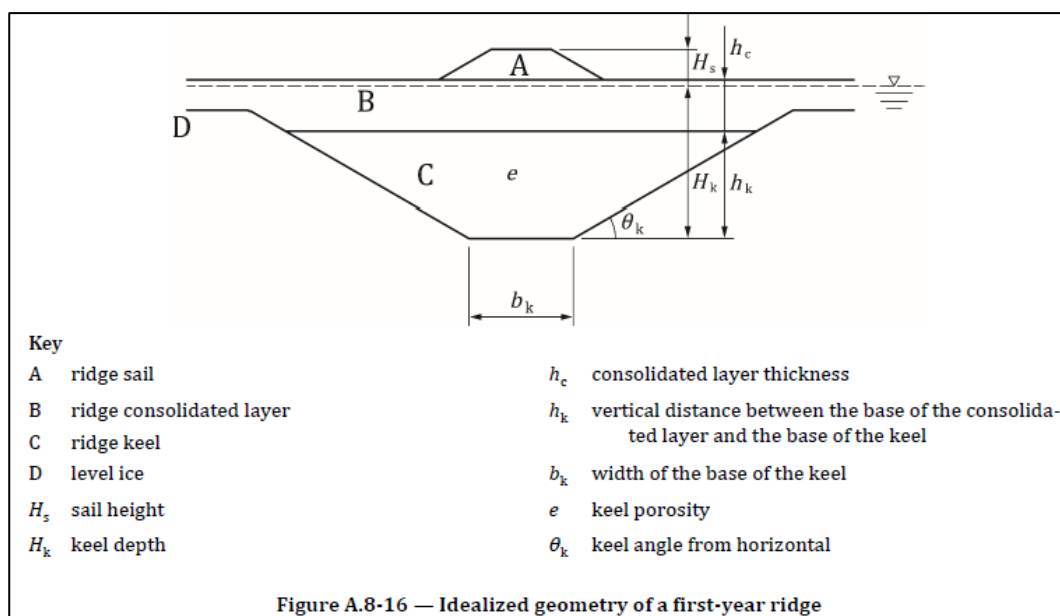


Figure 10-5 Idealised geometry of a first-year ice ridge ref. ISO 19906 [103].

Several models are available for the determination of the unconsolidated keel action component F_k . Passive failure models are generally used to determine the unconsolidated keel action component acting on vertical or inclined structures. Measurements indicate that the keel cohesion often varies from zero at the base of the keel to a maximum immediately beneath the consolidated layer. Under such conditions, the keel action can be determined for vertical structures (see Reference [148]), with suitable modification (see Reference [149]) as given by Formulae (A.8-50) and (A.8-51):

$$F_k = \mu_\phi h_k w \left(\frac{h_k \mu_\phi \gamma_e}{2} + 2c \right) \left(1 + \frac{h_k}{6w} \right) \quad (\text{A.8-50})$$

$$\mu_\phi = \tan \left(45^\circ + \frac{\phi}{2} \right) \quad (\text{A.8-51})$$

where

μ_ϕ is the passive pressure coefficient;

ϕ is the angle of internal friction;

c is the apparent keel cohesion (an average value over the keel volume should be used);

w is the width of the structure;

γ_e is the effective buoyancy, in units consistent with c .

The effective buoyancy is given by Formula (A.8-52):

$$\gamma_e = (1 - e)(\rho_w - \rho_i)g \quad (\text{A.8-52})$$

where

e is the keel porosity;

ρ_w is the water density;

ρ_i is the ice density.

Guidance for the specification of ridge keel parameters is provided in A.8.2.8.8.

Figure 10-6 Ridge keel load equation ref. ISO 19906 [103].

Ice ridge parameter guidelines are described in ISO 19906 [103] as shown in Figure 10-7.

The sail height and the level-ice thickness are often used as key parameters to define other geometrical shape parameters. For the ridge profile shown in Figure A.8-16, typical relationships are given as $h_c = 1,6h$, $H_k = 4,5H_s$ and $\theta_k = 26^\circ$. The width parameter can vary from $b_k = 0$ to $b_k = 5H_s$. The porosity of the ridge keel depends on the age of the ice ridge and varies in different sea areas. Some key indices of ridge shape are outlined in Reference [147].

The thickness parameters h_c and H_k depend on geographical location. Thicker consolidated layers and keels develop in highly dynamic sea areas due to the rafting process. Therefore, it is suggested that field data be used to specify statistical characteristics of the consolidated layer. Existing field data suggest that the parameters h_c and H_k are not correlated with each other. In the absence of field data, it can be assumed in a deterministic analysis that h_c is 2,0 times the thickness of an ice sheet that has grown in open water under the same conditions as the ice ridge.

The thickness h_c of the consolidated layer of an ice ridge is locally variable in the vicinity of the structure during an ice action. This can be considered if field data are available to create a probability distribution for the consolidated layer thickness. Using this probability distribution, an average value of the consolidated layer thickness can be determined for each event. The average value can be determined by considering the thickness variability in an area of $A = w^2$, where w is the width of the structure.

Figure 10-7 Ice ridge parameter guidelines ref. ISO 19906 [103].

Ice ridge assessment were prepared by Toumo Kärnä for the nearby Arkona OWF project in year 2012 where a consolidated layer of 45 cm and a parent ice thickness of 10 -15 cm were suggested. According to the Kriegers Flak ice ridge assessment [119] a consolidated ice thickness of 43 -67 cm is suggested and are formed of ice blocks of 20 cm in thickness. Both the Arkona and Kriegers Flak ice ridge assessments are based on data from much more severe ice locations (North Baltic Sea, Beaufort Sea, and Sea of Okhotsk). Further ice ridge measurements have not been made for OWFs where the ice is blocked by several structures located in a random structure seen from the ice. We consider the methods described in ISO 19906 [103] being very conservative with respect to ice ridge generation for Bornholm I and II OWF. But due to lack of analysis of ice ridge generation for the area of Bornholm I and II OWF it is suggested to specify the ice ridge parameters in line with ISO 19906.

Consolidated layer thickness: $h_{c50y} = 0.3 * 1.6 = 0.48$ m

Consolidated layer thickness: $h_{c100y} = 0.34 * 1.6 = 0.54$ m

Parent ice floe thickness: $h_p = 0.2$ m (usually assumed to be $h_c/3$)

Sail Height: $h_s = 4.2 * \sqrt{h_p = 0.2} = 1.88$ m

Keel depth: $h_k = 4.5 * 1.88 = 8.45$ m

The ice keel porosity has been measured to reduce from 0.45 to 0.29 in a month for a newly generated ice keel. A design value of 0.35 ref. [108] is suggested for a ten to fifteen days old ridge.

The internal friction and keel cohesion are selected based on the investigations as listed in ref. [108] "Table 4 Summary of Strength Properties of Ice Rubble" and discussions in ref. [108] for moderate sea ice conditions as considered for the Bornholm I and II OWF location.

Suggested parameters for the ice ridge loads for 1/50y and 1/100y case:

- Thickness of consolidated layer (1/50y): $h_c = 0.48$ m
- Thickness of consolidated layer (1/100y): $h_c = 0.54$ m
- Depth of the ridge keel: $H_k = 8.45$ m
- Keel porosity: $e = 0.35$
- Internal friction of the keel: $\varphi = 30^\circ$
- Keel cohesion: $c = 5$ kPa

Due to the relative short period with critical ice conditions, we estimate that the strength of the consolidated layer is corresponding to the generated ice sheet layer and not the assumed thickness of the consolidated layer.

Please be aware that for a down-bending cone the forces from breaking the consolidated layer is increased due to the rubbles in the ridge so this force component is approximately equal to the force component from an up-bending cone, see Croasdale et al 2019 [109].

The overall analysis shows in general (Annex B) that all foundations in Bornholm I and II OWF has a risk of being exposed to ice ridges, so ice ridge is a standard design case.

In the case that Bornholm I and II OWF foundations are constructed with cones the risk of ice ridge generation is reduced. Surrounding wind farm with foundations constructed without cones will increase the risk of ice ridge generation.

11 Icing (marine and atmospheric)

Ice accretion (or icing) refers to the accumulation of ice or snow on a structure. Icing can be categorised into two types: the atmospheric icing and the marine icing. Atmospheric icing includes freezing rain, supercooled fog, and snow, while marine icing mainly occurs by freezing sea spray from breaking waves and/or strong winds blowing over the sea surface. Atmospheric icing occurs when rain, fog, or snow freezes upon contact with a surface.

Required conditions for atmospheric icing are low air temperatures between -20°C and 0°C combined with low wind speeds (less than 10 m/s).

Marine icing occurs when sea spray from breaking waves or strong wind blowing over the sea surface freezes upon the contact with a surface. Required conditions for marine icing are wind speed greater than 10 m/s, air temperatures less than the freezing point of seawater, i.e. -0.4°C and sea surface temperature smaller than 8°C.

The occurrence of atmospheric icing in Europe is shown on Figure 11-1. It is assessed that the nearby onshore conditions for atmospheric icing can be extended to Bornholm I and II OWF. Hence the risk of atmospheric icing is moderate, corresponding to 2-7 days/year.

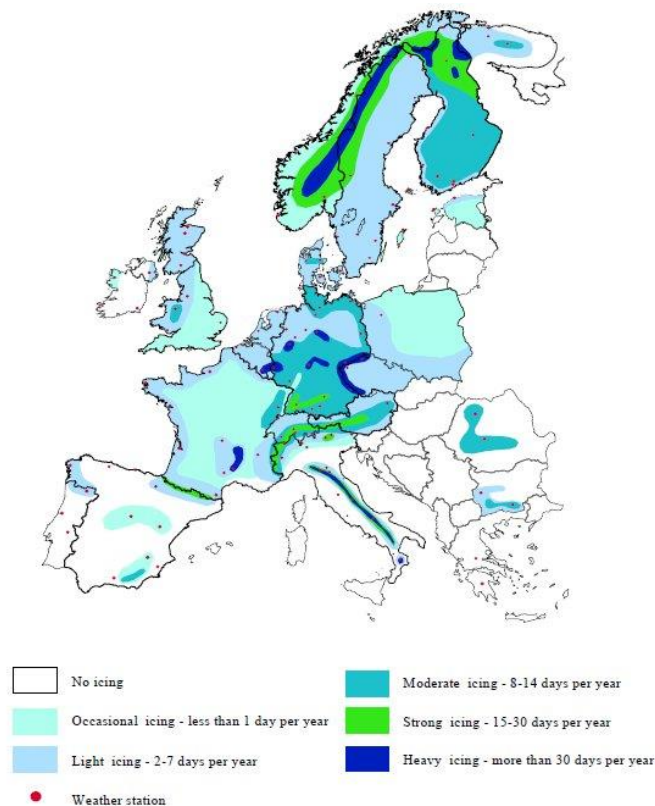


Figure 11-1 Atmospheric icing map of Europe.

Table 11-1 Type of snow or ice ref. DNV-ST-0437, [101].

Type of snow or ice	Area	Thickness and density
Marine icing Ice from freezing sea spray.	At sea level to highest wave elevation: From highest wave elevation: Linearly reduced up to +60mMSL:	100 mm 100 mm 0 mm Density: 850 kg/m ³
Atmospheric icing	In the full height of the structure from the water surface to the top of the WTG tower, nacelle, and blades.	Thickness: 30mm, Density: 700 kg/m ³

The recommended praxis DNV-RP-0175 [111] can be used for designing issues related to icing. However, this recommendation is not fully aligned with the load standard DNV-ST-0437 [101] and it is recommended to follow [101] where discrepancies are found.

For atmospheric icing on WTG blades, it is recommended to follow DNV-ST-0437 [101] ref. Figure 11-2.

With the rotor rotating under in-cloud icing conditions, the cases "ice formation on all rotor blades" and "ice formation on all rotor blades except one" shall be investigated. The mass distribution (mass/unit length) shall be assumed at the leading edge. It increases linearly from zero in the rotor axis to the value μ_E at half the radius, and then remains constant up to the outermost radius. The value μ_E is calculated as follows:

$$\mu_E = \rho_E \cdot k \cdot c_{min} (c_{max} + c_{min}) \quad (2.39)$$

where:

- μ_E = mass distribution on the leading edge of the rotor blade at half the rotor radius [kg/m]
- ρ_E = density of the ice (900 kg/m³)
- k = $0,00675 + 0,3 \exp(-0,32 R/R_1)$
- R = rotor radius
- R_1 = 1 m
- c_{max} = maximum chord length
- c_{min} = chord length at the blade tip, linearly extrapolated from the blade contour

Figure 11-2 Atmospheric icing for WTG blades ref. DNV-ST-0437 [101].

12 Design load cases

Ice loads shall be evaluated for different ice load situations according to IEC 61400-3-1 [102] Table 3 as copied in Table 12-1 below. Identical listing of design loads for ice conditions can be found in DNV-ST-0437 [101]. The DNV-RP-0175 [111] provides additional recommendations to consider for the ice loads assumptions. To perform the load analysis, wind turbine loads shall be combined with the ice loads on the support structure as specified in Table 12-1 and Table 12-2. In this report the ice load input is provided to enable the foundation designer to perform the required analysis of the combined model.

Table 12-1 Ice design load cases (DLC) according to IEC 61400-3-1 [102] (Table 3).

Table 3 – Design load cases for sea/lake ice

Design situation	DLC	Ice condition	Wind condition	Water level	Type of analysis	Partial safety factor
Power production	D1	Horizontal load from temperature fluctuations	NTM $V_{hub} = V_r \pm 2 \text{ m/s}$ and V_{out} Wind speed resulting in maximum thrust	NWLR	U	N
	D2	Horizontal load from water level fluctuations or arch effects	NTM $V_{hub} = V_r \pm 2 \text{ m/s}$ and V_{out} Wind speed resulting in maximum thrust	NWLR	U	N
	D3	Horizontal load from moving ice at relevant velocities $h = h_{50}$ or largest value of moving ice.	NTM $V_{in} < V_{hub} < V_{out}$	NWLR	U	N
	D4	Horizontal load from moving ice at relevant velocities <i>Use values of h corresponding to expected history of moving ice occurring.</i>	NTM $V_{in} < V_{hub} < V_{out}$	NWLR	F	*
	D5	Vertical force from fast ice covers due to water level fluctuations	No wind load applied	NWLR	U	N
Parked	D6	Pressure from hummocked ice and ice ridges	EWM Turbulent wind model $V_{hub} = V_1$	NWLR	U	N
	D7	Horizontal load from moving ice at relevant velocities <i>Use values of h corresponding to expected history of moving ice occurring.</i>	NTM $V_{hub} < 0,7 V_{ref}$	NWLR	F	*
	D8	Horizontal load from moving ice at relevant velocities $h = h_{50}$ or largest value of moving ice.	EWM Turbulent wind model $V_{hub} = V_1$	NWLR	U	N

To be added: DLC D9 Power production (as defined in Table 12-2, from DNV-RP-0175 (Table 3-1), [111]). Pressure from hummocked ice and ice ridges. Most situation where pressure from hummocked ice and ice ridges may occur is corresponding to Power production.

In the following, an initial assessment of the design load cases (DLC's) are made though without knowledge about the wind turbine to be mounted on the foundation. Any of the DLC's [102] can be design driving; however, DLC D1 and DLC D5 are likely not design driving due to the moderate water level and

temperature variations. For the Ultimate Limit State (ULS) DLC the ice load input in Table 1-1 is provided for calculation of DLC D2, D3, D5 and D6. DLC D3 is most likely dominant relative to DLC D6 due to the higher shear loads from a running turbine. Loads from passing or service vessels shall be taken into consideration.

Dynamic ice load analysis ref. Section 9.4 shall be carried out to check the load response. It is required to carry out dynamic analyses including an integrated dynamic model for DLC D3, D4, D6 and D7 based upon the load matrix. This calculation shall preferably be carried out by the WTG supplier to integrate the sea ice dynamic with the WTG dynamic model.

For a monopile structure without ice cone it is recommended to carry out model simulation analysis with dynamic ice crushing for all important frequencies of ice and structure interaction and the associated damping estimates. At present the Vanilla model is assumed to be most accurate. It is necessary to carefully evaluate how to treat the non-linearities and associated plastic deformation in the soil support, in case this leads to changed stiffness of the structure during the load simulation.

The main conclusion from other ice load calculation projects is that the major ice loads for vertical structures is ice loads from intermittent ice crushing or frequency lock-in. It only occurs with an ice floe velocity between 0.01 and 0.06 m/s (Figure 13-5). Continuous crushing results in ice forces much lower (order of magnitude 50 %) and with very limited fatigue components (Figure 13-5). So load case Table 12-1 can be misleading for vertical structures with respect to the load cases (D3, D4, D7 and D8). It has been seen from recent projects that the cases where the ice floe velocity is between 0.01 and 0.06 m/s are very rare been in the order of 1-10 events of 10 minutes during the foundation lifetime. So, the load cases with maximum ice load have a character of an accidental load case rather than an ULS case, but this must be proven in detailed design. Further, it is very likely that more critical ULS events only may occur for a design ice thickness 10-20% lower than the 50 year ice thickness, see Gravesen et al ref. [123] Ice drift and ice action on offshore wind farm structures.

Ice ridges load are assumed to be quasistatic as the rubble parts of the ice ridge are assumed to induce damping of the structure and consequently the dynamic effect may be disregarded.

Table 12-2 Additional load case for icing during operation according to DNV-RP-0175 Table 3-1 [111].

<i>DLC</i>	<i>Wind Conditions</i>	<i>Icing conditions</i>	<i>Load evaluation</i>	<i>Partial safety factor for loads</i>
13.1 Power production under icing conditions	NTM* $v_{in} < v_{hub} < v_{out}$	Icing modelling according to ice class	F (fatigue) U (ultimate)	N*
*defined according to DNVGL-ST-0437, IEC 61400-1, IEC 61400-2 and IEC 61400-3-1				

13 References

13.1 Project specific documents

- [1]. Energy Island Baltic Sea, Metocean Assessment Part A: Description and Verification of Data Basis, IO Number 4500092960, DHI, 2024-02-07.
- [2]. Climatological Ice Atlas for the western and southern Baltic Sea (1961-2010), ISBN-Nr. 978-3-86987-278-0, BSH-Nr. 2338. 2012, BSH
- [3]. BSH Ice reports and charts. Link: [BSH - Eisberichte und Eiskarten](#)
- [4]. Ice observation reports for the Danish waters from year 1861 to year 2019. SOK, Last one for the winter 2018-2019, ISSN 0106-5076
- [5]. Climatological Ice Atlas for the Kattegat, Kattegat, Skagerrak and Lake Vänern (1963-1979), SMHI, Swedish Meteorological and Hydrological Institute 1982.
- [6]. Bundesamt für Seeschifffahrt und Hydrographie, "Climatological Ice Atlas for the Western and Southern Baltic Sea (1961-2010)," 2012.
- [7]. State and Evolution of the Baltic Sea, 1952-2005, Rainer Feistel, Günther Nausch, Norbert Wasmund, April 2008
- [8]. Havis – Isobservationer, SMHI, Swedish Meteorological and Hydrological Institute. Link:<https://www.smhi.se/data/oceanografi/havis> (Last visited: 27.04.2023)
- [9]. NORA3, Oseanografi og maritim meteorologi, Link: <https://marine.met.no/node/19> (Last visited: 06.09.2023)

13.2 Normative and general references

- [101]. DNV-ST-0437, Loads and site conditions for wind turbines, DNV-GL, November 2016, Amended in November 2021.
- [102]. IEC International Standard, IEC 61400-3-1, Wind Turbines – Part 3: Design Requirements for offshore wind turbines, IEC. 2019.
- [103]. ISO 19906:2019 Petroleum and natural gas industries - Arctic offshore structures. 2019.
- [104]. Offshore Installations, IV Part 6, Chapter 7, Oil and Gas, Guidelines for the Construction of Fixed Offshore Installations in Ice Infested Waters, Germanisher Lloyd. GL Edition 2005.
- [105]. POAC 09, Ice Loads for Offshore Wind Turbines in Southern Kattegat. June 2009, Paper by: Helge Gravesen and Tuomo Kärnä.
- [106]. POAC 1993, Factors influencing the coefficient of friction between sea ice and various materials. Nakazawa et al. 1993.
- [107]. PERD/CHC Report 3-49, HYD-TR-067, Friction of Sea Ice on Various Construction Materials. Frederking, R. and Barker, A. Ottawa, Canada. 2001.
- [108]. An overview of first-year sea ice ridges, HYD-TR-047, PERD/CHC Report 5-112, August 2000.
- [109]. POAC 2019, Ice load signatures for ridge action on wind turbines with conical collars, Croasdale, K, Thijssen, J. and Allyn, N, Delft. The Netherlands. 2019.
- [110]. POAC 2003, Ice forces to wind turbine foundations in Denmark. Gravesen, H., Pedersen, B., Sørensen, S.L., and Vølund. P. Trondheim, Norway. Paper No. 187 (2003)
- [111]. DNV-RP-0175. Recommended Practice. Icing of wind turbines, December 2017, Amended in October 2021.

- [112]. Kärnä, T. (2008): Ice-induced vibrations of slender structures. In: Fransson, L. (ed.). Ice Mechanics and Shipping in Ice-infested waters. Luleå University of Technology. (2008)
- [113]. Kärnä, T., Gravesen, H., Fransson, L., and Løset, S. (2010): Simulation of multi-modal vibrations due to ice actions. 20th IAHR Intern. Symp. On Ice. Lahti, Fin-land. June 14-18th, 2010.
- [114]. Gravesen, H., Helkjær, A. and Kärnä, T. (2011): Improved practical ice load design methods for wind foundations. European Offshore Wind (EOW'11). PO 342. Amsterdam
- [115]. Nord, T. et al (incl. Hendrikse H.) (2018): Ice induced vibrations in the Nordstrømsgrund Lighthouse. Cold Region Technology 155/2018, pp 237-251.
- [116]. Willems, T., Hendrikse, H. (2019): Coupled simulation of ice structure interaction for offshore wind turbines in BHawc using Vanilla. Poac 2019. The Netherland.
- [117]. Owen, C.C., and Hendrikse, H. (2019): A study of the transition ice speed from intermittent crushing to frequency lock-in vibrations based on model-scale experiments. POAC 2019, Delft. The Netherlands.
- [118]. DMI. Future climate changes in Denmark (Danish language). Report no. 6 (2014).
- [119]. Tikanmäki M, Heinonen, J (2021). Estimating extreme level ice and ridge thickness for offshore wind turbine design: Case study Kriegers Flak. Doc.:10.1002/we.2690, 19/2 2021, Wiley
- [120]. POAC11-064, Data for crushing formula, T. Kärnä, D.M. Masterson, July 2011
- [121]. Hav- og Fiskeribiologi, Siz Madsen, Fiskericirklen, ISBN 87-90749-08-1, 2008
- [122]. Deutscher Wetterdienst, "German Climate Atlas," [Online]. Available: https://www.dwd.de/EN/climate_environment/climateatlas/climateatlas_node.html. [Accessed 15 09 2022].
- [123]. Ice drift and ice action on offshore wind farm structures, paper submitted to POAC'23. Glasgow. United Kingdom June 2023, Gravesen, H., Jørgensen, L.B., Høyland, K.V., and Svend Bicker, S. (2023).

Annex A Recorded ice data, Area 16

Figure 13-1 shows location of areas in the Baltic Sea, Kattegat, Skagerrak and Lake Vänern where ice thickness distribution is detailed recorded, ref. the Swedish Ice Atlas [5]. Comparison with Area 16 is made in Section 4.2 since this is the nearest location with detailed recorded ice conditions.

Ice thickness distribution areas
 Områden för vilka istjockleksfördelningen beräknats
 Jään paksuuden jakautumia vastaavat alueet

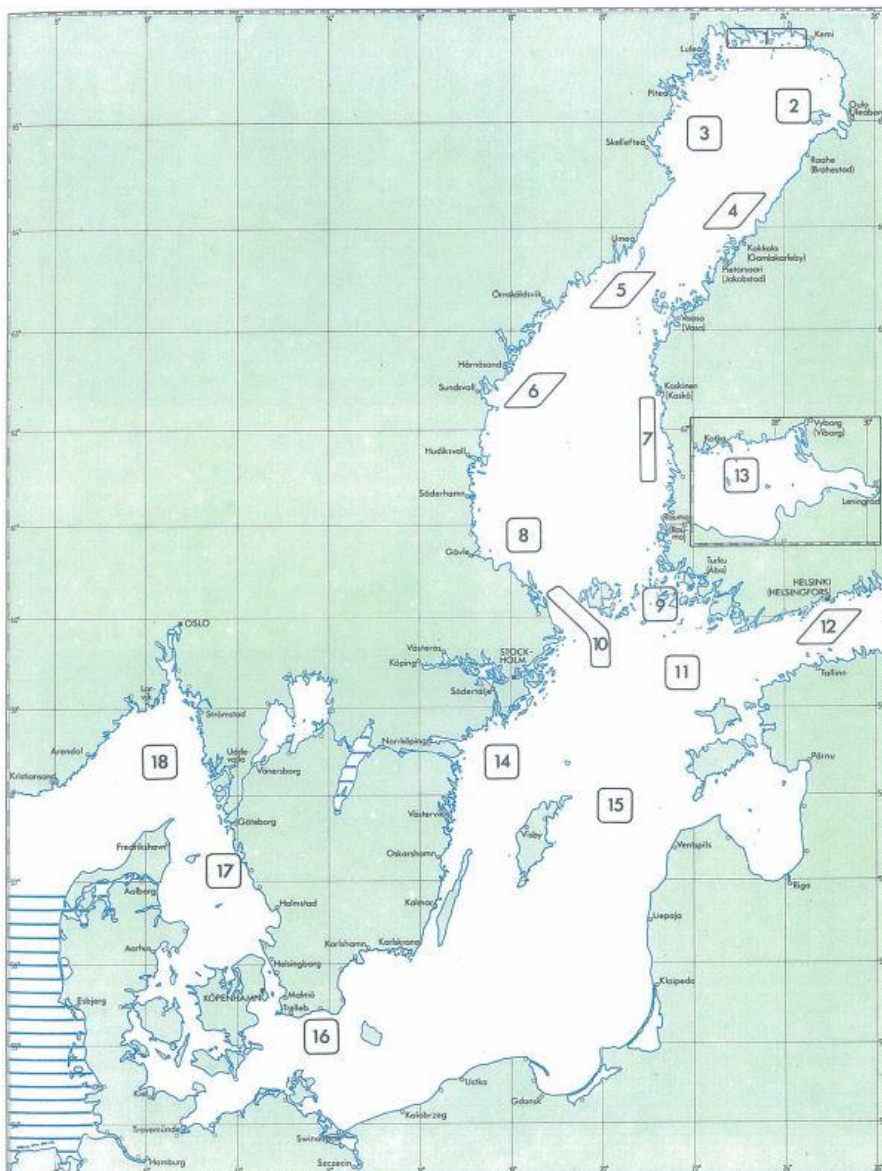


Figure 13-1 Numbered regions for calculated ice thickness distribution, [5].

For area 16 the distributions of ice thickness are further given in tabular form, which is shown in Table 13-1, [5], where probabilities over the cases with ice are given in percentage for nine thickness classes and mean level ice thickness in

cm are listed. In the top of the table are listed the given month and date to which the distribution of ice thickness is given. Furthermore, also the number of years with data and the number of thickness values used for estimating the distribution is listed in the table at the bottom.

Table 13-1 Table for Area 16 for calculated ice thickness distribution, [5].

Area 16

Day	1	11	21	1	11	21	1	11	21	1	11	21	1	11	21	1	11	21	1	11	21	1
Month	11	11	11	12	12	12	1	1	1	2	2	2	3	3	3	4	4	4	5	5	5	6
Ice frequency	0	0	0	0	0	0	0	0	0	5	5	13	17	16	17	10	7	3	0	0	0	0
Thickness																						
1- 2 cm	0	0	0	0	0	0	0	0	0	0	0	0	0	0	0	0	0	0	0	0	0	0
3- 6 cm	0	0	0	0	0	0	0	0	0	100	23	35	10	32	9	75	100	0	0	0	0	0
7-12 cm	0	0	0	0	0	0	0	0	0	0	77	60	60	58	82	25	0	0	0	0	0	0
13-20 cm	0	0	0	0	0	0	0	0	0	0	0	5	30	5	9	0	0	0	0	0	0	0
21-30 cm	0	0	0	0	0	0	0	0	0	0	0	0	0	0	0	0	0	0	0	0	0	0
31-42 cm	0	0	0	0	0	0	0	0	0	0	0	0	0	0	0	0	0	0	0	0	0	0
43-56 cm	0	0	0	0	0	0	0	0	0	0	0	0	0	0	0	0	0	0	0	0	0	0
57-72 cm	0	0	0	0	0	0	0	0	0	0	0	0	0	0	0	0	0	0	0	0	0	0
> 73 cm	0	0	0	0	0	0	0	0	0	0	0	0	0	0	0	0	0	0	0	0	0	0
Mean thickness	0	0	0	0	0	0	0	0	0	4	8	8	11	9	9	5	4	0	0	0	0	0
Number of ice years	0	0	0	0	0	0	0	0	0	1	2	3	2	2	2	2	1	0	0	0	0	0
Number of data	0	0	0	0	0	0	0	0	0	1	13	20	10	19	11	8	2	0	0	0	0	0

Annex B Ice ridge case study

B.1 Ice ridge generation in a wind farm.

The blocking effect is related to the shape of the foundation and the number of foundations that add to the blocking effect and thereby the ice ridge generation. A foundation with an ice cone will break the ice and is not considered to create ice ridges.

A foundation without an ice cone will have a considerably higher blocking effect and is in special situations considered to generate ice ridges. In this annex examples of typical relevant wind turbine foundations are considered to evaluate the blocking effect. In both cases the total blocking effect is a summation of the blocking effect by the individual foundations in the direction of the ice floe.

The ice floe movement is primarily generated by the wind acting on the ice floe.

B.2 Ice blocking effect for Bornholm I and II OWF

Ice floe drift from all directions can create the ice ridge building pressure as there are minimum 3 number of foundations in a row in nearly all directions.

It can also be assumed that the distance to shore has a sufficient length, so ice ridge exposure is possible for all incident ice drift directions.

Additionally, neighbouring wind farm foundations will influence the ice blocking and ice ridge generation. There is a risk that ice ridges can be released from a neighbouring wind farm depending on the wind and current direction.

There exists no way of analysing if and when the ridges are released. It is generally assumed that the ridges most frequently are generated in periods with heavy frost and are frozen together with the ice sheet in the wind farms. The most likely release occurs with milder weather potentially associated with waves and different wind patterns.

B.3 Foundations with cones

The basis for calculating the ice ridge generating pressure is described in Section 10.

The resistance for relevant foundations (dia. 9m) with cones is typically 0.02 MN on foundation for an ice sheet of 10 cm and typically 0.042 MN for an ice sheet of 15 cm.

So, for structures with cones the ice scenario will be that the ice sheets will be pressed through the wind farm without generating a ridge. It is further considered statistically unlikely that there is a sufficient number of repeated passings of the ice sheets so the broken pieces from the cone effect can create an ice ridge.

In the case that Bornholm I and II OWF are constructed with cones and the surrounding wind farms are with vertical structures without cones it cannot be excluded that ice ridges been created from wind farms without cones can move over to Bornholm I and II OWF. It is deemed that the risk for ice ridges generated in other wind farm is moving to Bornholm I and II OWF is much lesser than if Bornholm I and II OWF are constructed without cones.

B.4 Monopiles and jackets without cones

The resistance for relevant foundations without ice cones is typically 0.9 MN for a monopile with diameter of 9 m and an ice sheet of 10 cm and typically 1.1 MN for an ice sheet of 15 cm. A jacket will have ice forces of the same order of magnitude.

This means that typically 11 foundations (range 4 to 18) are required to create the ridge generation pressure for ice thickness of 10 cm and typically 15 foundations (range 5 to 25) for an ice thickness of 15 cm, see Section 9 Ice ridges for ice ridge generation pressure. With assumed 1,5 turbines per 1500 m a wind farm with say 10 rows of foundations (range 3 to 15) can generate the ridge building pressure.

B.5 Summation of ice ridge blocking effects

The ice ridge blocking effects analysis can be summarized in Table 13-2.

Table 13-2 Numbers of foundations to create forces sufficient to ice ridges generation.

Examples of ridge blocking			Case 1	Case 2
Flow size (load length)	D	m	1500	1500
Ridge generation factor	R_{min}		2	2
Ref. ISO 19906 Figure A.8-21	R_{ave}		6	6
	R_{max}		10	10
Ice thickness	h	m	0.1	0.15
Ridge generating load acc. ISO 19906 formulae (A.8-65)				
Load minimum for R_{min}	F_{min}	MN	3.3	5.4
Load average for R_{ave}	F_{ave}	MN	9.8	16.2
Load maximum for R_{max}	F_{max}	MN	16.3	27.0
Blocking effect for structures with cones	Cone			
Blocking load per foundation	F_{cone}	MN	0.02	0.042
Number of foundations, Minimum	N_{min}		163	128
Number of foundations, Average	N_{ave}		488	385
Number of foundations, Maximum	N_{max}		813	642
Blocking effect for straight structures	Vertical			
Blocking load per foundation	F_{vert}	MN	0.9	1.1
Number of foundations, Minimum	N_{min}		4	5
Number of foundations, Average	N_{ave}		11	15
Number of foundations, Maximum	N_{max}		18	25

It is concluded that Bornholm I and II OWF has to be designed for ice ridges if constructed without cones. But mainly due to risk of ice ridges at present. The risk for that the wind farm can induce ice ridges by itself is considered limited.

Order of magnitude for Ice ridge on structure with basic diameter of 9 m:

Ice ridge keel force:	1.8 MN
Cone down-bending: by a 2 factor	0.3 MN rubble increases the load
Cone up-bending:	0.6 MN
Vertical structure consolidated layer:	2.3 MN
Total load up- or downbending cone	2.4 MN
Total load vertical structure:	4.1 MN

Annex C Discussion of dynamic ice loading scenarios

The dynamic design ice condition shall be found for:

- Idling with low damping of first system mode (this can occur due to wind velocity at nacelle less than 4 m/s, general error incl. errors at transformer stations, icing at rotor or other reasons for no production)
- power production with higher damping of first system mode
- power production with low damping of first system mode due to large misalignment

The incident kinetic energy even from larger ice floe (of km size) is very small for low V_{ice} so only a limited amount of load circles occur before the ice floe are stopped. Weak wind and current also means that it is unrealistic to assume that the required additional shear stress to an ice rubble field behind the ice floes can maintain the velocity. So at least at smaller ice velocities the ice floes are stopped within few metres penetration. During this transition until the ice floes are stopped, very different ice velocities will cause a limited number of load circles with incident ice velocities between 0 and 0.1 m/s, where the ice force is maximum.

The different scenarios have to be selected interactive with the detailed dynamic ice loading carried out interactive with the turbine model (idling or production) so the final scenarios have to await the results from the detailed modelling. Below is given some rough estimates.

Incidence of ice floes:

There does not exist information on the extend of ice rubble behind incident ice floes. A rough estimate could be that for fatigue load one assumes:

- for 70 % of the cases a 500 m ice floe with maximum 5 km open to close pack ice exposed to the shear force corresponding to the ice velocity considered ($\tau_{pa} = 3 V_{ice}^2$, vice in m/s) (no kinetic energy contribution is assumed for the pack ice)
- For 20 % of the cases a 500 m floe with 5 km area of ice floes in close contact + shear force
- For 10 % of the cases a 500 m floe with 10 km area of ice floes in close contact + shear force

For ULS a rough estimate could be a 2 km ice floe with 5 km ice rubble behind.

Incidence of ice ridges:

Apply the estimate of the ice ridge geometry only for ULS and only as a equivalent static load as the rubble in the ridge will create that large damping so there will not be coincidence of maximum ice ridge load and high dynamic ice loads from failure of the consolidated layer.

Assume a 5 km zone of ice sheet with a thickness of typical 15 cm behind the ridge. Include shear stress corresponding to the V_{ice} . Calculate which incidence ice velocities (V_{ice}) will make it possible for the ice ridge to penetrate so maximum ice ridge forces is obtained. In case the maximum ridge force can only be obtained for rare combinations of high ice velocities, the risk could be less than 1/50 y so the ice ridge design should be carried out without a partial coefficient or with reduced partial coefficients.

Owen, C.C., and Hendrikse, H. has made a study of the transition ice speed from intermittent crushing to frequency lock-in vibrations based om model-scale

experiments. [117]. From there the following four figures are included to illustrate the shift in intermittent crushing, frequency lock-in and continuous brittle crushing during ice floe movements.

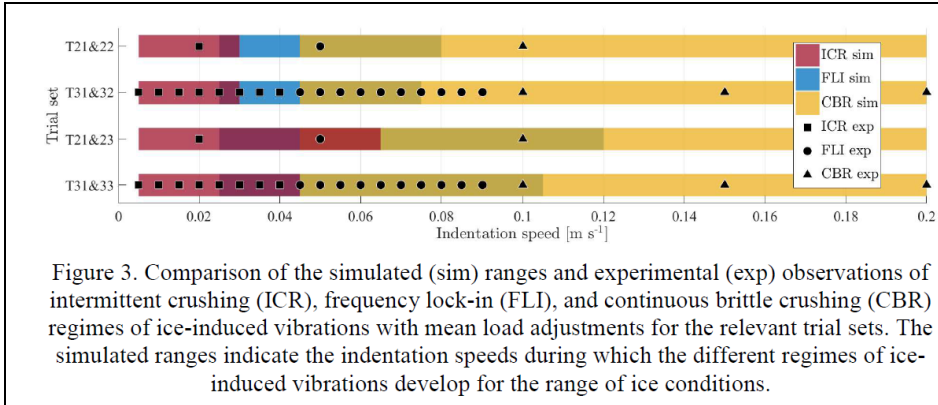


Figure 13-2 Comparison of simulated and experimental observations. [117] Figure 3.

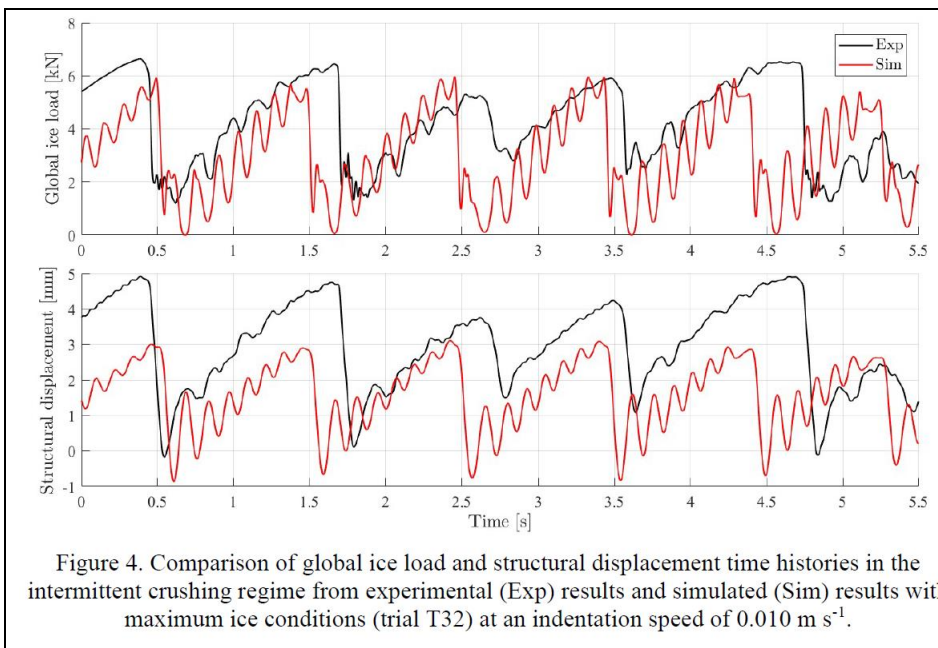


Figure 13-3 Comparison of global ice load and structural displacement. [117] Figure 4.

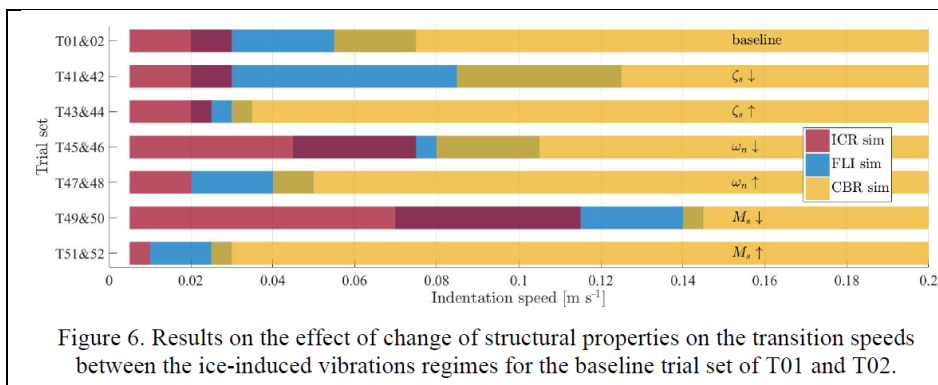


Figure 13-4 Results on effect of change in structural properties [117] Figure 6.

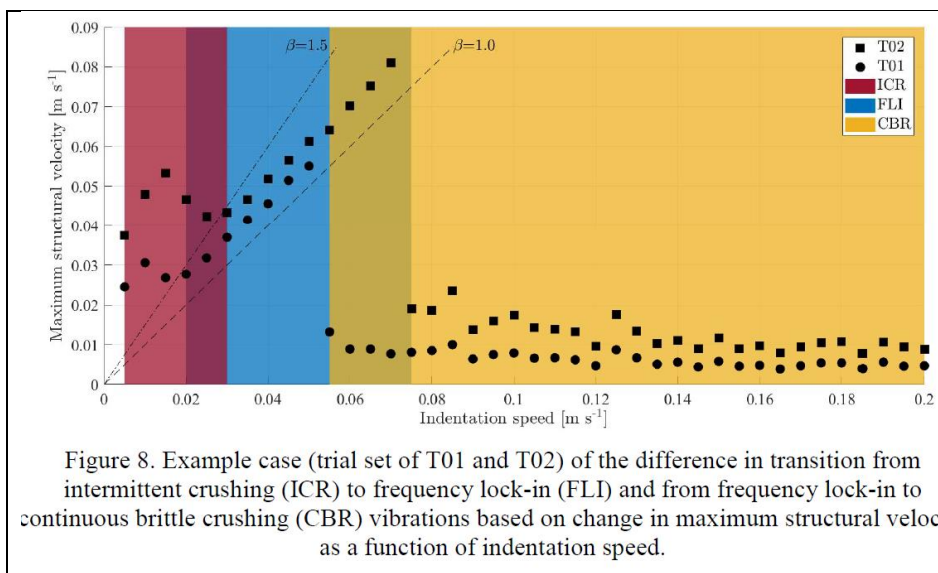


Figure 13-5 Example case (trial T01 and T02) [117] Figure 8.

Above figures (Figure 13-2, Figure 13-3, Figure 13-4 and Figure 13-5) illustrates that the structural conditions may limit the frequency lock-in to quite a narrow ice floe range or in certain cases it does not occur.

The conditions are further complicated for the actual OWF:

- There are rarely ice concentrations above 0.8 even at the reference Area 16 and intermittent crushing require heavy ice conditions, where an ice concentration of less than 0.8 maybe will make intermittent crushing to a very rare event.
- Even if there is a potential for intermittent crushing and frequency lock-in the kinetic energy in the incoming ice floes is that low so ice penetration stops after 1-2 dynamic events. Even if a certain 1-few km ice belt is behind the incoming ice floes, the penetration will stop after a few force oscillations. For larger incoming velocities there is a risk that a few load cycles in the frequency lock-in range can occur when the floe velocity is de-accelerated and hit the 0.02-0.06 m/s range.